

8-26-2015 12:00 AM

# The Development of Cyclic RGD Peptides Stabilized Through $^{99m}\text{Tc}/\text{Re}(\text{CO})_3^+$

Aagam Patel, *The University of Western Ontario*

Supervisor: Dr. Leonard Luyt, *The University of Western Ontario*

A thesis submitted in partial fulfillment of the requirements for the Master of Science degree in Chemistry

© Aagam Patel 2015

Follow this and additional works at: <https://ir.lib.uwo.ca/etd>

 Part of the [Inorganic Chemistry Commons](#), and the [Radiochemistry Commons](#)

---

## Recommended Citation

Patel, Aagam, "The Development of Cyclic RGD Peptides Stabilized Through  $^{99m}\text{Tc}/\text{Re}(\text{CO})_3^+$ " (2015). *Electronic Thesis and Dissertation Repository*. 3207.  
<https://ir.lib.uwo.ca/etd/3207>

This Dissertation/Thesis is brought to you for free and open access by Scholarship@Western. It has been accepted for inclusion in Electronic Thesis and Dissertation Repository by an authorized administrator of Scholarship@Western. For more information, please contact [wlsadmin@uwo.ca](mailto:wlsadmin@uwo.ca).

The Development of Cyclic RGD Peptides Stabilized Through  $^{99m}\text{Tc}/\text{Re}(\text{CO})_3^+$

Integrated Article

by

Aagam Patel

Graduate Program in Chemistry

A thesis submitted in partial fulfillment  
of the requirements for the degree of  
**Master of Science**

The School of Graduate and Postdoctoral Studies  
The University of Western Ontario  
London, Ontario, Canada

© Aagam Patel 2015

## Abstract

Protein secondary structure can be mimicked by incorporating structural constraints into peptides and this can be facilitated by metal coordination. The objective of this project is to establish a chelation system with a cancer targeting peptide sequence, where the coordination to a metal centre results in a cyclic metallopeptide. Cyclic RGD peptides are antagonists for  $\alpha_v\beta_3$  and other integrins, which are present during tumour angiogenesis. Arg-Gly-Asp (RGD) sequence is employed in the peptide backbone, with an un-natural amino acid (3-Pal) and a chelating molecule (pyridyl-triazole, pyta) present on opposite ends of the peptide sequence to form a linear peptide sequence, pyta-RGD-3-Pal-NH<sub>2</sub>. The linear peptide was reacted with  $[\text{Re}(\text{OH}_2)_3(\text{CO})_3]^+$  to form a cyclic system, with the pyridyl-triazole coordinating in a bidentate fashion. The linear peptide and resulting cyclic metallopeptide were characterized by high resolution mass spectrometry (HRMS), Circular Dichroism (CD) spectroscopy, one- and two-dimensional <sup>1</sup>H-NMR spectroscopy, and variable temperature (VT) NMR spectroscopy, with purity > 90% as determined by HPLC. Computational studies on the coordinated peptide suggested intra-molecular hydrogen bonding consistent with VT NMR data. The linear peptide was successfully radiolabelled with Tc-99m demonstrating the potential application as a SPECT (single photon emission computed tomography) imaging agent for angiogenesis. This approach to adding a structural constraint, through metal-based peptide cyclization, results in a metallopeptide where the metal is central to creating the turn mimetic.

## Keywords

Molecular imaging probe, Technetium-99m, metal-based peptide cyclization, cyclic RGD, <sup>99m</sup>Tc/Re(CO)<sub>3</sub><sup>+</sup>

## Co-Authorship Statement

The computational study presented in Chapter 3 was completed by Dr. Jinqiang Hou, a postdoctoral fellow in Dr. Leonard Luyt's Lab.

## Acknowledgments

First of all, I would like to thank Dr. Len Luyt for the opportunity to work in his lab. Thanks for all the support and motivation you provided over the last couple years.

Next, I would to thank Milan for teaching me peptide synthesis and being a great bud, in and out of the lab. I would also like to thank Neha and Axie for putting up with me last couple years, and giving helpful insights on the project.

Special thanks to all the lab members, past and present, in the Luyt lab. It's been a pleasure knowing and working with you guys. Cheers.

Finally, I would like to thank my family and close friends for all their love and support during the good and bad times.

# Table of Contents

Abstract .....	ii
Co-Authorship Statement.....	iii
Acknowledgments.....	iv
Table of Contents .....	v
List of Tables .....	viii
List of Figures .....	ix
List of Schemes .....	xi
List of Appendices .....	xii
List of Abbreviations and Symbols.....	xiii
Chapter 1 .....	1
1 Introduction .....	1
1.1 Molecular Imaging.....	1
1.2 Targeting Entity .....	1
1.3 Solid Phase Peptide Synthesis (SPPS).....	2
1.4 Structural Constraints.....	4
1.5 Metal Induced Structural Constraints .....	6
1.6 Signaling Source .....	8
1.7 Single Photon Emission Computed Tomography (SPECT) .....	9
1.8 Technetium-99m as Signaling Source .....	10
1.9 Using $^{99m}\text{Tc}/\text{Re}(\text{CO})_3^+$ as a “2+1” Chelation System to Induce a Turn Conformation in a Linear Pentapeptide .....	12
1.10 Integrin, $\alpha_v\beta_3$ , as a Biological Target .....	13
1.11 Thesis Scope .....	17
1.12 References .....	17
Chapter 2.....	23

2	Employing Amino Acids to Cyclize Pentapeptides Through “2+1” Chelation System Using $^{99m}\text{Tc}/\text{Re}(\text{CO})_3^+$ .....	23
2.1	Introduction .....	23
2.2	Results and Discussion .....	26
2.2.1	Synthesis of $[\text{Re}(\text{CO})_3(\text{OH}_2)_3]\text{OTf}^{12}$ .....	26
2.2.2	Synthesis of Ac-HRGDH-OH .....	26
2.2.3	Characterization of Ac-HRGDH-OH .....	28
2.2.4	“2+1” Coordination Using Natural Amino Acids as Metal Chelators .....	29
2.2.5	“2+1” Mixed Coordination with an External Mono-Dentate Chelator .....	32
2.2.6	“2+1” Coordination with Un-natural Amino Acids as Metal Chelators ..	33
2.3	Conclusion .....	37
2.4	Experimental .....	37
2.4.1	Small Molecule Synthesis .....	38
2.4.2	Peptide Synthesis .....	38
2.4.3	$\text{Re}(\text{CO})_3^+$ Coordination .....	41
2.5	References .....	42
	Chapter 3 .....	45
3	A Turn Induced by $^{99m}\text{Tc}/\text{Re}$ (I) Tricarbonyl Coordination to Form Cyclic Metallopeptides .....	45
3.1	Introduction .....	45
3.2	Results and Discussion .....	46
3.2.1	Strategy .....	46
3.2.2	Peptide Synthesis .....	47
3.2.3	$^1\text{H}$ -NMR Analysis of pyta-RGD-3-Pal-NH <sub>2</sub> .....	48
3.2.4	$\text{Re}(\text{CO})_3^+$ Coordination .....	49
3.2.5	Characterization of $[\text{Re}(\text{CO})_3(\text{pyta-RGD-3-Pal-NH}_2)]\text{OTf}$ .....	50
3.2.6	Circular Dichroism (CD) Spectroscopy .....	52

3.2.7	Variable Temperature (VT) NMR .....	53
3.2.8	Computational Study .....	55
3.2.9	<sup>99m</sup> Tc Labelling .....	56
3.2.10	Derivatives of [Re(CO) <sub>3</sub> (pyta-RGD-3-Pal-NH <sub>2</sub> )] <sup>+</sup> .....	57
3.3	Conclusion .....	58
3.4	Experimental .....	58
3.4.1	Small Molecule Synthesis.....	59
3.4.2	Peptide Synthesis .....	60
3.4.3	Metal Coordination .....	62
3.4.4	Circular Dichroism (CD) spectroscopy .....	64
3.4.5	Computational Studies .....	64
3.5	References .....	65
Chapter 4	.....	69
4	Conclusion .....	69
4.1	References.....	71
Appendices	.....	73
Appendix A: Chromatograms of selected compounds	.....	73
Appendix B: <sup>1</sup> H-NMR spectra of linear and Re(CO) <sub>3</sub> <sup>+</sup> coordinated peptides	.....	79
Appendix C: Computational study on Re(CO) <sub>3</sub> <sup>+</sup> , <b>3.5</b>	.....	95
Curriculum Vitae	.....	98

## List of Tables

Table 2.1 Calculated and observed m/z ratio of Ac-HRGDH-OH, 2.4. ....	27
Table 2.2 Reaction conditions used to coordinate Ac-HRGDH-OH with $[\text{Re}(\text{CO})_3(\text{OH}_2)_3]^+$ .30	
Table 2.3 Increasing molar equivalent of pyridine led higher % of $[\text{Re}(\text{CO})_3(\text{Ac-HRGDH-NH}_2)(\text{py})]^+$ .....	33
Table 2.4 Number of dominant isomers displayed upon coordination with $\text{Re}(\text{CO})_3^+$ , for 2/3-Pal-RGD-3/4-Pal series.....	35
Table 3.1 Amino acids' proton shifts (ppm) of the linear peptide, pyta-RGD-3-Pal-NH <sub>2</sub> .....	49
Table 3.2 Amino acids' proton chemical shifts (ppm) of the coordinated peptide, pyta-RGD-3Pal-NH <sub>2</sub> - $\text{Re}(\text{CO})_3^+$ . ....	50
Table 3.3 Chemical shifts of amide protons expressed in numerical values, $\Delta\delta/\Delta T$ (ppb/K) for each amino acid residues. ....	54

# List of Figures

Figure 1.1 Schematic for a molecular imaging probe.....	1
Figure 1.2 Solid phase peptide synthesis (SPPS) employing 9-fluorenylmethoxycarbonyl (Fmoc) strategy .....	3
Figure 1.3 Structural constraints introduced through different bond types; cilengitide, cyclization through amide bond, and octreotide, cyclization introduced by di-sulfide bonds .	6
Figure 1.4 Dominant isomer of Ac-HAAAH-NH <sub>2</sub> coordinated with Pd <sup>2+</sup> , through N1 nitrogen atoms on both imidazole rings. <sup>18</sup> .....	8
Figure 1.5 Decay scheme of <sup>99</sup> Mo to <sup>99</sup> Ru.....	10
Figure 1.6 Coordination of Ac-HAAAH with Re(CO) <sub>3</sub> <sup>+</sup> through N1 and N3 nitrogen atoms of the imidazole rings, and carboxyl oxygen at the C-terminus. <sup>31</sup> .....	13
Figure 1.7 Simple schematic of integrin consisting of $\alpha$ and $\beta$ subunits. ....	14
Figure 1.8 Integrins exhibiting binding towards different membrane proteins. <sup>36</sup> .....	15
Figure 1.9 Interactions between cyclic RGD peptide and integrin, $\alpha_v\beta_3$ . The cyclic peptide (yellow) making important interactions (dashed lines) with the amino acid residues of $\alpha_v$ (blue) and $\beta_3$ (red) subunits. <sup>39</sup> .....	15
Figure 1.10 Project design rationale .....	17
Figure 2.1 Schematic of pendant and integrated technetium-99m radiopharmaceutical designs .....	24
Figure 2.2 Model “2+1” chelation system .....	27
Figure 2.3 Linear Ac-HRGD <sup>H</sup> -OH peptide.....	27
Figure 2.4 <sup>1</sup> H-NMR spectrum of Ac-HRGD <sup>H</sup> -OH in CD <sub>3</sub> OD. ....	28
Figure 2.5 <sup>1</sup> H-NMR splits of Glycine and Aspartic acid in in CD <sub>3</sub> OD. ....	29

Figure 2.6 Coordination of di-aspartic acid to $\text{Re}(\text{CO})_3^+{}^{11}$ .....	31
Figure 2.7 Bidentate coordination at the C-terminal or N-terminal when using histidine residue as a metal chelator .....	34
Figure 2.8 Bidentate coordination at the N-terminus using un-natural amino acids as a metal chelators .....	35
Figure 2.9 LC-MS traces of 3Pal-RGD-3Pal-OH crude mixture and of an isolated isomer ..	37
Figure 3.1 Structures of pyridyl-triazole (pyta) and 3-pyridylalanine (3-Pal).....	51
Figure 3.2 Partial $^1\text{H}$ -NMR spectra (600 MHz, $\text{DMSO-d}_6$ , 25 °C) of the linear peptide and coordinated peptide .....	51
Figure 3.3 Partial $^1\text{H}$ -NMR spectra (600 MHz, $\text{DMSO-d}_6$ ) of the linear peptide (top) and coordinated peptide, $[\text{Re}(\text{CO})_3(\text{pyta-RGD-3Pal-NH}_2)]\text{OTf}$ (below).....	52
Figure 3.4 Circular Dichroism (CD) analysis of linear peptide and $\text{Re}(\text{CO})_3^+$ coordinated peptide in $\text{H}_2\text{O}$ at 25 °C.....	53
Figure 3.5 VT NMR analysis of the rhenium coordinated peptide in $\text{DMSO-d}_6$ at 600 MHz. ....	54
Figure 3.6 Optimized structure of Re-coordinated peptide, 3.5, displaying intra-molecular hydrogen bonding. ....	56
Figure 3.7 U-HPLC analysis showing correlations between $\gamma$ trace of $^{99\text{m}}\text{Tc}(\text{CO})_3^+$ labelled peptide and UV trace of $\text{Re}(\text{CO})_3^+$ coordinated peptide. ....	57
Figure 3.8 Derivatives of $[\text{Re}(\text{CO})_3(\text{pyta-RGD-3-Pal-NH}_2)]\text{OTf}$ . ....	58

## List of Schemes

Scheme 2.1 Synthetic route for $[\text{Re}(\text{OH}_2)_3(\text{CO})_3]\text{OTf}$ , as 0.1 M solution.....	7
Scheme 2.2 Synthetic approach for Ac-HRGDh-OH coordination with $[\text{Re}(\text{CO})_3(\text{OH}_2)_3]^+$ and proposed coordination product.....	29
Scheme 2.3 Synthetic approach towards mixed “2+1” $\text{Re}(\text{CO})_3^+$ complexes, and a proposed coordination product .....	32
Scheme 2.4 Synthetic approach for Ac-3-Pal-RGD-3-Pal-OH coordination with $[\text{Re}(\text{CO})_3(\text{OH}_2)_3]^+$ , and proposed coordination structure.....	36
Scheme 3.1 Synthetic route for pyridyl-triazole (pyta) .....	47
Scheme 3.2 Synthesis of pyta-RGD-3Pal-NH <sub>2</sub> employing SPPS.....	47
Scheme 3.3 $\text{Re}(\text{CO})_3^+$ coordination of pyta-RGD-3-Pal-NH <sub>2</sub> .....	49
Scheme 3.4 $^{99\text{m}}\text{Tc}(\text{CO})_3^+$ coordination of pyta-RGD-3-Pal-NH <sub>2</sub> to give <b>3.6</b> . ....	55

## List of Appendices

Appendix A: Chromatograms .....	70
Appendix B: $^1\text{H}$ - and COSY NMR spectra of linear and $\text{Re}(\text{CO})_3^+$ coordinated peptides.....	77
Appendix A: Computational study on $\text{Re}(\text{CO})_3^+$ coordinated peptide, <b>3.5</b> .....	91

## List of Abbreviations and Symbols

**2D:** two-dimensional

**2-Pal:** 2-pyridylalanine

**3-Pal:** 3-pyridylalanine

**4-Pal:** 4-pyridylalanine

**Ac:** acetyl

**Boc:** *tert*-butoxycarbonyl

**CD:** circular dichroism

**CT:** computed tomography

**CD<sub>3</sub>OD:** deuterated methanol

**DCM:** dichloromethane

**DIPEA:** *N,N*-diisopropylethylamine

**DMF:** *N,N*-dimethylformamide

**DMSO-*d*<sub>6</sub>:** deuterated dimethyl sulfoxide

**ECM:** extracellular matrix

**en:** ethylenediamine

**ESI:** electrospray ionization

**Fmoc:** 9-fluorenylmethoxycarbonyl

**gCOSY:** correlation spectroscopy

**HATU:** (2-(7-aza-1*H*-benzotriazole-1-yl)-1,1,3,3-tetramethyluronium hexafluorophosphate)

**HCTU:** (2-(6-chloro-1H-benzotriazole-1-yl)-1,1,3,3-tetramethylaminium hexafluorophosphate)

**His:** histidine

**HPLC:** high performance liquid chromatography

**IC<sub>50</sub>:** half-maximal inhibitory concentration

**K:** Kelvin

**K<sub>d</sub>:** dissociation constant

**keV:** kilo electron volt

**LC:** liquid chromatography

**M:** molar

**MIDAS:** metal-ion dependent adhesion site

**MRI:** magnetic resonance imaging

**MS:** mass spectroscopy

**NaOH:** sodium hydroxide

**nM:** nano molar

**NMR:** nuclear magnetic resonance

**OtBu:** *tert*-butyl ester

**OTf:** trifluoromethanesulfonate

**Pbf:** 2,2,4,6,7-Pentamethyldihydrobenzofuran-5-sulfonyl

**PBS:** phosphate buffer saline

**PET:** positron emission tomography

**PM:** photon multiplier

**ppb:** parts per billion

**Py:** pyridine

**pyta:** pyridyl-triazole

**RGD:** arginine-glycine-aspartic acid

**ROE:** rotating frame overhauser enhancement

**ROSEY:** rotating frame nuclear overhauser effect

**RP:** reverse phase

**SPECT:** single photon emission computed tomography

**SPPS:** solid phase peptide synthesis

**TBME:** *tert*-butyl methyl ether

**TIPS:** triisopropylsilane

**TFA:** trifluoroacetic acid

**Trt:** triphenylmethane

**TSTU:** (*O*-(*N*-succinimidyl)-1,1,3,3-tetramethyl uranium tetrafluoroborate)

**US:** ultrasound

**VT:** variable temperature

## Chapter 1

### 1 Introduction

#### 1.1 Molecular Imaging

The methods used to evaluate and visualize biological events have changed over the years. Different imaging techniques have been introduced that provide insight into the biological processes taking place within our body. Molecular imaging is one such technique and can be defined as the non-invasive characterization and visualization of biological events taking place at the cellular and molecular level.<sup>1,2</sup> Molecular imaging allows diseased cells and normal tissue cells to be differentiated, by targeting those biological receptors that are overexpressed in diseased cells, while present at low concentrations in the normal tissue cells. Several factors are taken into account when designing a molecular imaging probe (Figure 1.1), which include: a) an appropriate biological target, b) a targeting entity with high affinity for the chosen biological target; a good binding target would have a dissociation constant ( $K_d$ ) in nM range, and c) an appropriate signaling source that allows the target to be detected by an external imaging modality.<sup>1</sup>

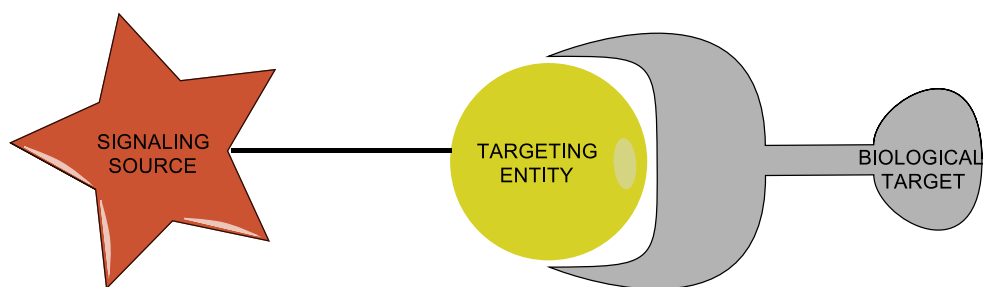


**Figure 1.1** Schematic for a molecular imaging probe.

#### 1.2 Targeting Entity

There are a number of different kinds of targeting entities that exist, ranging from small molecules and peptides to large biologics such as antibodies or nucleic acids. Peptides

have increasingly gained attention as a targeting component, as they have a number of desirable properties.<sup>2,3</sup> The advantages of using peptides as a targeting entity include: 1) they can be readily synthesized and the monomeric amino acid residues can be chemically modified; 2) there are many biological receptors that display good binding affinity towards small peptides; 3) their low molecular weight and small size allow them to penetrate tissue and tumours, as well as to be removed from the plasma and body relatively quickly; 4) a variety of bi-functional ligands can be attached at a peptide's C-terminus and N-terminus; and 5) peptides display good tumour-background ratios.<sup>2-4</sup> In addition, small molecule drugs, and imaging molecules can be attached to peptides for a variety of applications.<sup>5</sup>

The use of peptides as targeting entities also suffer from a number of disadvantages. Firstly, the *in vivo* stability of short linear peptides is a major concern, as they readily undergo degradation by proteases and peptidases.<sup>3,6</sup> Secondly, the flexible nature of linear peptides allows them to bind to multiple receptors, which reduces their specific binding towards the biological target.<sup>3,6</sup> Furthermore, the addition of an imaging source can affect the peptide conformation and reduce the specific binding of the peptide.<sup>1</sup> Despite these difficulties, structural constraints, such as through cyclization of the peptide backbone, can resolve some of the difficulties seen with short linear peptides.

### 1.3 Solid Phase Peptide Synthesis (SPPS)

Peptides can be synthesized either in solution-phase or on a solid-phase support. Solution-phase peptide synthesis is an efficient method; however, isolation, purification and characterization steps are required after the addition of each amino acid, making this a rather expensive and time consuming technique. On the other hand, solid phase peptide synthesis (SPPS), introduced by Merrifield in 1963<sup>7</sup>, is more efficient to construct large and complex peptide sequences. With this technique, a peptide is constructed in a stepwise manner, using an insoluble resin that fixes, the C-terminus of the peptide to the resin. This allows the use of excess reagents, in order to ensure that the addition of each amino acid proceeds to completion. When using this technique, the reagents and by-products are soluble, and can therefore, be easily removed with excess washing and

filtering without affecting the peptide which remains attached to the resin. As a result, this eliminates the need for a purification step after each amino acid coupling.

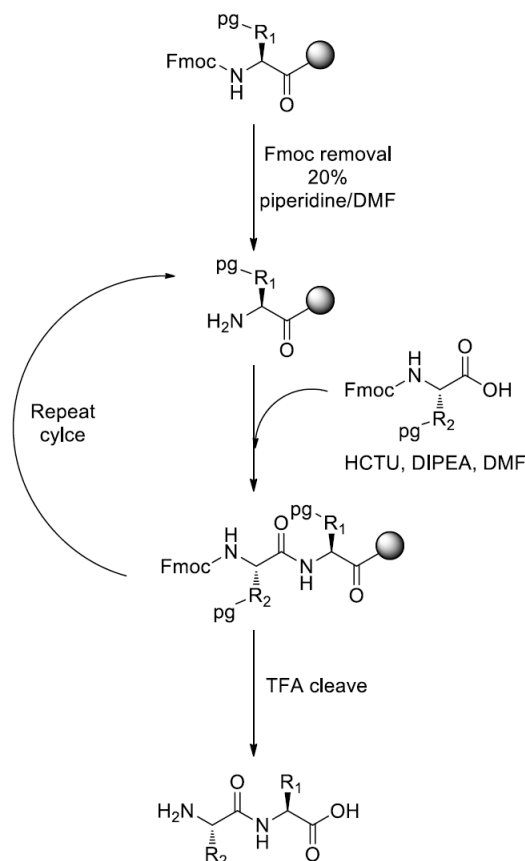


**Figure 1.2** Solid phase peptide synthesis (SPPS) employing 9-fluorenylmethoxycarbonyl (Fmoc) strategy

In SPPS, the peptide is constructed from the C-terminus to the N-terminus, with the C-terminus attached to an insoluble resin. There are two common strategies involved with SPPS based upon the protecting group being used, 9-fluorenylmethoxycarbonyl (Fmoc) and tert-butoxycarbonyl (Boc). These strategies both involve orthogonal protecting groups, which allows only the N-terminal protecting group of the peptide to be selectively removed for the addition of the next amino acid, and the other amino acids already coupled to the resin to remain protected. In the Fmoc strategy (Figure 1.2), the Fmoc group is a base labile, and can be removed with piperidine in *N,N*-

dimethylformamide (DMF). On the other hand, the resin, and the protecting groups on the side chains of amino acid residues are acid labile. Once the Fmoc group is removed, the next amino acid in the sequence is added in excess, in addition to the coupling reagent, 2-(6-chloro-1H-benzotriazole-1-yl)-1,1,3,3-tetramethylaminium hexafluorophosphate (HCTU) and a base, *N,N*-diisopropylethylamine (DIPEA) in DMF. This cycle repeats until the desired peptide is constructed. The peptide is cleaved off of the resin, and all of the protecting groups are removed by vortexing the resin in an acidic solution containing a carbocation scavenger, triisopropylsilane (TIPS). In suitable acidic conditions, trialkylsilanes can act as hydrogen donors, and de-block the protecting groups from additional reactions with the peptide.<sup>8</sup> This results in a linear peptide that is purified with reverse phase high performance liquid chromatography (RP-HPLC) and characterized by mass spectroscopy (MS).

## 1.4 Structural Constraints

The exploration of peptide geometry has been of major interest in peptide chemistry. Principal interest is the introduction of structural constraints within the peptide backbone, in order to create effective probes for targeting biological receptors. Cyclized peptides are to have a more rigid geometry, and therefore, when present in favorable conformations, would result in better binding and selectivity towards the targeted receptors.<sup>5</sup> Cyclization of peptides results in reduced molecular conformations in solution as compared to their linear counterparts. When these constrained peptides are used as targeting entities, the limited number of conformations results in less competition for targeting biological receptors. On the other hand, linear peptides undergo numerous conformations in solution, and these conformations are present in very fast equilibrium. As a result, the specific binding towards the targeted receptor is reduced, as different conformations compete for interaction with the biological target.<sup>5, 9</sup>

Numerous examples have been presented, where introducing a structural constraint results in better binding towards the targeted receptor. Kumar et al. reported cyclic analogues of linear peptide sequence, Ac-CIYKYY, as an inhibitory agent against activated Src tyrosine kinase.<sup>10</sup> Src kinase inhibitors prevent kinases from

phosphorylating proteins at the tyrosine site, and this inhibition slows down the downstream signal transduction. This mechanism is used in an attempt to treat tumours. Kumar et al. compared the linear peptide with cyclic head-to-tail peptide analogues, and found that the cyclic peptide ( $IC_{50} = 6.4 \mu M$ ) had an inhibitory effect, 62.5-fold higher than that of the linear peptide ( $IC_{50} = 400 \mu M$ ), which is believed to be due to the introduction of a structural constraint within the peptide backbone. They further reported eight other cyclic derivatives of the same linear peptide sequence, using different strategies to cyclize the peptide. Seven out of eight derivatives displayed better potency against tyrosine kinase than the linear sequence.

Cyclization can be introduced using different strategies, such as head-to-tail cyclization, and side-chain to side-chain cyclization. Cyclization can be presented by different bond types, such as the formation of amide bond, disulfide bridges, metal coordination, and several others. An example of where cyclization was introduced through amide bond formation is cilengitide (Figure 1.3), a pentapeptide cyclized from head-to-tail by the formation of an amide bond.<sup>11</sup> Cilengitide,  $c(RGDf(N-Me)V)$ , contains a tripeptide sequence, Arg-Gly-Asp (RGD), and is an antagonist for integrin,  $\alpha_v\beta_3$ . Numerous RGD peptides have shown good binding towards integrin,  $\alpha_v\beta_3$ . Vitronectin competitive assays displayed cilengitide ( $IC_{50} = 0.58 \text{ nM}$ ) to have 360-fold better binding towards  $\alpha_v\beta_3$  than the linear peptide sequence, GRGDSPK ( $IC_{50} = 0.58 \mu M$ ).<sup>12</sup> Octreotide is an example where cyclization is introduced through disulfide bonds, formed through side chain interactions of cysteine residues. Octreotide is a synthetic octapeptide that mimics somatostatin, a naturally occurring hormone; it binds to the somatostatin receptor. Both linear and cyclic octreotide displayed binding towards somatostatin receptors; however, linear octreotide exhibits poorer binding than its cyclic analogue.<sup>13</sup>

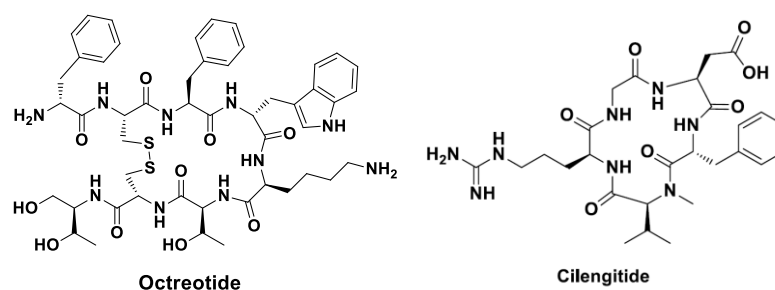


**Figure 1.3** Structural constraints introduced through different bond types; cilengitide, cyclization through amide bond, and octreotide, cyclization introduced by di-sulfide bonds

Cyclization has shown improved *in-vivo* stability of peptides. Pakkala et al. compared the stability of linear and cyclic peptides targeting human glandular kallikrein (KLK2) with the sequence GAARFKVWWAAG (KLK2b).<sup>5,14</sup> The KLK2 protein is a highly specific prostate serine protease that is overexpressed in aggressive prostate tumors. Targeting this protein serves a potential therapeutic to reduce the metastasis of prostate cancer. As mentioned earlier, the *in-vivo* stability of short linear peptides is a major concern, as they are readily broken down through enzymatic degradation. Here, the stability of linear and head-to-tail cyclized KLK2b peptides in trypsin and human plasma was compared. Trypsin behaves as a protease, and cleaves amide bond following lysine or arginine residues. The linear KLK2b peptide completely degraded after 30 minutes in trypsin; however, only 57% of head-to-tail cyclized peptide degraded after 4 hours, according to HPLC analysis. In addition, the linear peptide completely degraded after 30 minutes in human plasma, while, the cyclized peptide was still intact after 24 hours. This study demonstrated that stability of peptides can be achieved through head-to-tail amide cyclization.

## 1.5 Metal Induced Structural Constraints

Cyclization can also be introduced through metal coordination. Metals have been shown to exhibit structural constraints when introduced within the peptide sequences. This is commonly accomplished by developing a metal clip that will coordinate to a metal. In literature, metal complexes have been reported to stabilize peptide sequences.<sup>15-16</sup> A turn

can be induced within the peptide backbone by metal coordination where the metal acts as a central core around which a turn occurs. This is demonstrated by incorporating metal chelators or metal chelating amino acids within the peptide backbone. A turn is an element of secondary structure, and occurs when the peptide backbone that is in a random coil sharply bends on itself, separated by a minimum of two amino acid residues. A turn can be characterized based on the number of amino acids that are separating the two ends of the cyclized peptide. Various types of turns include  $\gamma$  ( $i, i\pm 2$ ),  $\beta$  ( $i, i\pm 3$ ),  $\alpha$  ( $i, i\pm 4$ ),  $\alpha$  helix ( $i, i\pm 3.6$ );  $i$  represents the amino acid where the turn is created.<sup>17,18</sup>

Hoang et al., demonstrated helicity within the peptide backbone upon metal coordination.<sup>19</sup> In their study, a linear peptide, in random coil, was cyclized and a turn was induced upon metal coordination. The natural amino acid, histidine, was used to coordinate with the metal center. The study reported that cyclization of linear pentapeptide, Ac-HAAAH-NH<sub>2</sub>, through Pd(en)<sup>2+</sup> core being coordinated through nitrogen atoms of the imidazole ring on histidine residues, present at the opposite ends of the pentapeptide. Three linkage isomers were observed when Ac-HAAAH-NH<sub>2</sub> was coordinated with Pd<sup>2+</sup>, which differed in the pair of imidazole nitrogen atoms bound to the metal. The dominant linkage isomer was a 22-membered macrocyclic metallopeptide, which had palladium (II) bound to the peptide through two N1 atoms of the imidazole rings (Figure 1.4). From the ROSEY NMR spectra, ROE correlations were observed for hydrogens of the imidazole rings on His<sub>1</sub> and His<sub>5</sub>, which suggested that they were present in close vicinity, and that Pd<sup>2+</sup> was bound through the imidazole nitrogen atoms of one peptide, instead of acting as a bridging metal for two different peptides. An upfield chemical shift in the <sup>1</sup>H-NMR spectra of CH $\alpha$  is characteristic for the presence of  $\alpha$  helicity in the peptide backbone.<sup>20</sup> This upfield chemical shift was observed for all CH $\alpha$  atoms present in the coordinated peptide backbone, which may suggest the presence of  $\alpha$  helicity. The Pd<sup>2+</sup> complexes were able to establish a reverse turn through cyclization, and the pentapeptide was held in a stable conformational lock.

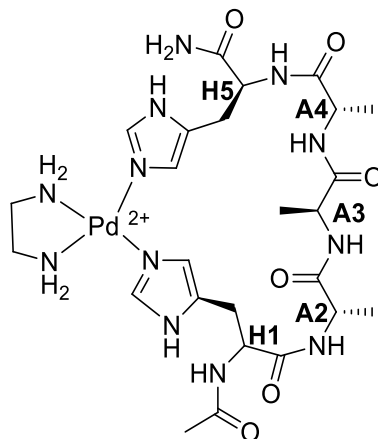


**Figure 1.4** Dominant isomer of Ac-HAAAH-NH<sub>2</sub> coordinated with Pd<sup>2+</sup>, through N1 nitrogen atoms on both imidazole rings.<sup>19</sup>

Albrecht et al. demonstrated activation of a biological relevant linear peptide sequence upon metal coordination.<sup>21</sup> They introduced a metal chelator, catechol, at the opposite ends of a tripeptide sequence, Trp-Ala-Val. This tri-peptide sequence is the backbone of Segetalins, cyclic peptides that possess estrogen-like activity.<sup>22</sup> Upon coordination with molybdenum, a turn was created, giving the tri-peptide sequence a conformational lock, and making the linear tri-peptide sequence biologically relevant. This concept can be used to develop imaging probes that employ metal clipped peptides whose biological activity is activated, upon coordinating with an appropriate radiometal signaling source.

## 1.6 Signaling Source

The signaling source is an integral component of an imaging probe. It provides energy that is detected by imaging modalities. More commonly used imaging modalities include computed tomography (CT), magnetic resonance imaging (MRI), positron emission tomography (PET), single photon emission computed tomography (SPECT), and ultrasound (US). PET and SPECT imaging employ radioactive materials as their signaling source. PET and SPECT share similar techniques that are based on the radiotracer principle, which states that biological events are monitored by the movement of a radiotracer circulating within the body. However, the pathway in which radiation is emitted and detected for PET and SPECT is fairly different.

In both PET and SPECT imaging the radiotracer is introduced within body fluids and is allowed to circulate until it binds to the target receptor. In both types of imaging,  $\gamma$ -rays are produced and detected by gamma cameras. The gamma camera most commonly contains sodium iodide (NaI) crystals with small amount of thallium that converts the  $\gamma$ -rays to photons. These photons are then captured by the photon multiplier (PM) tube, which converts the photons to an electronic signal. This electronic signal is then amplified and converted to a digital signal, which produces an image.<sup>23</sup> PET and SPECT isotopes are produced either by a cyclotron or a generator.

PET differs from SPECT in the way that  $\gamma$ -rays are emitted and subsequently detected by gamma cameras. For example, PET isotopes, which include  $^{18}\text{F}$ ,  $^{68}\text{Ga}$ ,  $^{64}\text{Cu}$ , undergo  $\beta^+$  decay by emitting a positron. The positron travels a short distance before coming in contact with an electron. This results in an annihilation event that produces two gamma rays of 511 keV each, which travel in opposite directions ( $180^\circ$  apart). These gamma rays are detected by gamma cameras that are placed  $360^\circ$  around the body. In addition, the half-life of PET and SPECT isotopes are different, PET radionuclides typically have half-lives ranging from minutes to hours, while those of SPECT isotopes range from hours to days.

## 1.7 Single Photon Emission Computed Tomography (SPECT)

SPECT imaging employs commonly used radionuclides such as  $^{99\text{m}}\text{Tc}$ ,  $^{111}\text{In}$ , and  $^{123}\text{I}$ ; all radioisotopes decay by releasing  $\gamma$ -rays with different energies. The energies released from SPECT radiotracers usually range from 100 – 300 KeV, which is strong enough to penetrate the skin without harming other tissues. SPECT radiotracers releases a single  $\gamma$ -ray that is detected by a gamma camera that circulates the whole body. SPECT radionuclides are less expensive, low energy, and readily available. They are ideally produced by on-site generators. SPECT radionuclides have longer half-lives ranging from 6 hours to 2.8 days, allowing for multiple syntheses, purification, and imaging of the body.

## 1.8 Technetium-99m as Signaling Source

Technetium-99m has been one of the more widely used radioactive metals to label biomolecules. It is used as a signaling source for more than 70% of nuclear medicine procedures.<sup>24</sup> Technetium-99m has many desirable properties, some of which include: i) easy availability, ii) low cost, iii) easy handling, iv), good imaging characteristics, and v) absence of strong radiation such as  $\alpha$  and  $\beta$  decay.<sup>3</sup>  $^{99m}\text{Tc}$  is an artificial element that is generated by a  $^{99}\text{Mo}/^{99m}\text{Tc}$  generator, in which  $^{99}\text{Mo}$  decays to  $^{99m}\text{Tc}$  by  $\beta^-$  decay.  $^{99m}\text{Tc}$  is a nuclear isomer of  $^{99}\text{Tc}$  present in a metastable state, which decays to  $^{99}\text{Tc}$  by emitting a  $\gamma$  ray with an energy equal to 140 keV (Figure 1.5). The  $\gamma$  emission can be detected by Single Photon Emission Computer Tomography (SPECT).  $^{99m}\text{Tc}$  has a half-life of 6 hours, which is suitable for radiolabeling biomolecules, as well as acquiring images.

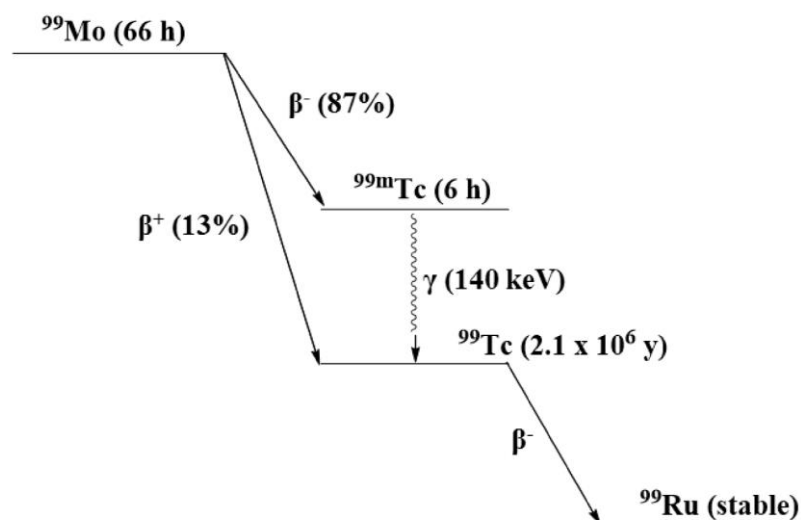


**Figure 1.5** Decay scheme of  $^{99}\text{Mo}$  to  $^{99}\text{Ru}$

The  $^{99m}\text{Tc}$  metal can exist in various oxidation states; for example a +V oxidation state of  $^{99m}\text{Tc}$  is observed in  $[\text{}^{99m}\text{Tc}=\text{O}]^{3+}$  and  $[\text{}^{99m}\text{Tc}\equiv\text{N}]^{2+}$ , a +III oxidation state in  $^{99m}\text{Tc(III)}$  complexes, and a +I oxidation state in  $[\text{}^{99m}\text{Tc}(\text{CO})_3]^+$  complexes. All of these oxidation states are the reduced form of  $[\text{}^{99m}\text{TcO}_4]^-$ , where the oxidation state of  $^{99m}\text{Tc}$  is +VII, which is the form when eluted from the  $^{99}\text{Mo}/^{99m}\text{Tc}$  generator. The  $[\text{}^{99m}\text{Tc}(\text{CO})_3]^+$  complexes can be stabilized either by a tridentate chelator, a '2+1' chelation system, or

three mono-dentate ligands. A '2+1' chelation system is the combination of bi-dentate and mono-dentate ligands attached to a metal.

The +1 oxidation state of  $^{99m}\text{Tc}/\text{Re}(\text{I})$  octahedral complexes, results in the  $d^6$  electrons occupying degenerate  $t_{2g}$  orbitals ( $d_{xy}$ ,  $d_{yz}$ , and  $d_{xz}$ ) leaving the doubly degenerate  $e_g$  orbitals ( $d_{x^2-y^2}$ ,  $d_{z^2}$ ) empty.<sup>25</sup> Tc/Re (I) are usually referred to as soft metals due to the low charge to size ratio and their preference for soft ligands, because soft-soft interactions are considered to be stronger than soft-hard interactions.

The  $^{99m}\text{Tc}(\text{CO})_3^+$  core is a versatile building block for a variety of biomolecules. The carbonyl groups are known to stabilize metals with low oxidation states, such as  $[\text{Mn}(\text{CO})_6]^+$ .<sup>25</sup> According to the molecular orbital energy diagram of a carbonyl group, the highest occupied molecular orbital (HOMO) is a  $3\sigma$  orbital and lowest unoccupied molecular orbitals (LUMO) are antibonding  $\pi$  ( $\pi^*$ ). The metal-carbonyl bond involves the HOMO ( $3\sigma$ ) participating in a sigma bond, whereas the LUMO ( $\pi^*$ ) form  $\pi$  bonds with the metal center.<sup>25</sup> The  $\pi$  bonding is achieved by donation of electrons from occupied  $d$  orbitals of the metal to doubly degenerate empty  $\pi^*$  orbitals of the carbonyl group; this lowers the electron density on the metal center while increasing it on the carbonyl group. Increase in the electron density helps stabilize the carbonyl group, and in return enhances the sigma donation to the metal center.<sup>25</sup> The  $\pi$  bonding can also be referred to as  $\pi$ -backbonding.

The  $^{99m}\text{Tc}(\text{CO})_3(\text{OH}_2)_3^+$  complex is a convenient starting material for labeling various biomolecules. Previously, the complex  $^{99m}\text{Tc}(\text{CO})_3(\text{OH}_2)_3^+$  was synthesized from aqueous  $^{99m}\text{TcO}_4^-$  in the presence of gaseous carbon monoxide, CO, and borohydride,  $\text{BH}_4^-$ , as a reducing agent.<sup>26</sup> However, the use of carbon monoxide is unsuitable for developing radiopharmaceutical 'isolink' kits. Each 'isolink' kit contains a lyophilized mixture of sodium carbonate, disodium boranocarbonate, sodium tartrate, and sodium tetraborate.<sup>27</sup> The compound  $\text{K}_2[\text{H}_3\text{BCO}_2]$  has been reported to release CO in aqueous solution at high temperatures.<sup>28, 29</sup> Alberto et al. employed  $[\text{H}_3\text{BCO}_2]^{2-}$ , as a reducing agent and a potential source for CO, to form a water soluble and water stable  $^{99m}\text{Tc}(\text{CO})_3(\text{OH}_2)_3^+$  complex.<sup>30</sup> The reaction was performed at 90 °C for 10 minutes, in

an appropriate buffer solution and a complexing agent (sodium tartrate), for stabilizing the intermediate complexes. Pitchumony et al. reported microwave assisted synthesis of  $[^{99m}\text{Tc}(\text{CO})_3(\text{OH}_2)_3]^+$ , with reduced reaction time to 3.5 minutes at 110 °C.<sup>31</sup> According to the reaction conditions described above, an octahedral complex was formed with the carbonyls *trans* to the aqua ligands to provide a facial orientation. The aqua ligands can be readily replaced with incoming biomolecules.

The  $^{99m}\text{Tc}$  chemistry is performed at a microgram scale. To explore the coordination chemistry, rhenium ( $^{185/187}\text{Re}$ ) is used as a non-radioactive analogue. Rhenium follows technetium in Group VII of the periodic table. Elements in the same group share similar physical and chemical characteristics. Thus, rhenium is a suitable metal to explore coordination chemistry for radioactive technetium.

The  $^{99m}\text{Tc}/\text{Re}(\text{CO})_3^+$  octahedral complexes commonly exist as facial isomers; however, a report on meridional isomer has been published.<sup>32</sup> Due to the strong bonding between the metal center and the carbonyl groups, the *trans* aqua ligands are very labile and can be easily substituted with incoming biomolecules. Electron density from nitrogen, oxygen, and sulfur atoms of various ligands, can be donated to the empty d orbitals of  $^{99m}\text{Tc}/\text{Re}(\text{CO})_3^+$  metal core, resulting in formation of  $\sigma$  bonds.

## 1.9 Using $^{99m}\text{Tc}/\text{Re}(\text{CO})_3^+$ as a “2+1” Chelation System to Induce a Turn Conformation in a Linear Pentapeptide

The  $^{99m}\text{Tc}/\text{Re}(\text{CO})_3^+$  core has not been reported to create and stabilize a turn conformation within a biologically relevant peptide. However, in 2014, Simpson reported coordination of Ac-HAAAH with the  $\text{Tc}/\text{Re}(\text{CO})_3^+$  core to create a turn conformation.<sup>33</sup> The  $^{99m}\text{Tc}/\text{Re}$  (I) core was coordinated through imidazole nitrogen atoms of histidine residues present at opposite ends of the peptide. This was based on a similar approach employed by Hoang et al.<sup>19</sup> The facially oriented octahedral complex was cyclized through the oxygen atom of the carboxyl group, at the C-terminus. However, instead of having both the N1 nitrogen atoms of imidazole rings coordinated to the metal centre, as

reported by Hoang et al.<sup>19</sup>, the peptide was coordinated through N1 and N3 nitrogen atoms (Figure 1.6). The metalloprotein complex resulted in a 21 membered macrocycle, and a small 7 membered ring. The peptide can be referred to as a “2+1” chelation system, where a bidentate attack from imidazole nitrogen and carboxyl oxygen is observed at one end, and a monodentate attack of imidazole nitrogen atom is observed on the other end. Hydrogen bonding in the peptide backbone was reported by variable temperature (VT) NMR and computational studies. Four hydrogen bonds were observed within the peptide backbone. The radiolabeled peptide, with  $^{99m}\text{Tc}(\text{CO})_3^+$ , resulted in the identical dominant isomer when coordination was demonstrated with  $\text{Re}(\text{CO})_3^+$ .

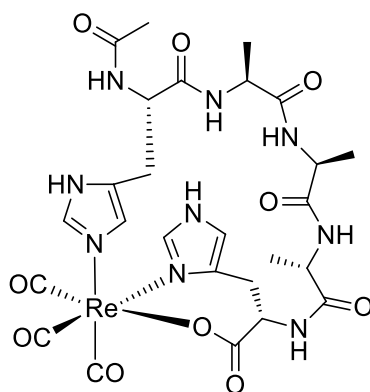


**Figure 1.6** Coordination of Ac-HAAAH with  $\text{Re}(\text{CO})_3^+$  through N1 and N3 nitrogen atoms of the imidazole rings, and carboxyl oxygen at the C-terminus.<sup>33</sup>

## 1.10 Integrin $\alpha_v\beta_3$ , as a Biological Target

Integrins are heterodimeric type I transmembrane proteins that mediate cell-cell and cell-extracellular matrix (ECM) interactions. Integrin signaling regulates cell shape, cell cycle, and cell migration.<sup>34</sup> This is achieved by one of two ways: ‘outside-in signaling’ and ‘inside-out signaling’. For “inside-out signaling” to occur, an intracellular activator binds to the  $\beta$  subunit of the integrin, resulting in a conformational change, and increasing the binding affinity for the extracellular proteins. On the other hand, ‘outside-in signaling’ involves a ligand binding to the integrin at the extracellular domain, resulting in a conformational change of the integrin structure. This subsequently promotes intracellular signaling through signaling proteins. The “outside-in signaling” regulates

cell polarity, cytoskeletal structure, and cell survival, while ‘inside-out signaling’ results in cell invasion and migration. The detached cells result in apoptosis through a series of events.<sup>35</sup> Preventing the binding of extracellular membrane proteins to integrins leads to cell death and suppresses the aggression of tumour such as metastasis and angiogenesis.<sup>36</sup> The development of antagonists that prevent the binding of ECM proteins can serve as a potential therapeutic for tumour suppression. Besides assessing integrins as therapeutic targets, they also make good imaging biomarkers. The targeting of integrins allows for the evaluation anti-angiogenic and anti-therapeutic agents, and also preliminary diagnosis of cancer.<sup>34</sup>

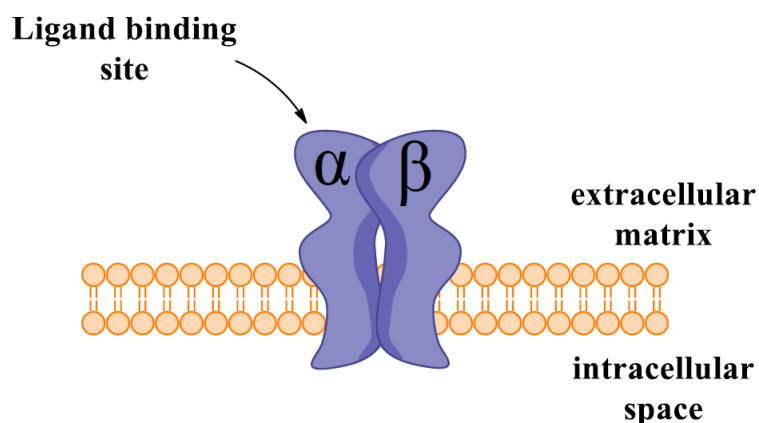


**Figure 1.7** Simple schematic of integrin consisting of  $\alpha$  and  $\beta$  subunits.

There exist 18 $\alpha$  and 8 $\beta$  subunits that are non-covalently bonded to make up 24 different pairs of integrins.  $\alpha$  and  $\beta$  subunits are non-homologous in structure, but similarities within the subunits have been observed. Integrins are composed of three major units: large extracellular domain, single spanning transmembrane domain, and short cytoplasmic domain.

Integrins  $\alpha_v\beta_3$ ,  $\alpha_5\beta_1$  and  $\alpha_v\beta_6$  are present at low concentration in normal tissues, but are overexpressed in tumour tissues. They are known to play an important role in tumour angiogenesis, making them an attractive target for tumour imaging.<sup>34</sup> Some of the ECM proteins that bind to integrins include fibronectin, fibrinogen, vitronectin, collagens, osteopontin, etc. They all share the same cellular recognition site, a tripeptide sequence, Arg-Gly-Asp (RGD).<sup>37</sup> Eight of the 24 different integrins, including  $\alpha_v\beta_3$ , have affinity

towards the tripeptide sequence RGD (Figure 1.8).  $\alpha_v\beta_3$  is a well-studied integrin; many antagonists, such as cilengitide, and imaging probes, have been developed to target the receptor. It is known to be overexpressed at multiple tumour sites, including prostate, breast, ovarian, cervical, pancreatic, melanoma, and glioblastoma tumours.

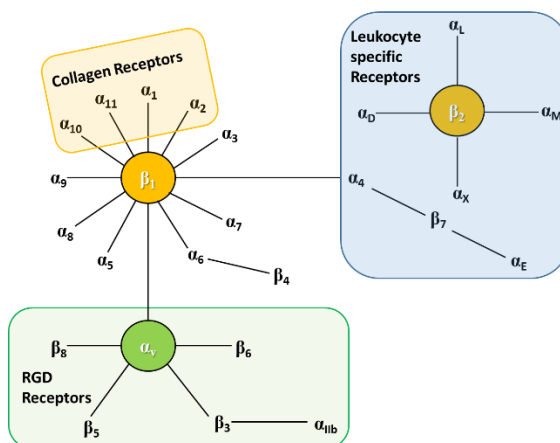


**Figure 1.8** Integrins exhibiting binding towards different membrane proteins.<sup>38</sup>

Xiong et al., published the first crystal structure of Arg-Gly-Asp cyclic ligand bonded to the extracellular domain of the integrin  $\alpha_v\beta_3$  (Figure 1.9).<sup>39</sup> Interesting characteristics about the tri-peptide sequence were observed. The side chains of the amino acids play an important role in the binding of the RGD ligand to the integrin. The side chain of arginine, which contains a guanidinium group, was held together by a bidentate salt bridge formed with Asp<sup>218</sup> and Asp<sup>150</sup>. The arginine interaction occurs at the  $\alpha$  subunit of the extracellular domain. The glycine residue occupies the space between  $\alpha$  and  $\beta$  subunits. It makes numerous important hydrophobic interactions, including hydrophobic interactions with the carbonyl oxygen of Arg<sup>216</sup>, of the  $\alpha$  subunit. The side chain of aspartic acid, a carboxylate group, makes vital interactions with amino acids of the  $\beta$  subunit. One of the oxygen atoms of the carboxylate group forms hydrogen bonds with amides of Tyr<sup>122</sup> and Asn<sup>215</sup>. The other oxygen correlates with Mn<sup>2+</sup> at the metal-ion dependent adhesion site (MIDAS). The side chain of aspartic acid also makes hydrophobic interaction with the beta carbon atom of Asn<sup>215</sup>. Thus, all three amino acids of the tri-peptide are critical for binding with integrin,  $\alpha_v\beta_3$ .

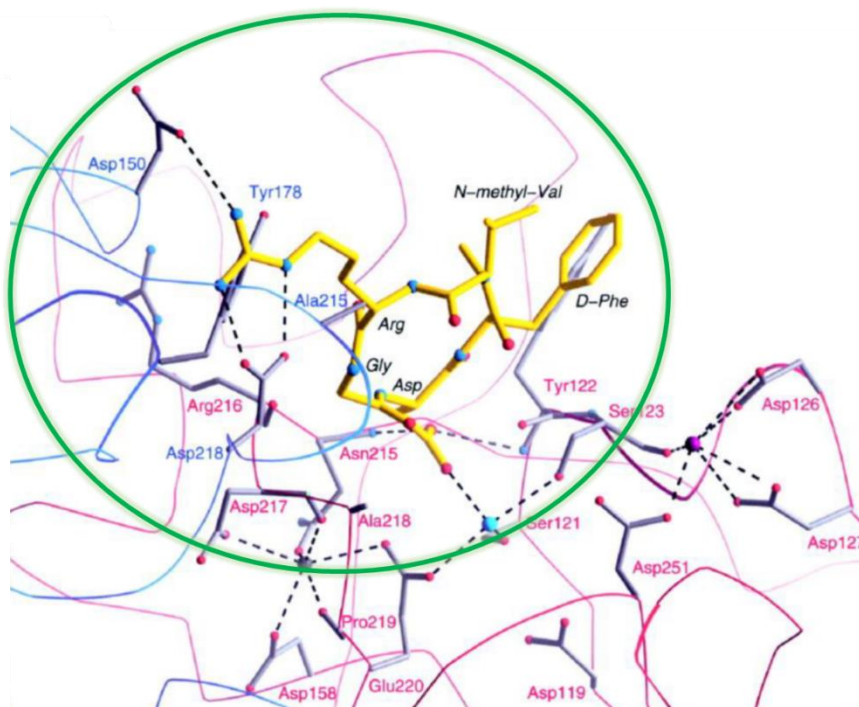


**Figure 1.9** Interactions between cyclic RGD peptide and integrin,  $\alpha_v\beta_3$ . The cyclic peptide (yellow) making important interactions (dashed lines) with the amino acid residues of  $\alpha_v$  (blue) and  $\beta_3$  (red) subunits (image adapted from Xiong et al.<sup>39</sup>)

Several linear and cyclic radiolabeled RGD peptides have been published for both SPECT and PET imaging modalities.<sup>40,41</sup> A  $^{99m}\text{Tc}$  labelled linear peptide  $\alpha\text{P2}$  (RGDSCRGDSY) has been used to image metastatic melanoma in cancer patients.<sup>41,42</sup> However, the lack of specificity, low binding affinity, and rapid degradation makes the linear peptide less suitable for tumor imaging.<sup>41,43</sup> On the other hand, cyclic RGD peptides have shown to enhance binding affinity and improve stability. Examples of cyclic radiotracers for PET imaging include, [ $^{18}\text{F}$ ]Galacto-RGD and [ $^{18}\text{F}$ ]AH111585.<sup>40,44,45,46</sup> Both cyclic RGD peptides are currently being evaluated as non-invasive imaging agents for  $\alpha_v\beta_3$  in cancer patients.<sup>40</sup> The high cost, low tumor uptake, and lack of preparative method for repetitive radio-synthesis, will limit the use of these peptides as imaging entities.<sup>40</sup> A  $^{99m}\text{Tc}$  labelled cyclic peptide,  $^{99m}\text{Tc}$ -NC100692, containing RGD in the backbone, has displayed good binding towards integrin  $\alpha_v\beta_3$ . It has also been used to identify malignant lesions in patients with breast cancer.<sup>40,47</sup> However, the cyclic  $^{99m}\text{Tc}$  labeled peptide ( $^{99m}\text{Tc}$ -NC100692) has high liver uptake, and

is rapidly excreted from the body due to the lipophilic nature of the  $^{99\text{m}}\text{Tc}$  chelator.<sup>40</sup> Hence, there is a continuous need to develop new techniques for the designing radiopharmaceuticals that allows for both quick and efficient ways to introduce radionuclides, as well as to improve *in-vivo* stability and targeting capability.

## 1.11 Thesis Scope

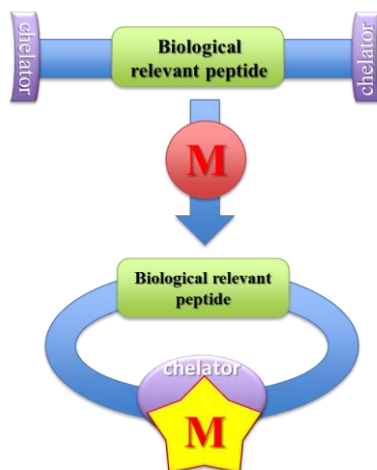


**Figure 1.10** Project design rationale

Prior work has demonstrated that  $^{99\text{m}}\text{Tc}/\text{Re}(\text{CO})_3^+$  is able to establish a turn within a linear peptide sequence. This results in a conformational lock and hydrogen bonding within the peptide backbone. We now propose cyclization of a linear peptide, with a biological relevant sequence, RGD, through  $^{99\text{m}}\text{Tc}/\text{Re}(\text{CO})_3^+$ . To coordinate with  $^{99\text{m}}\text{Tc}/\text{Re}(\text{CO})_3^+$ , use of natural and un-natural amino acids as well as metal chelators were explored. The linear and cyclized peptides were characterized with LC-MS,  $^1\text{H}$ -NMR, and 2D-NMR spectroscopy. The turn was characterized with Circular Dichroism (CD), and Variable Temperature (VT) NMR spectroscopy.

## 1.12 References

1. James, M. L.; Gambhir, S. S., A Molecular Imaging Primer: Modalities, Imaging Agents, and Applications. *Physiol Rev* **2012**, 92 (2), 897-965.

2. Chen, K.; Chen, X. Y., Design and Development of Molecular Imaging Probes. *Curr Top Med Chem* **2010**, *10* (12), 1227-1236.
3. Okarvi, S. M., Peptide-based radiopharmaceuticals: Future tools for diagnostic imaging of cancers and other diseases. *Med Res Rev* **2004**, *24* (3), 357-397.
4. Danthi, S. N.; Pandit, S. D.; Li, K. C. P., A primer on molecular biology for imagers: VII. Molecular imaging probes. *Acad Radiol* **2004**, *11* (9), 1047-1054.
5. Roxin, A.; Zheng, G., Flexible or fixed: a comparative review of linear and cyclic cancer-targeting peptides. *Future Med Chem* **2012**, *4* (12), 1601-1618.
6. (a) Mansi, R.; Tesauro, D.; Pedone, C.; Benedetti, E.; Morelli, G., Peptide based radiopharmaceuticals for imaging of two different receptors. *Journal of Peptide Science* **2006**, *12*, 229-229; (b) Dong, C.; Liu, Z.; Wang, F., Peptide-based Radiopharmaceuticals for Targeted Tumor Therapy. *Curr Med Chem* **2014**, *21* (1), 139-152.
7. Carpino, L. A.; Han, G. Y., 9-Fluorenylmethoxycarbonyl Function, a New Base-Sensitive Amino-Protecting Group. *J Am Chem Soc* **1970**, *92* (19), 5748-&.
8. Pearson, D. A.; Blanchette, M.; Baker, M. L.; Guindon, C. A., Trialkylsilanes as Scavengers for the Trifluoroacetic-Acid Deblocking of Protecting Groups in Peptide-Synthesis. *Tetrahedron Lett* **1989**, *30* (21), 2739-2742.
9. (a) Ovchinnikov, Y. A.; Ivanov, V. T., Conformational States and Biological-Activity of Cyclic Peptides. *Tetrahedron* **1975**, *31* (18), 2177-2209; (b) Blout, E. R., Cyclic-Peptides - Past, Present, and Future. *Biopolymers* **1981**, *20* (9), 1901-1912; (c) Ramakrishnan, C.; Paul, P. K. C.; Ramnarayan, K., Cyclic-Peptides - Small and Big and Their Conformational Aspects. *J Bioscience* **1985**, *8* (1-2), 239-251; (d) Deber, C. M.; Madison, V.; Blout, E. R., Why Cyclic Peptides - Complementary Approaches to Conformations. *Accounts Chem Res* **1976**, *9* (3), 106-113.
10. Kumar, A.; Ye, G. F.; Wang, Y. H.; Lin, X. F.; Sun, G. Q.; Parang, K., Synthesis and structure-activity relationships of linear and conformationally constrained peptide analogues of CIYKYY as src tyrosine kinase inhibitors. *J Med Chem* **2006**, *49* (11), 3395-3401.
11. Eskens, F. A. L. M.; Dumez, H.; Hoekstra, R.; Perschl, A.; Brindley, C.; Bottcher, S.; Wynendaele, W.; Dreys, J.; Verweij, J.; van Oosterom, A. T., Phase I and pharmacokinetic study of continuous twice weekly intravenous administration of

Cilengitide (EMD 121974), a novel inhibitor of the integrins  $\alpha v \beta 3$  and  $\alpha v \beta 5$  in patients with advanced solid tumours. *European Journal of Cancer* **2003**, *39* (7), 917-926.

12. Mas-Moruno, C.; Rechenmacher, F.; Kessler, H., Cilengitide: The First Anti-Angiogenic Small Molecule Drug Candidate. Design, Synthesis and Clinical Evaluation. *Anti-Cancer Agent Me* **2010**, *10* (10), 753-768.

13. Patel, Y. C.; Murthy, K. K.; Escher, E. E.; Banville, D.; Spiess, J.; Srikant, C. B., Mechanism of Action of Somatostatin - an Overview of Receptor Function and Studies of the Molecular Characterization and Purification of Somatostatin Receptor Proteins. *Metabolism* **1990**, *39* (9), 63-69.

14. Pakkala, M.; Hekim, C.; Soininen, P.; Leinonen, J.; Koistinen, H.; Weisell, J.; Stenman, U. H.; Vepsäläinen, J.; Narvanen, A., Activity and stability of human kalikrein-2-specific linear and cyclic peptide inhibitors. *Journal of Peptide Science* **2007**, *13* (5), 348-353.

15. (a) Ruan, F. Q.; Chen, Y. Q.; Hopkins, P. B., Metal-Ion Enhanced Helicity in Synthetic Peptides Containing Unnatural, Metal-Ligating Residues. *J Am Chem Soc* **1990**, *112* (25), 9403-9404; (b) Torrado, A.; Imperiali, B., New synthetic amino acids for the design and synthesis of peptide-based metal ion sensors. *J Org Chem* **1996**, *61* (25), 8940-8948.

16. Kelso, M. J.; Hoang, H. N.; Appleton, T. G.; Fairlie, D. P., The first solution structure of a single  $\alpha$ -helical turn. A pentapeptide  $\alpha$ -helix stabilized by a metal clip. *J Am Chem Soc* **2000**, *122* (42), 10488-10489.

17. Gunasekaran, K.; Gomathi, L.; Ramakrishnan, C.; Chandrasekhar, J.; Balaram, P., Conformational interconversions in peptide  $\beta$ -turns: Analysis of turns in proteins and computational estimates of barriers. *J Mol Biol* **1998**, *284* (5), 1505-1516.

18. Kabsch, W.; Sander, C., Dictionary of Protein Secondary Structure - Pattern-Recognition of Hydrogen-Bonded and Geometrical Features. *Biopolymers* **1983**, *22* (12), 2577-2637.

19. Hoang, H. N.; Bryant, G. K.; Kelso, M. J.; Beyer, R. L.; Appleton, T. G.; Fairlie, D. P., Linkage Isomerism in the Binding of Pentapeptide Ac-His(Ala)(3)His-NH<sub>2</sub> to

- (Ethylenediamine)Palladium(II): Effect of the Binding Mode on Peptide Conformation. *Inorganic chemistry* **2008**, 47 (20), 9439-9449.
20. Wishart, D. S.; Sykes, B. D.; Richards, F. M., The Chemical-Shift Index - a Fast and Simple Method for the Assignment of Protein Secondary Structure through Nmr-Spectroscopy. *Biochemistry-Us* **1992**, 31 (6), 1647-1651.
  21. Albrecht, M.; Stortz, P.; Weis, P., Mimicking the biologically active part of the cyclopeptides segetalin A and B by "clipping" of a linear tripeptide derivative by metal coordination. *Supramol Chem* **2003**, 15 (7-8), 477-483.
  22. (a) Morita, H.; Yun, Y. S.; Takeya, K.; Itokawa, H.; Shiro, M., Conformational-Analysis of a Cyclic Hexapeptide, Segetalin-a from Vaccaria-Segetalis. *Tetrahedron* **1995**, 51 (21), 5987-6002; (b) Morita, H.; Yun, Y. S.; Takeya, K.; Itokawa, H.; Yamada, K., Segetalin-B, Segetalin-C and Segetalin-D, 3 New Cyclic-Peptides from Vaccaria-Segetalis. *Tetrahedron* **1995**, 51 (21), 6003-6014.
  23. Saha, G. B., *Fundamentals of nuclear pharmacy*. 6th ed.; Springer: New York, 2010; p xviii, 409 p.
  24. *Technetium-99m Radiopharmaceuticals: Status and Trends*. International Atomic Energy Agency: 2009.
  25. Atkins, P. W.; Shriver, D. F., *Inorganic chemistry*. 4th ed.; W.H. Freeman: New York, 2006; p xxi, 822 p.
  26. Alberto, R.; Schibli, R.; Egli, A.; Schubiger, A. P.; Abram, U.; Kaden, T. A., A novel organometallic aqua complex of technetium for the labeling of biomolecules: Synthesis of [Tc-99m(OH<sub>2</sub>)(3)(CO)(3)](+) from [(TcO<sub>4</sub>)-Tc-99m](-) in aqueous solution and its reaction with a bifunctional ligand. *J Am Chem Soc* **1998**, 120 (31), 7987-7988.
  27. Liu, G. Z.; Dou, S. P.; He, J.; Vanderheyden, J. L.; Rusckowski, M.; Hnatowich, D. J., Preparation and properties of Tc-99m(CO)(3)(+)-labeled N,N-bis(2-pyridylmethyl)-4-aminobutyric acid. *Bioconjugate Chem* **2004**, 15 (6), 1441-1446.
  28. Malone, L. J.; Manley, M. R., Hydrolysis of Carbon Monoxide Borane. *Inorganic chemistry* **1967**, 6 (12), 2260-&.
  29. Malone, L. J.; Parry, R. W., Preparation and Properties of Boranocarbonates. *Inorganic chemistry* **1967**, 6 (4), 817-&.

30. Alberto, R.; Ortner, K.; Wheatley, N.; Schibli, R.; Schubiger, A. P., Synthesis and properties of boranocarbonate: A convenient in situ CO source for the aqueous preparation of [(TC)-T-99m(OH<sub>2</sub>)(3)(CO)(3)](+). *J Am Chem Soc* **2001**, *123* (13), 3135-3136.
31. Pitchumony, T. S.; Banevicius, L.; Janzen, N.; Zubieta, J.; Valliant, J. F., Isostructural Nuclear and Luminescent Probes Derived From Stabilized [2+1] Rhenium(I)/Technetium(I) Organometallic Complexes. *Inorganic chemistry* **2013**, *52* (23), 13521-13528.
32. Banerjee, S. R.; Babich, J. W.; Zubieta, J., Site directed maleimide bifunctional chelators for the M(CO)(3)(+) core (M=Tc-99m, Re). *Chem Commun* **2005**, (13), 1784-1786.
33. Simpson, E. The Development of Metal-Organic Compounds for Use as Molecular Imaging Agents. University of Western Ontario, 2014.
34. Desgrosellier, J. S.; Cheresch, D. A., Integrins in cancer: biological implications and therapeutic opportunities. *Nat Rev Cancer* **2010**, *10* (1), 9-22.
35. Hynes, R. O., A reevaluation of integrins as regulators of angiogenesis. *Nat Med* **2002**, *8* (9), 918-921.
36. Brooks, P. C.; Montgomery, A. M. P.; Rosenfeld, M.; Reisfeld, R. A.; Hu, T. H.; Klier, G.; Cheresch, D. A., Integrin Alpha(V)Beta(3) Antagonists Promote Tumor-Regression by Inducing Apoptosis of Angiogenic Blood-Vessels. *Cell* **1994**, *79* (7), 1157-1164.
37. Ruoslahti, E.; Pierschbacher, M. D., New Perspectives in Cell-Adhesion - Rgd and Integrins. *Science* **1987**, *238* (4826), 491-497.
38. Hynes, R. O., Integrins: Bidirectional, allosteric signaling machines. *Cell* **2002**, *110* (6), 673-687.
39. Xiong, J. P.; Stehle, T.; Zhang, R. G.; Joachimiak, A.; Frech, M.; Goodman, S. L.; Arnaout, M. A., Crystal structure of the extracellular segment of integrin alpha V beta 3 in complex with an Arg-Gly-Asp ligand. *Science* **2002**, *296* (5565), 151-155.
40. Zhou, Y.; Chakraborty, S.; Liu, S., Radiolabeled Cyclic RGD Peptides as Radiotracers for Imaging Tumors and Thrombosis by SPECT. *Theranostics* **2011**, *1*, 58-82.

41. Liu, S., Radiolabeled multimeric cyclic RGD peptides as integrin  $\alpha(v)\beta(3)$  targeted radiotracers for tumor imaging. *Mol Pharmaceut* **2006**, 3 (5), 472-487.
42. Sivolapenko, G. B.; Skarlos, D.; Pectasides, D.; Stathopoulou, E.; Milonakis, A.; Sirmalis, G.; Stuttle, A.; Courtenay-Luck, N. S.; Konstantinides, K.; Epenetos, A. A., Imaging of metastatic melanoma utilising a technetium-99m labelled RGD-containing synthetic peptide. *Eur J Nucl Med* **1998**, 25 (10), 1383-1389.
43. Liu, S.; Edwards, D. S., Fundamentals of receptor-based diagnostic metalloradiopharmaceuticals. *Top Curr Chem* **2002**, 222, 259-278.
44. Morrison, M. S.; Ricketts, S. A.; Barnett, J.; Cuthbertson, A.; Tessier, J.; Wedge, S. R., Use of a Novel Arg-Gly-Asp Radioligand,  $(18)\text{F}$ -AH111585, to Determine Changes in Tumor Vascularity After Antitumor Therapy. *J Nucl Med* **2009**, 50 (1), 116-122.
45. Kenny, L. M.; Coombes, R. C.; Oulie, I.; Contractor, K. B.; Miller, M.; Spinks, T. J.; McParland, B.; Cohen, P. S.; Hui, A. M.; Palmieri, C.; Osman, S.; Glaser, M.; Turton, D.; At-Nahhas, A.; Aboagye, E. O., Phase I trial of the positron-emitting Arg-Gly-Asp (RGD) peptide radioligand F-18-AH111585 in breast cancer patients. *J Nucl Med* **2008**, 49 (6), 879-886.
46. Beer, A. J.; Haubner, R.; Goebel, M.; Luderschmidt, S.; Spilker, M. E.; Wester, H. J.; Weber, W. A.; Schwaiger, M., Biodistribution and pharmacokinetics of the  $\alpha(v)\beta(3)$ -Selective tracer F-18-Galacto-RGD in cancer patients. *J Nucl Med* **2005**, 46 (8), 1333-1341.
47. Bach-Gansmo, T.; Danielsson, R.; Saracco, A.; Wilczek, B.; Bogsrud, T. V.; Fangberget, A.; Tangerud, A.; Tobin, D., Integrin receptor imaging of breast cancer: A proof-of-concept study to evaluate Tc-99m-NC100692. *J Nucl Med* **2006**, 47 (9), 1434-1439.

## Chapter 2

# 2 Employing Amino Acids to Cyclize Pentapeptides Through “2+1” Chelation System Using $^{99m}\text{Tc}/\text{Re}(\text{CO})_3^+$

## 2.1 Introduction

Structural constraints play an important role when designing peptides that mimic native proteins as discussed in section 1.4. Short linear peptides, less than twelve amino acids, display poor *in-vivo* stability as they are rapidly broken down through enzymatic degradation.<sup>1</sup> Linear peptides adapt numerous molecular conformations in solution and these conformations compete to bind to a biological target, reducing the specific binding of the original peptide.<sup>2</sup> Structural constraints introduced through cyclization results in limited molecular conformations, with fewer competing for the targeted receptor, resulting in enhanced specific binding.<sup>2</sup>

Structural constraints can be introduced by different bonds types, including cyclization through metal coordination. Short linear peptides, less than twelve amino acids, do not have enough flexibility and energy to induce a secondary structure within a peptide backbone. However, a metal clip can stabilize a turn upon metal coordination.<sup>1</sup> Palladium, iridium, rhenium, and technetium have established and stabilized a turn within the peptide backbone.<sup>3,4,5</sup> Histidine residues have shown to coordinate with different metal centers in native metallo-proteins, such as copper in hemocyanin,<sup>6</sup> zinc in thermolysin,<sup>7</sup> and iron in hemoglobin.<sup>8</sup> This is normally demonstrated by coordination of nitrogen atoms on the imidazole ring with the metal center. Metal chelating di-histidine residues are known to be present within protein secondary structure, affecting the overall structure of the protein, such as His-X-His in a  $\beta$ strand, His-X<sub>2</sub>-His in a reverse  $\beta$  turn, and His-X<sub>3</sub>-His in a  $\alpha$ -helix.<sup>9,10</sup> Studies have shown that incorporating metal chelating di-histidine residues enhances binding affinity, and also improves stabilization of the protein. Kellis et al., incorporated di-histidine residues, His-X<sub>3</sub>-His, into the N-terminal  $\alpha$  helix of yeast cytochrome *c*, at the 4 and 8 position.<sup>10c</sup> Upon coordinating with Cu (II)

iminodiacetate complex, the coordinated protein exhibited 24 times higher affinity than the protein without the di-histidine residues. This study showed that incorporating a suitable clip for a metal, such as histidine residues, not only improved stability of the protein, but also enhanced its binding affinity.

Targeted technetium radiopharmaceuticals generally consist of a biological peptide sequence for the target receptor, a pharmacokinetic modifier linker, and a bi-functional chelator for the attachment of the metal. Technetium-99m can be introduced, either through a pendant or an integrated design. The pendant design is a classical approach where a bi-functional chelator is attached to the peptide, through a side chain of an amino acid or the end terminus of the peptide, Figure 2.1a. An advantage of using this design is that it does not interfere with the targeting entity; however, because the bi-functional chelator is covalently attached to the peptide, the metal complex is placed at a position that can be easily cleaved through hydrolysis.<sup>11</sup> Also, due to the bulkiness of the chelator, it could perhaps influence the conformation of the peptide and result in decreased binding affinity to the receptor. Therefore, structural modifications of the metal complex must be further explored to improve the binding affinity of the peptide. Numerous examples have been provided for

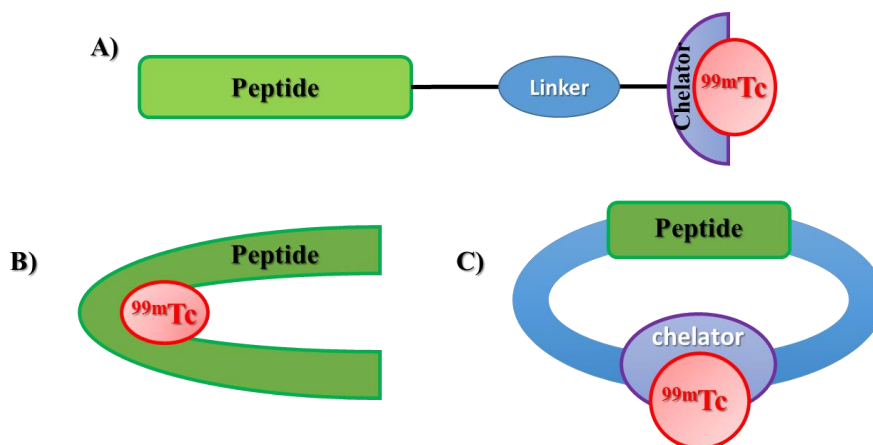


**Figure 2.1** Schematic of pendant and integrated technetium-99m radiopharmaceutical designs

An integrated design introduces the metal complex directly into the peptide backbone, making the labelling component an integral part of the biologically active region. This

approach ‘hides’ the metal complex within the peptide framework resulting in a more stable, compact, and low molecular weight chelation system. Integration can be a result of peptide cyclization or turn mimics, where the metal chelator is introduced into the turn region of the peptide sequence (Figure 2.1b), or a chelator is formed when the peptide is cyclized through metal coordination (Figure 2.1c). This approach eliminates the use of an external bulky chelator resulting in low molecular weight radiopharmaceuticals.<sup>12</sup>

One of the more widely used technetium-99m core has been  $^{99m}\text{Tc}(\text{CO})_3^+$ . The  $^{99m}\text{Tc}/\text{Re}(\text{CO})_3^+$  core has been shown to stabilize through a “2+1” chelation system.<sup>13</sup> A “2+1” chelation system is comprised of bi-dentate and mono-dentate ligands. There are two ways to introduce “2+1” chelation system, through a pendant design or an integrated design. Figure 2.2 represents a simplistic model of “2+1” chelation systems. Figure 2.2a represents a pendant design, where a bi-dentate chelator is attached to the peptide through a spacer; on the other hand, Figure 2.2b is an integrated design, where the metal complex is incorporated into the peptide framework.

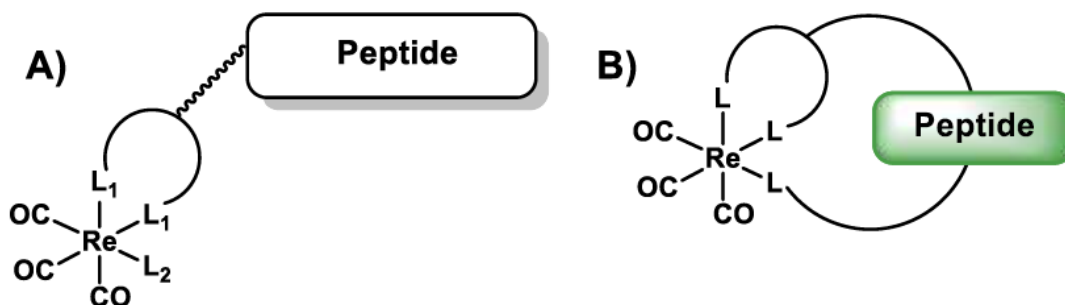


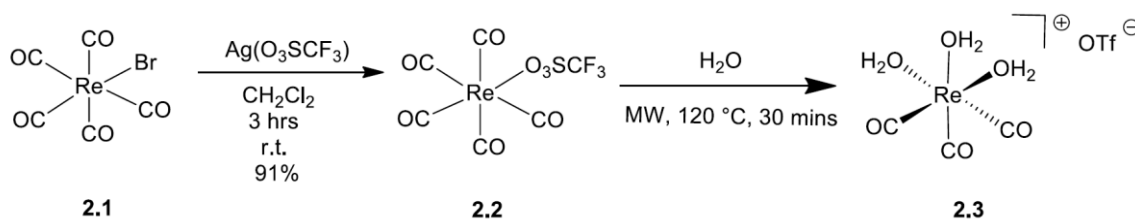
**Figure 2.2** Model “2+1” chelation system

Simpson reported cyclization of the pentapeptide, Ac-HAAAH-OH, through  $^{99m}\text{Tc}/\text{Re}(\text{CO})_3^+$ , with a mono-dentate coordination through imidazole nitrogen at the N-terminus, and a bi-dentate chelation through a carboxyl oxygen and imidazole nitrogen at the C-terminus.<sup>5</sup> We can now replace the tri-alanine sequence with a biological relevant peptide, RGD, to target receptor, integrin  $\alpha_v\beta_3$ , for imaging and therapeutic purposes. Here, efforts to cyclize RGD peptide in a “2+1” chelation fashion, with natural and unnatural amino acids, was attempted.

## 2.2 Results and Discussion

### 2.2.1 Synthesis of $[\text{Re}(\text{CO})_3(\text{OH}_2)_3]\text{OTf}^{14}$

The  $^{99\text{m}}\text{Tc}/\text{Re}(\text{CO})_3^+$  species is one of the widely used metal cores for radiochemistry, with the aqua ligands as a convenient starting point. The aqua ligands are very labile due to the *trans* effect presented by the carbonyls. The aqua ligands can be easily displaced with the incoming ligands. Commercially available bromopentacarbonyl rhenium, **2.1**, was reacted with silver triflate,  $[\text{Ag}(\text{O}_3\text{SCF}_3)]$ , in freshly distilled dichloromethane (DCM), under subdued light for three hours at room temperature. The reaction mixture was gravity filtered to remove by-product salts, silver bromide (AgBr). The product was precipitated with addition of hexanes, and slow evaporation resulted in pentacarbonyltriflate rhenium (I), **2.2**. Compound **2.2** was reacted with water under microwave conditions to result tris-aqua tris-carbonyl rhenium (I) species, as a 0.1 M solution, **2.3**.



**Scheme 2.1** Synthetic route for  $[\text{Re}(\text{OH}_2)_3(\text{CO})_3]\text{OTf}^{14}$ , as 0.1 M solution

### 2.2.2 Synthesis of Ac-HRGDH-OH

The peptide was constructed from C→N terminus on a solid phase support, with the C-terminus attached to an insoluble resin. The synthesis of the linear peptide employed 9-fluorenylmethyloxycarbonyl (Fmoc) chemistry. The N-terminus of each amino acid was already protected with the Fmoc group, and the side chain of amino acid residues were protected with acid labile groups. After the removal of the Fmoc group, an amino acid with a base and coupling reagent in *N,N*-dimethylformamide (DMF) were added. The amino acid couplings were repeated until the desired peptide was constructed. The Fmoc group on the last amino acid, at the N-terminus, was removed and acetylated with acetic

anhydride in DMF. The removal of protecting groups, and the cleavage of the peptide off the resin was performed by vortexing the resin in a cleavage cocktail. The linear peptide was precipitated with excess *tert*-butyl methyl ether (TBME) and centrifuged. The centrifuged precipitates were dissolved in water and frozen over dry ice. The frozen peptide was lyophilized to remove solvents. The peptide was purified with reverse-phase preparative HPLC-MS (RP HPLC-MS), with a purity of >95%.

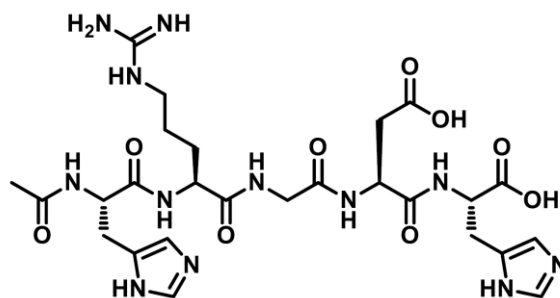


**Figure 2.3** Linear Ac-HRGDH-OH, **2.4**, peptide

Ac-HRGHD-OH	Calculated ( $m/z$ )	Observed ( $m/z$ )
$[M+H]^+$	663.66	663.34
$[M+2H]^{2+}$	332.33	332.25

**Table 2.1** Calculated and observed  $m/z$  ratio of Ac-HRGDH-OH, **2.4**, analyzed by ESI-LC-MS.

## 2.2.3 Characterization of Ac-HRGD<sup>H</sup>-OH

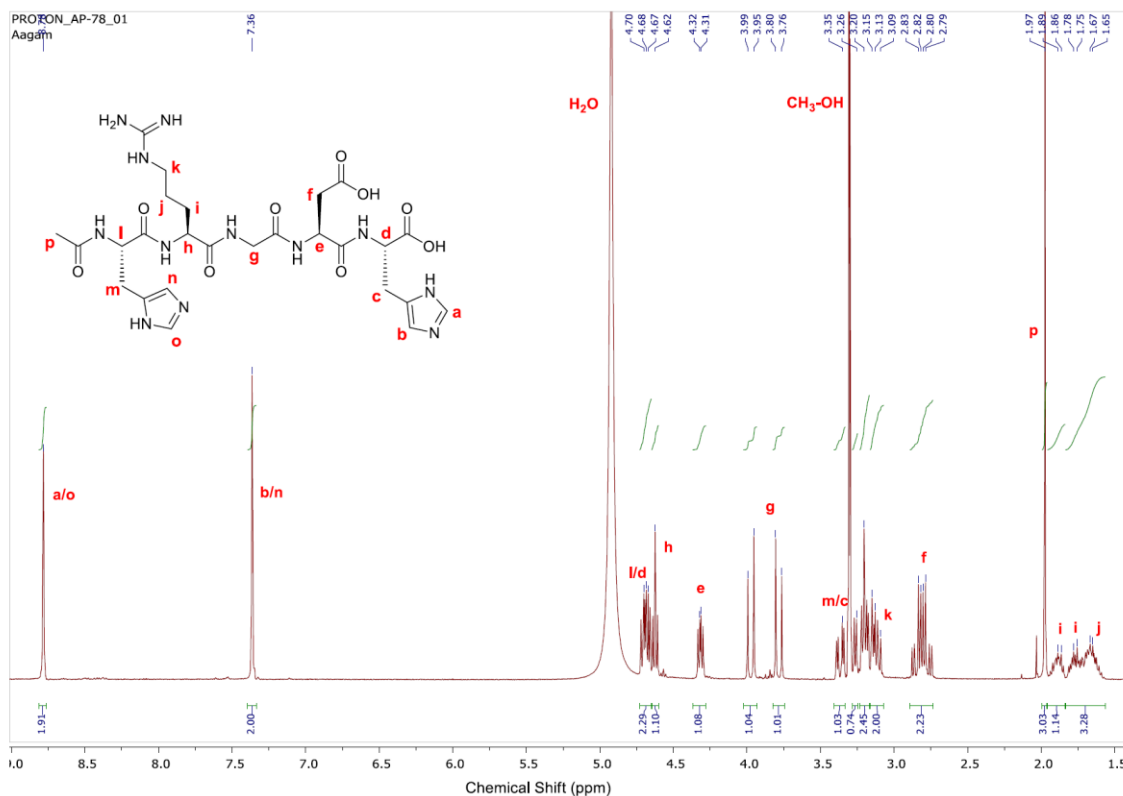


**Figure 2.4** <sup>1</sup>H-NMR spectrum of Ac-HRGD<sup>H</sup>-OH, 2.4, in CD<sub>3</sub>OD.

The acetylated RGD peptide was characterized with HPLC-MS and <sup>1</sup>H-NMR spectroscopy. Table 2.1 reports the calculated and observed  $m/z$  ratio of the peptide, and Figure 2.4 displays the <sup>1</sup>H-NMR spectrum in CD<sub>3</sub>-OD. After analyzing the spectra, interesting observations were made, with glycine appearing as a prochiral molecule and the splitting of hydrogens were observed with a pair of doublets near 3.88 ppm. The same prochirality was observed with other methylene groups, adjacent to CH $\alpha$  atoms, of other amino acids. The methylene group of aspartic acid was observed to follow an ABM spin system, where the methylene hydrogens (H<sub>f</sub>) were coupled with each other and at the same time were coupled with CH $\alpha$  (H<sub>e</sub>). The arginine methylene groups were present around 1.5–2.0 ppm, and coupling was hard to observe. The CH $\alpha$  atoms were spread from 3.75–4.75 ppm. The CH hydrogen atoms of the imidazole rings were overlapped due to their similar chemical environment. The H<sub>a/o</sub> was observed to have a more

downfield chemical shift when compared with  $H_{b/n}$ , due to the electron withdrawing nitrogen atoms present on both side of the proton.

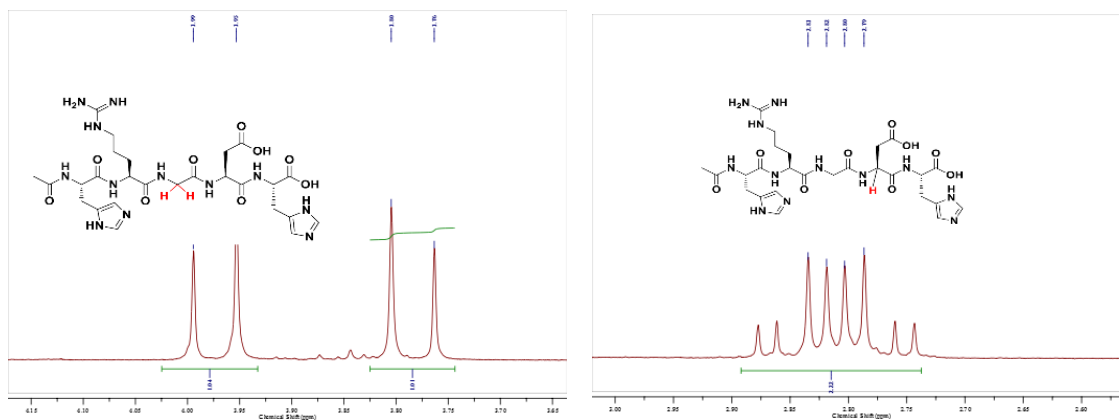
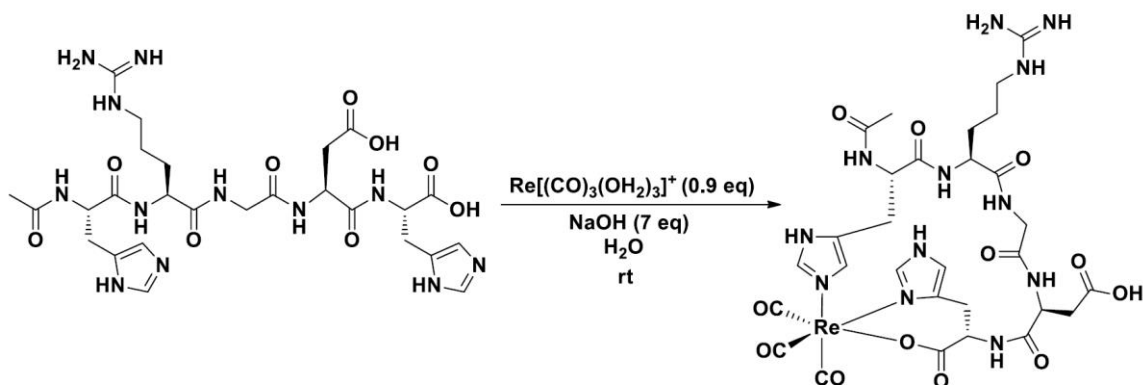


**Figure 2.5**  $^1\text{H}$ -NMR splits of Glycine and Aspartic acid in  $\text{CD}_3\text{OD}$ .

#### 2.2.4 “2+1” Coordination Using Natural Amino Acids as Metal Chelators

Following the coordination procedure reported by Simpson<sup>5</sup>,  $\text{Ac-H}_1\text{RGDH}_5\text{-OH}$  was reacted with  $[\text{Re}(\text{CO})_3(\text{OH}_2)_3]^+$ . The peptide was dissolved in water,  $[\text{Re}(\text{CO})_3(\text{OH}_2)_3]^+$  and concentrated base, 5M NaOH, were added to the solution. Upon completion of the reaction, the solution was lyophilized to remove the solvent. LC-MS showed the uncoordinated peptide left at the end of the reaction. There were numerous peaks at different retention times that corresponded to the same  $m/z$  ratio of the peptide coordinated with  $\text{Re}(\text{CO})_3^+$ , which suggested that there might be linkage isomers present. No dominant coordinated isomeric peak was observed. The reaction was optimized to obtain a single dominant isomeric peptide. A generic scheme used for the coordination is displayed in Scheme 2.2, and Table 2.2 reports various conditions used to optimize the reaction. The peaks were compared based on the area under the curve, from the LC-MS chromatogram.



**Scheme 2.2** Synthetic approach for Ac-HRGDH-OH, **2.4**, coordination with  $[\text{Re}(\text{CO})_3(\text{OH}_2)_3]^+$ , and proposed coordination product.

#	0.1 M $[\text{Re}(\text{CO})_3(\text{OH}_2)_3]^+$ (molar Eq.)	5M NaOH (molar Eq.)	Temp (°C)	Time (hours)	% coordinated vs uncoordinated peptide
01	1.25	1.8	110 (microwave)	0.6	NR
02	1.20	1.0	rt	48	NR
03	1.20	1.0	rt	5	96
04	1.75	1.0	rt	2	56
05	1.75	0.6	rt	3	18
06	1.75	-	50	3.5	NR
07	1.65	1.0	rt	1	NR
<b>08</b>	<b>0.90</b>	<b>7</b>	<b>rt</b>	<b>3</b>	<b>97</b>

**Table 2.2** Reaction conditions used to coordinate Ac-HRGDH-OH, **2.4**, with  $[\text{Re}(\text{CO})_3(\text{OH}_2)_3]^+$ .

Analysis of the data suggested that increasing the molar equivalent of the  $\text{Re}(\text{CO})_3^+$  species led to a lower percentage of the coordinated peptide; this could be due to side reactions taking place when excess  $\text{Re}(\text{CO})_3^+$  was used. Unfortunately, the masses corresponding to the undesired side products were not observed from LC-MS analysis. It was also noted that the concentration of the base plays an important role in peptide coordination. The reaction proceeded to completion at a higher pH (~9-10); this could be due to high pH allowing for full deprotonation of the carboxyl group at the C-terminus

and aspartic acid. Compound 8, showed near complete conversion of the linear peptide to the coordinated peptide, with the peptide coordinated in the tridentate fashion.

After optimizing the reaction, a reproducible method was obtained that produced a dominant isomer. A sub-stoichiometric  $[\text{Re}(\text{CO})_3(\text{OH}_2)_3]^+$  and a basic pH solution, led to a higher percentage of the coordinate peptide, and a single dominant isomer (major peak of the spectrum) was observed. The coordinated peptide was purified by RP HPLC-MS, but unfortunately the major peak was not isolated as it was present in close proximity with other isomeric peaks. An appropriate preparative gradient was not found that was capable of separating the peaks.

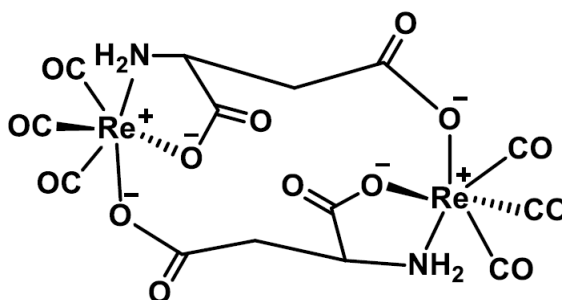


**Figure 2.6** Coordination of di-aspartic acid to  $\text{Re}(\text{CO})_3^+$ <sup>15</sup>

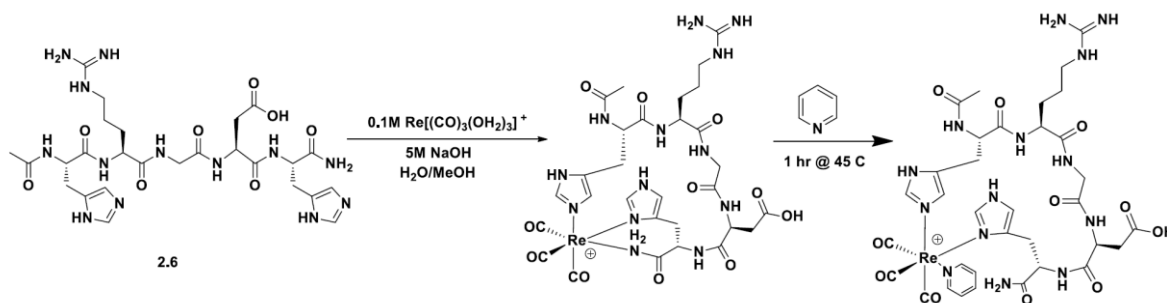
The side chain functional groups of arginine (guanidine) and aspartic acid (carboxylate, Figure 2.6) have potential to be involved in coordination with the Tc/Re (I).<sup>15</sup> Protecting the side chain functional groups of amino acids could perhaps have led to a lower number of coordination sites and linkage isomers. The protected peptide (Ac-His(trt)-Arg(pbf)-Gly-Asp(OtBu)-His(trt)-OH, **2.5**) was synthesized on a 2-chlorotrityl resin and cleaved off the resin with acetic acid, trifluoroethanol and DCM. This resulted in a linear peptide with all the protecting groups present on the amino acid side chains. The peptide was purified with preparative RP HPLC-MS, with a purity of >95%. Coordination to  $[\text{Re}(\text{CO})_3(\text{OH}_2)_3]^+$  was demonstrated by dissolving the peptide in methanol, adding  $[\text{Re}(\text{CO})_3(\text{OH}_2)_3]^+$  and 5M NaOH to the solution. The reaction was stirred at 50 °C for 3 hours. Upon completion of the reaction, the solvent was removed under reduced pressure. The LC-MS spectra showed traces of the peptide coordinated to  $\text{Re}(\text{CO})_3^+$ , but the

quantity was very low and did not permit further analysis. The peptide might have been too bulky and sterically hindered to coordinate with  $\text{Re}(\text{CO})_3^+$ .

### 2.2.5 “2+1” Mixed Coordination with an External Mono-Dentate Chelator

From literature, the heterocycles imidazole and pyridine are known ligands that bind to different metals, including  $^{99\text{m}}\text{Tc}/\text{Re}$ .<sup>16</sup> Using peptides to result in a “2+1” chelation system gave numerous isomers, therefore, attempts to use a mixed chelation system was proposed. The concept was to employ the imidazole rings on the terminal histidine residues to act as mono-dentate ligands, replacing two of three aqua ligands. This results in the peptide acting as a bidentate chelator in whole, creating a turn within the peptide backbone. Replacement of the remaining aqua molecule was explored with different metal ligands. This still follows the integrated design. The “2+1” mixed chelation system was recently proposed by Pitchumony et al.<sup>13</sup> and Connell et al.<sup>17</sup>

To reduce the number of coordination sites on the peptide, the free carboxyl group at the C-terminus was replaced with a terminal amide. The linear peptide, Ac-HRGD $\text{H}$ -NH $_2$  (**2.6**), was first reacted with  $[\text{Re}(\text{CO})_3(\text{OH}_2)_3]\text{OTf}$ , and after the first step was completed, pyridine was added and the reaction mixture was heated. The reaction was monitored with LC-MS. Table 2.3 reports the reaction with different molar equivalent of pyridine.



**Scheme 2.3** Synthetic approach towards mixed “2+1”  $\text{Re}(\text{CO})_3^+$  complexes, and a proposed coordination product.

#	Pyridine (molar Eq.)	% of “2+1” mixed coordination system
1	1.3	90.5
2	10	90.9
3	100	99.5
4	1000	99.8
5	1300	No evidence of the peptide acting as a tridentate chelator

**Table 2.3** Increasing molar equivalent of pyridine led to higher % of  $[\text{Re}(\text{CO})_3(\text{Ac-HRGDH-NH}_2)(\text{py})]^+$ .

Analysis of the reaction prior to the addition of the pyridine suggested that the peptide was coordinated to Re (I) core in a tridentate fashion. The specific connectivity of the peptide with the Re (I) metal center is uncertain; this could be due to functional groups of amino acids, such as aspartic acid or arginine coordinating to  $\text{Re}(\text{CO})_3^+$ . When the second step of the reaction proceeded using a low molar equivalent of pyridine, the majority of the product was still the peptide coordinated to the Re (I) center in a tridentate fashion. Attempting the reaction with excess pyridine led to a mixed “2+1” coordination of the peptide with the pyridine attached to the Re (I) center. The resulting complex was positively charged. Two isomeric peaks were observed by analytical HPLC-MS, which can be separated with preparative RP HPLC-MS. However, the “2+1” mixed coordination system resulted in very poor yields. Upon addition of an external ligand, the pyridine displaced previously formed coordination bonds. This resulted in three pyridine molecules attached to the Re (I) center to form  $[\text{Re}(\text{CO})_3(\text{py})_3]^+$ , with each pyridine acting as a mono-dentate ligand. Other metal coordinating ligands, such as N-methylimidazole, imidazole and methylbenzylimidazole were also explored; however, none of them displayed good yields. The “2+1” mixed coordination system was abandoned due to poor yields.

## 2.2.6 “2+1” Coordination with Un-natural Amino Acids as Metal Chelators

Using histidine as a metal chelator resulted in numerous coordinated isomers. This could have been due to histidine residues having multiple coordinating sites. Histidine, when

employed as a bi-dentate chelator, was placed at the C-terminal and N-terminal of the peptide. Histidine, when coordinated, formed a 7 or 8 membered ring, when used as a bi-dentate chelator at the C-terminus; and 6 or 7 membered ring when placed at the N-terminus. The five membered chelate rings are generally very stable, as they don't present extra ring strain.<sup>18</sup> The larger chelate rings, such as seven membered ring, are generally less stable due to the distortions of the bond angles and unfavorable steric interactions.<sup>18</sup> A better chelator with less coordinating sites, and forming favorable sizes, was explored.

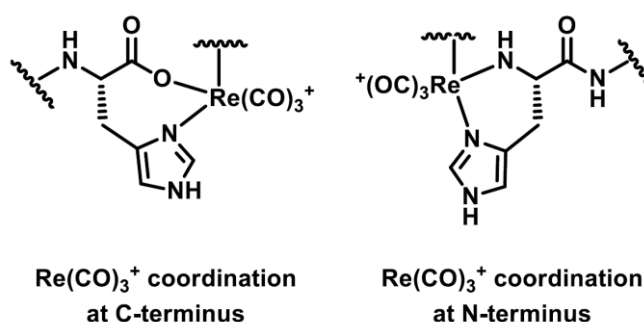


**Figure 2.7** Bi-dentate coordination at the C-terminal or N-terminal when using histidine residue as a metal chelator

Pyridine and pyridine analogues are metal ligands that can coordinate with various metal centers in a mono-dentate fashion. Un-natural amino acids (Figure 2.8) containing pyridine as their side chain, such as 3-pyridylalanine, 2-pyridylalanine, and 4-pyridylalanine, were explored. 2-pyridylalanine (2-Pal) and 3-pyridylalanine (3-Pal) forms 6 and 7 membered rings, respectively, when used as bi-dentate chelators at the N-terminus. 2-/3-Pal amino acid residues were incorporated at the N-terminus of a peptide, while 3-/4-Pal amino acid residues were incorporated at the C-terminus as a mono-dentate ligand. Different combinations of pyridylalanine amino acid residues were used at the two end terminals, to derive a variety of linear peptide sequences with RGD in the backbone, for example 2-Pal-RGD-4-Pal-NH<sub>2</sub>. Each linear peptide was manually synthesized with Fmoc chemistry, and characterized with LC-MS. Each peptide was purified with RP HPLC-MS, with a purity > 95%.

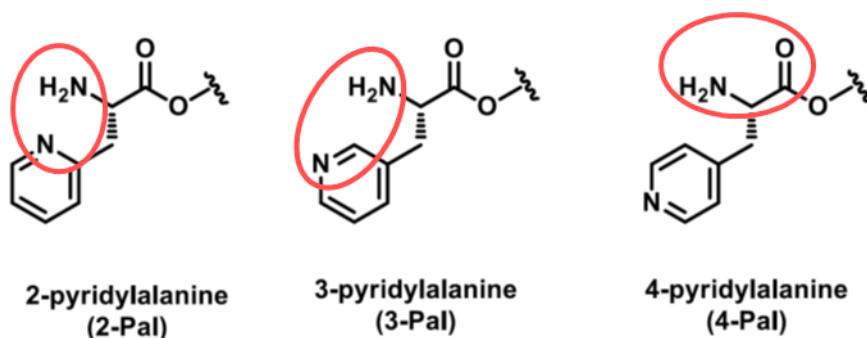


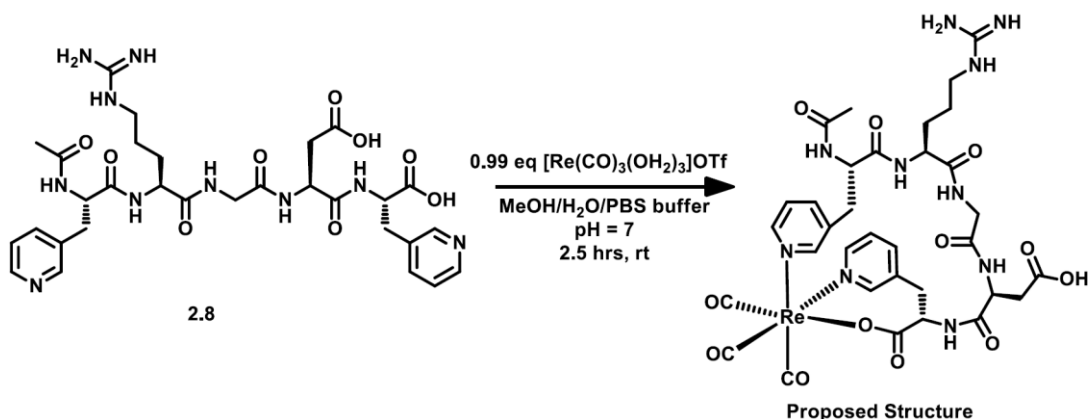
**Figure 2.8** Bidentate coordination at the N-terminus of pentapeptides using un-natural amino acids as metal chelators

Compound	Peptide sequence	Calculated [M+H] <sup>+</sup>	Observed [M+H] <sup>+</sup>
<b>2.7</b>	Ac-3-Pal-RGD-3-Pal-OH	685.71	685.29
<b>2.8</b>	Ac-3-Pal-RGD-3-Pal-NH <sub>2</sub>	684.73	684.25
<b>2.9</b>	H-3-Pal-RGD-3-Pal-OH	685.71	686.22
<b>2.10</b>	H-2-Pal-RGD-4-Pal-NH <sub>2</sub>	642.69	643.11
<b>2.11</b>	H-2-Pal-RGD-3-Pal-NH <sub>2</sub>	642.69	643.16

**Table 2.4** Synthesized peptide sequences for coordination with Re(CO)<sub>3</sub><sup>+</sup>, employing pyridylalanine amino acid residues at end termini.

The linear peptides were reacted with Re(CO)<sub>3</sub><sup>+</sup> under various conditions, such as acidic pH, basic pH, neutral pH, microwave heating, and traditional heating. LC-MS analysis displayed multiple isomers forming when the peptide was coordinated with Re(CO)<sub>3</sub><sup>+</sup>. Table 2.4 reports linear peptides that were synthesized and reacted with Re(CO)<sub>3</sub><sup>+</sup>. Fewer isomers were observed compared to when histidine residues were used as metal chelators. However, dominant isomers were present in close proximity with other isomers, and isolating a single isomer presented a challenge. Of all peptides, Ac-3-Pal-RGD-3-Pal-

OH, **2.8**, displayed good separations between the isomers, and a single isomer was isolated.



**Scheme 2.4** Synthetic approach for Ac-3-Pal-RGD-3-Pal-OH, **2.8**, coordination with  $[\text{Re}(\text{CO})_3(\text{OH}_2)_3]^+$ , and proposed product.

The bi-dentate coordination could occur at the C-terminus through the free carboxyl and through the nitrogen atom of the pyridine on 3-Pal, forming an eight membered ring. A single isomer was isolated, at the retention time of 4.5 minutes; however, the stability of the isolated isomer was an issue. The stability of the coordinated isomer was monitored by leaving the isomer in water/acetonitrile solution over couple days at room temperature, and then characterizing by LC-MS. Figure 2.9 shows the MS traces of  $[\text{Re}(\text{CO})_3(3\text{Pal-RGD-3Pal-OH})]\text{OTf}$  as a crude mixture and of an isolated isomer. In solution, the isomer was interconverted into different isomeric form. The difference in the retention time of the peaks, could be a result of different injection time.

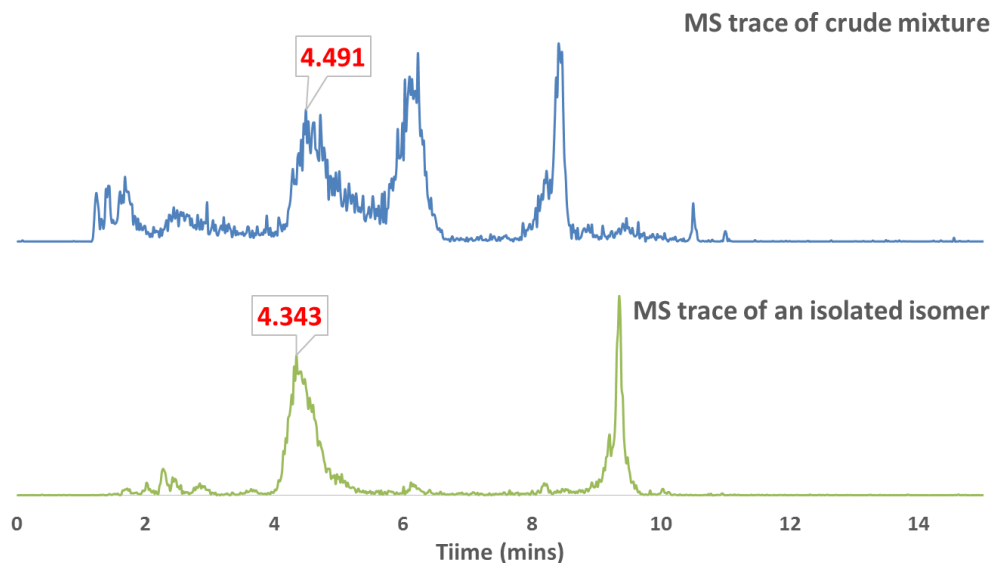


**Figure 2.9** MS traces of  $[\text{Re}(\text{CO})_3(3\text{Pal-RGD-3Pal-OH})]\text{OTf}$  as crude mixture and isolated isomer

## 2.3 Conclusion

Cyclization of a pentapeptide containing a biological relevant sequence, RGD, in the peptide backbone was attempted. Natural, histidine, and un-natural amino acids, 2/3/4-pyridylalanine, were employed to accomplish the coordination with  $\text{Re}(\text{CO})_3^+$ . Most peptides resulted in multiple isomers that were formed upon metal coordination and the isomers were present in close proximity with other isomers. Isolating a single isomer for further analysis presented a challenge. Ac-3-Pal-RGD-3-Pal-OH demonstrated good separation between its isomers, and a single isomer was isolated. However, stability of the isolated isomer was a major issue as it interconverted to different isomer over days at room temperature in a mixture of acetonitrile and water. A strong chelation system that results in limited linkage isomers, with good chromatographic separation is desired.

## 2.4 Experimental

All the reagents and solvents were purchased from Sigma Aldrich, Chem-Impex, Nova BioChem, and the Fmoc protected amino acids were purchased from Peptide International and Apptec, and were used without further purification. Analytical HPLC-

MS was performed using a Waters Atlantis T3 C18 column 4.6 x 150 mm, 5  $\mu$ m.

Preparative RP HPLC-MS was performed using a Waters Atlantis T3 Prep C18 OBD column 19 x 150 mm, 5  $\mu$ m. A gradient system was used consisting of: CH<sub>3</sub>CN + 0.1% v/v trifluoroacetic acid, TFA, (solvent A) and H<sub>2</sub>O + 0.1% v/v TFA (solvent B), and the absorbance was detected using a Waters 2998 Photodiode Array Detector. Electrospray Ionization (ESI) mass spectrum was obtained using a Micromass Quatro Micro LCT mass spectrometer.

### 2.4.1 Small Molecule Synthesis

#### *Tris-aqua tris-carbonylrhenium (I) triflate, 2.3*

Commercially available bromopentacarbonyl rhenium (I) (1.22 g, 3.0 mmol) was added to a dry round bottom flask, and dissolved in freshly distilled dichloromethane (40 ml). Silver triflate (0.98g, 3.8 mmol) was weighed out under subdued light, and added to the flask with increased nitrogen flow. The flask was covered with aluminum foil, and stirred at room temperature for three hours. After three hours, the side product, silver bromide, was removed with vacuum filtration. The resulting solution was evaporated with reduced pressure to half volume (20 ml). Hexanes (20 ml) were degased in a 50 ml round bottom flask, by bubbling nitrogen through for 30 minutes. Dry hexanes were added, and the solvent was slowly removed with reduced pressure, resulting in 1.3 g (91%) of white powder. A suspension of pentacarbonylrhenium (I) triflate (0.5 g) in water (10.41 ml) was prepared for microwave reaction. The reaction was performed at 120 °C for 30 minutes, which resulted in 0.1 M [Re(CO)<sub>3</sub>(OH<sub>2</sub>)<sub>3</sub>]<sup>+</sup> solution. The resulting solution was characterized by LC-MS.

### 2.4.2 Peptide Synthesis

Peptides were synthesized from C→N terminus using standard Fmoc Solid Phase Synthesis (Fmoc-SPPS) approach. Synthesis was carried out manually at room temperature. Fmoc protected Rink amide (0.54 mmol/g), Wang (0.48 mmol/g loading), and 2-chlorotrityl (0.34 mmol/g loading) resins were used as solid support. Wang and 2-chlorotrityl resin were pre-loaded with Histidine with trityl as a protecting group. The

resin was swollen in dichloromethane (DCM) for 15 minutes. The Fmoc group was removed using 20% piperidine in *N,N*-dimethylformamide (DMF) over two cycles (5 and 15 minutes). Coupling reactions were carried out with 3 eq. Fmoc protected amino acid, 3 eq. HCTU (2-(6-chloro-1H-benzotriazole-1-yl)-1,1,3,3-tetramethylaminiumhexafluorophosphate) and 6 eq. of DIPEA (*N,N*-diisopropylethylamine). Each cycle was vortexed for 60-90 minutes. The resin was washed with excess DMF and DCM after each coupling and de-protection cycles. The N terminus of the peptide was acetylated after removing the Fmoc protection from the last amino acid, using 15% acetic anhydride in DMF for 20 minutes, repeated twice. The acetylated peptide was cleaved off the resin with 95% (v/v) trifluoroacetic acid (TFA), 2.5% (v/v) triisopropylsilane (TIPS) and 2.5% (v/v) H<sub>2</sub>O. The cleavage was performed for 4 hours. The cleaved peptide was precipitated with tert-butyl methyl ether (TBME), and centrifuged at 4000 rpm for 10 minutes. After decanting, the peptide was frozen and lyophilized to remove any remaining solvents. The peptide was purified with reverse phase preparative LC-MS, and the purity was checked by analytical HPLC. Each of the following peptides synthesized resulted in purity > 95%.

#### *Ac-HRGDH-OH*, **2.4**

The peptide was synthesized manually on a Wang resin employing the same methodology that is explained above. ESI-LC-MS *m/z* calcd. for C<sub>26</sub>H<sub>38</sub>N<sub>12</sub>O<sub>9</sub> [M+H]<sup>+</sup> 663.66 and [M+2H]<sup>2+</sup> 332.33, found [M+H]<sup>+</sup> 663.34 and [M+2H]<sup>2+</sup> 332.25. <sup>1</sup>H-NMR Spectrum (400 MHz, CD<sub>3</sub>-OD,  $\delta$ ): 8.79 (1H, d, imidazole, <sup>4</sup>J<sub>H-H</sub> = 1.6 Hz), 8.78 (1H, d, imidazole, <sup>4</sup>J<sub>H-H</sub> = 1.6 Hz), 7.36 (1H, s, imidazole), 7.36 (1H, s, imidazole), 4.70 (1H, dd, CH of His, <sup>3</sup>J<sub>H-H</sub> = 6 Hz, <sup>3</sup>J<sub>H-H</sub> = 4.4 Hz), 4.68 (1H, dd, CH of His, <sup>3</sup>J<sub>H-H</sub> = 6.4 Hz, <sup>3</sup>J<sub>H-H</sub> = 4.4 Hz), 4.62 (1H, t, CH of Arg, <sup>3</sup>J<sub>H-H</sub> = 6.4 Hz), 4.32 (1H, dd, CH of Asp, <sup>3</sup>J<sub>H-H</sub> = 5.6 Hz), 3.88 (1H, pair of doublets, CH<sub>2</sub> of Gly, <sup>2</sup>J<sub>H-H</sub> = 16.8 Hz, <sup>2</sup>J<sub>H-H</sub> = 16.4 Hz), 3.80 (1H, d, CH<sub>2</sub> of Gly), 3.37 (1H, dd, CH<sub>2</sub> of His, <sup>2</sup>J<sub>H-H</sub> = 11.2 Hz, <sup>3</sup>J<sub>H-H</sub> = 4.8 Hz), 3.28 (1H, dd, CH<sub>2</sub> of His, <sup>2</sup>J<sub>H-H</sub> = 10 Hz, <sup>3</sup>J<sub>H-H</sub> = 6 Hz), 3.20 (1H, dd, CH<sub>2</sub> of His, <sup>2</sup>J<sub>H-H</sub> = 7.4 Hz, <sup>3</sup>J<sub>H-H</sub> = 4.4 Hz), 3.12 (1H, dd, CH<sub>2</sub> of His, <sup>2</sup>J<sub>H-H</sub> = 10 Hz, <sup>3</sup>J<sub>H-H</sub> = 7.2 Hz), 3.22 – 3.09 (2H, m, CH<sub>2</sub> of Arg), 2.81 (2H, m, CH<sub>2</sub> of Asp, <sup>2</sup>J<sub>H-H</sub> = 17.2, <sup>3</sup>J<sub>H-H</sub> = 7.96 Hz), 1.97 (3H, s,

CH<sub>3</sub>C(O)NH), 1.90 (1H, m, CH<sub>2</sub> of Arg), 1.77 (1H, m, CH<sub>2</sub> of Arg), 1.67 (2H, m, CH<sub>2</sub> of Arg).

*Ac-His(trt)-Arg(pbf)-Gly-Asp(OtBu)-His(trt)-OH, 2.5*

The peptide was synthesized manually on a 2-chlorotrityl resin using standard SPPS. The peptide was cleaved off the resin using cleavage cocktail with (v/v) equivalence (1eq) acetic acid: (2eq) trifluoroethanol: (7eq) DCM solution. The peptide was stirred in the cleavage cocktail for 2.5 hours, and the solvent was removed with reduced pressure. The peptide was purified with preparative RP LC-MS, and the purity was checked with analytical HPLC-MS. ESI-LC-MS *m/z* calcd. for C<sub>81</sub>H<sub>90</sub>N<sub>12</sub>O<sub>12</sub>S [M+H]<sup>+</sup> 1456.7 and [M+2H]<sup>2+</sup> 728.9, found [M+H]<sup>+</sup> 1456.6 and [M+2H]<sup>2+</sup> 728.6

*Ac-HRGD<sub>2</sub>-NH<sub>2</sub>, 2.6*

The peptide was synthesized manually on a Rink Amide resin using general SPPS. ESI-LC-MS *m/z* calcd. for C<sub>26</sub>H<sub>39</sub>N<sub>13</sub>O<sub>8</sub> [M+H]<sup>+</sup> 662.7 and [M+2H]<sup>2+</sup> 331.8, found [M+H]<sup>+</sup> 662.3 and [M+2H]<sup>2+</sup> 331.7

*Ac-3-Pal-RGD-3-Pal-OH, 2.7*

The peptide was manually synthesized on 2-chlorotrityl resin using general SPPS. Removal of all the protecting groups and cleavage of the peptide of the resin was achieved with 95% (v/v) trifluoroacetic acid (TFA), 2.5% (v/v) triisopropylsilane (TIPS) and 2.5% (v/v) H<sub>2</sub>O. The cleavage was performed for 4 hours at room temperature. ESI-LC-MS *m/z* calcd. for C<sub>30</sub>H<sub>40</sub>N<sub>10</sub>O<sub>9</sub> [M+H]<sup>+</sup> 685.71 and [M+2H]<sup>2+</sup> 343.36, found [M+H]<sup>+</sup> 685.29 and [M+2H]<sup>2+</sup> 343.22.

*Ac-3-Pal-RGD-3-Pal-NH<sub>2</sub>, 2.8*

The peptide was manually synthesized on a Rink Amide resin using general SPPS. ESI-LC-MS *m/z* calcd. for C<sub>30</sub>H<sub>41</sub>N<sub>11</sub>O<sub>8</sub> [M+H]<sup>+</sup> 684.73 and [M+2H]<sup>2+</sup> 342.87, found [M+H]<sup>+</sup> 684.25 and [M+2H]<sup>2+</sup> 342.72.

*H-3-Pal-RGD-3-Pal-OH, 2.9*

The peptide was synthesized manually on a Rink Amide resin using general SPPS. The N-terminal amino acid was not acetylated. ESI-LC-MS  $m/z$  calcd. for  $C_{28}H_{38}N_{10}O_8$   $[M+H]^+$  685.71, found  $[M+H]^+$  686.22.

***H-2-Pal-RGD-4-Pal-NH<sub>2</sub>, 2.10***

The peptide was synthesized manually on a Rink Amide resin using general SPPS. The N-terminal amino acid was not acetylated. ESI-LC-MS  $m/z$  calcd. for  $C_{28}H_{39}N_{11}O_7$   $[M+H]^+$  642.69, found  $[M+H]^+$  643.11.

***H-2-Pal-RGD-3-Pal-NH<sub>2</sub>, 2.11***

The peptide was synthesized manually on a Rink Amide resin using general SPPS. The N-terminal amino acid was not acetylated. ESI-LC-MS  $m/z$  calcd. for  $C_{28}H_{39}N_{11}O_7$   $[M+H]^+$  642.69, found  $[M+H]^+$  643.16.

### 2.4.3 $Re(CO)_3^+$ Coordination

*Coordination of Ac-HRGDH-OH with  $[Re(CO)_3(OH_2)_3]^+$*

The acetylated peptide, **2.4**, (11.5 mg, 0.011 mmol, 1.0 eq) was dissolved in water (5 ml) and methanol (0.5 ml);  $Re[(CO)_3(OH_2)_3]^+$  (103.33  $\mu$ L, 0.010 mmol, 0.9 eq) and 5 M NaOH (80.4  $\mu$ L, 0.080 mmol, 7 eq) were added to the solution. The reaction was performed for 3 hours, and monitored by UPLC-MS every half hour. The solution was frozen and lyophilized to remove solvents. A RP SNAP C-18 cartridge was used to purify the coordinated peptide on an automated Isolera flash column. Water and methanol were used as solvents. Gradient included (water in methanol): 0-15% (150 ml), 15-15% (45 ml), 15-50% (150ml), 50-50% (45ml), 50-95% (105 ml), and 95-95% (45ml). ESI-LC-MS  $m/z$  calcd. for  $C_{29}H_{37}N_{12}O_{12}Re$   $[M+H]^+$  932.9 and  $[M+2H]^{2+}$  466.9, found  $[M+H]^+$  933.3 and  $[M+2H]^{2+}$  467.1

*Synthesis of  $Re[(CO)_3(Ac-HRGDH-NH_2)(py)]^+$*

The acetylated peptide, **2.6**, (10 mg, 9.0  $\mu$ mol, 1.0 eq) was dissolved in methanol (5 ml), 0.1 M  $[Re(CO)_3(OH_2)_3]^+$  (90  $\mu$ L, 8.1  $\mu$ mol, 0.9 eq) and 5 M NaOH (50  $\mu$ L,  $4.5 \times 10^{-2}$

mmol, 5.0 eq) were added to the solution. The reaction was performed for 3 hours, and then pyridine (100 eq, 80.5 uL) was added to the reaction mixture. The reaction mixture was further stirred for an hour at 45 °C. An excess TBME was added to the reaction mixture, and the resulting solution was centrifuged for 10 minutes at 3000 rpm. The precipitates were frozen and lyophilized for further analysis. ESI-LC-MS  $m/z$  calcd. for  $C_{34}H_{44}N_{12}O_{11}Re^+$   $[M]^+$  1011.0 and  $[M+H]^{2+}$  506.5, found  $[M+H]^+$  1011.7 and  $[M+2H]^{2+}$  506.1

#### *Synthesis of $[Re(CO)_3(Ac-3-Pal-RGD-3-Pal-NH_2)]OTf$*

The acetylated peptide, **2.8**, (30 mg, 44  $\mu$ mol, 1 eq) was dissolved in a mixture of methanol (2 mL) and water (1 mL). The pH of the solution was adjusted to 7 by adding phosphate buffer saline (3 mL). The  $[Re(CO)_3(OH_2)_3]OTf$  (434  $\mu$ L, 43.4  $\mu$ mol, 0.99 eq) solution was then added to the reaction mixture, and stirred at room temperature for 2.5 hours. The reaction mixture was lyophilized and purified by preparative HPLC-MS. ESI-LC-MS  $m/z$  calcd. for  $C_{33}H_{41}N_{10}O_{12}Re$   $[M+H]^+$  955.24 and  $[M+2H]^{2+}$  478.12, found  $[M+H]^+$  955.40 and  $[M+2H]^{2+}$  478.09.

## 2.5 References

1. James, M. L.; Gambhir, S. S., A Molecular Imaging Primer: Modalities, Imaging Agents, and Applications. *Physiol Rev* **2012**, 92 (2), 897-965.
2. Roxin, A.; Zheng, G., Flexible or fixed: a comparative review of linear and cyclic cancer-targeting peptides. *Future Med Chem* **2012**, 4 (12), 1601-1618.
3. (a) Ruan, F. Q.; Chen, Y. Q.; Hopkins, P. B., Metal-Ion Enhanced Helicity in Synthetic Peptides Containing Unnatural, Metal-Ligating Residues. *J Am Chem Soc* **1990**, 112 (25), 9403-9404; (b) Torrado, A.; Imperiali, B., New synthetic amino acids for the design and synthesis of peptide-based metal ion sensors. *J Org Chem* **1996**, 61 (25), 8940-8948.
4. Snyder, J. P.; Lakdawala, A. S.; Kelso, M. J., On the stability of a single-turn alpha-helix: The single versus multiconformation problem. *J Am Chem Soc* **2003**, 125 (3), 632-633.

5. Simpson, E. The Development of Metal-Organic Compounds for Use as Molecular Imaging Agents. University of Western Ontario, 2014.
6. Magnus, K. A.; Hazes, B.; Tonthat, H.; Bonaventura, C.; Bonaventura, J.; Hol, W. G. J., Crystallographic Analysis of Oxygenated and Deoxygenated States of Arthropod Hemocyanin Shows Unusual Differences. *Proteins-Structure Function and Genetics* **1994**, *19* (4), 302-309.
7. Holland, K. D.; Mathews, G. C.; Bolossy, A. M.; Tucker, J. B.; Reddy, P. A.; Covey, D. F.; Ferrendelli, J. A.; Rothman, S. M., Dual Modulation of the Gamma-Aminobutyric-Acid Type-a Receptor Ionophore by Alkyl-Substituted Gamma-Butyrolactones. *Mol Pharmacol* **1995**, *47* (6), 1217-1223.
8. Perutz, M. F., Stereochemistry of Cooperative Effects in Haemoglobin. *Nature* **1970**, *228* (5273), 726-734.
9. Roberts, V. A.; Iverson, B. L.; Iverson, S. A.; Benkovic, S. J.; Lerner, R. A.; Getzoff, E. D.; Tainer, J. A., Antibody Remodeling - a General-Solution to the Design of a Metal-Coordination Site in an Antibody-Binding Pocket. *P Natl Acad Sci USA* **1990**, *87* (17), 6654-6658.
10. (a) Arnold, F. H.; Haymore, B. L., Engineered Metal-Binding Proteins - Purification to Protein Folding. *Science* **1991**, *252* (5014), 1796-1797; (b) Suh, S. S.; Haymore, B. L.; Arnold, F. H., Characterization of His-X3-His Sites in Alpha-Helices of Synthetic Metal-Binding Bovine Somatotropin. *Protein Eng* **1991**, *4* (3), 301-305; (c) Todd, R. J.; Vandam, M. E.; Casimiro, D.; Haymore, B. L.; Arnold, F. H., Cu(II)-Binding Properties of a Cytochrome-C with a Synthetic Metal-Binding Site - His-X3-His in an Alpha-Helix. *Proteins-Structure Function and Genetics* **1991**, *10* (2), 156-161.
11. Hickey, J. L. THE DEVELOPMENT OF PEPTIDE MIMICS FOR USE AS INTEGRATED RADIOPHARMACEUTICALS. The University of Western Ontario, 2011.
12. Schibli, R.; Schubiger, P. A., Current use and future potential of organometallic radiopharmaceuticals. *Eur J Nucl Med Mol I* **2002**, *29* (11), 1529-1542.
13. Pitchumony, T. S.; Banevicius, L.; Janzen, N.; Zubieta, J.; Valliant, J. F., Isostructural Nuclear and Luminescent Probes Derived From Stabilized [2+1]

Rhenium(I)/Technetium(I) Organometallic Complexes. *Inorganic chemistry* **2013**, 52 (23), 13521-13528.

14. Schmidt, S. P.; Nitschke, J.; Trogler, W. C.; Hockett, S. I.; Angelici, R. J., Manganese(I) and Rhenium(I) Pentacarbonyl(Trifluoromethanesulfonato) Complexes. *Inorg Syn* **1989**, 26, 113-117.

15. Nayak, D. K.; Halder, K. K.; Baishya, R.; Sen, T.; Mitra, P.; Debnath, M. C., Tricarbonyltechnetium(I) and tricarbonylrhenium(I) complexes of amino acids: crystal and molecular structure of a novel cyclic dimeric  $\text{Re}(\text{CO})_3$ -amino acid complex comprised of the OON donor atom set of the tridentate ligand. *Dalton T* **2013**, 42 (37), 13565-13575.

16. Viguri, M. E.; Perez, J.; Riera, L., C-C coupling of N-heterocycles at the fac- $\text{Re}(\text{CO})_3$  fragment: synthesis of pyridylimidazole and bipyridine ligands. *Chemistry* **2014**, 20 (19), 5732-40.

17. Connell, T. U.; Hayne, D. J.; Ackermann, U.; Tochon-Danguy, H. J.; White, J. M.; Donnelly, P. S., Rhenium and technetium tricarbonyl complexes of 1,4-Substituted pyridyl-1,2, 3-triazole bidentate 'click' ligands conjugated to a targeting RGD peptide. *J Labelled Compd Rad* **2014**, 57 (4), 262-269.

18. Atkins, P. W.; Shriver, D. F., *Inorganic chemistry*. 4th ed.; W.H. Freeman: New York, 2006;

## Chapter 3

### 3 A Turn Induced by $^{99m}\text{Tc}/\text{Re}$ (I) Tricarbonyl Coordination to Form Cyclic Metallopeptides

#### 3.1 Introduction

Peptides over the past decade have gained a great interest as targeting entities for drug delivery and discovery agent. There are wide range of biological receptors that have affinity towards peptides, for example integrins, growth hormone secretagogue receptor 1a, and gastrin releasing peptide receptor.<sup>1,2,3</sup> Peptides as a class of biomolecules have many desirable properties such as rapid body clearance, high binding affinity towards targeted receptors, easy chemical synthesis.<sup>4,5</sup> With all these advantages using peptides as targeting entities for imaging molecules present, the *in-vivo* stability of short linear peptides still remains a major concern, as they are readily broken down through enzymatic degradation. Many techniques have been presented to improve the stability and binding affinity of linear peptides; introducing structural constraints within the peptide backbone is one such technique. Peptide macro-cyclization can be introduced through various bond types such as covalent bonds, for example disulfide bridge and amide linkage, and also hydrocarbon stapling. Metal based cyclization provides another approach to introduce structural constraints within peptides. Many studies have been presented that investigate the effect of metals on stabilizing peptide turns.<sup>6,7,8</sup>

In 2014, Ma et al. reported cyclization of a linear peptide, HAAAH, through Ir (III) complexation.<sup>9</sup> They further evaluated this easy-to-use cyclization by replacing the tri-alanine sequence with a biological relevant peptide, RGD. The cyclized RGD peptide showed better protein-protein interactions than the linear peptide. Peptide cyclization through rhenium and technetium, instantly allows the peptide to have potential use as an imaging agent and radio-therapeutic. In 2014, Simpson reported cyclization of the HAAAH through rhenium and technetium centres.<sup>10</sup> We now report on peptide

cyclization through rhenium and technetium coordination, with a biological applicable peptide in the backbone.

## 3.2 Results and Discussion

### 3.2.1 Strategy

The addition of structural constraints is an approach to peptide modification that has been shown to improve *in-vivo* stability and receptor affinity for biologically relevant peptides. Cyclizing a peptide backbone through  $^{99m}\text{Tc}/\text{Re}(\text{CO})_3^+$  coordination is a unique approach that has not been thoroughly investigated. Employing  $^{99m}\text{Tc}/\text{Re}(\text{CO})_3^+$  as a structural constraint allows the peptide to be potentially used as an imaging probe.  $^{99m}\text{Tc}/\text{Re}(\text{CO})_3^+$  as octahedral complexes, occupies lower energy orbitals, which can be stabilized with aromatic amines, such as pyridine, triazole, and imidazole.<sup>11</sup> Pyridyl-triazole have been shown to coordinate with  $\text{Re}(\text{CO})_3^+$  in a bi-dentate fashion.<sup>12,13</sup> Derivative of pyridyl-triazole can be incorporated within the peptide backbone for metal coordination. Pyridyl-triazole, pyta, is established at the C-terminus of the peptide sequence; and 3-pyridylalanine (3-Pal), containing pyridine as a side chain, is inserted at the N-terminus of the peptide. We demonstrate the cyclization of a biologically relevant peptide sequence, comprised of the tripeptide RGD in the backbone, upon metal coordination with full in-depth characterization and analysis. To further investigate the structural geometry within the RGD backbone, D-amino acids were explored.

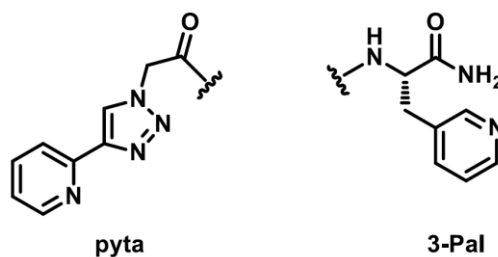
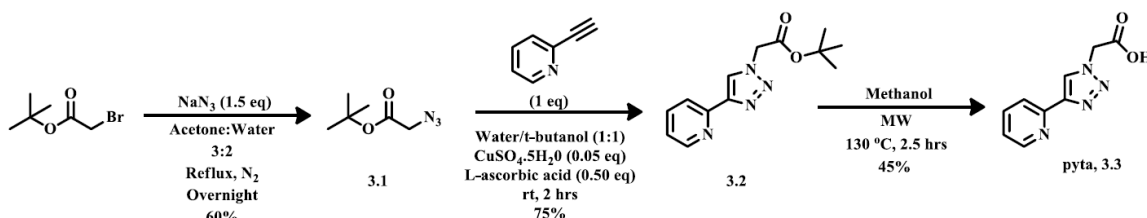


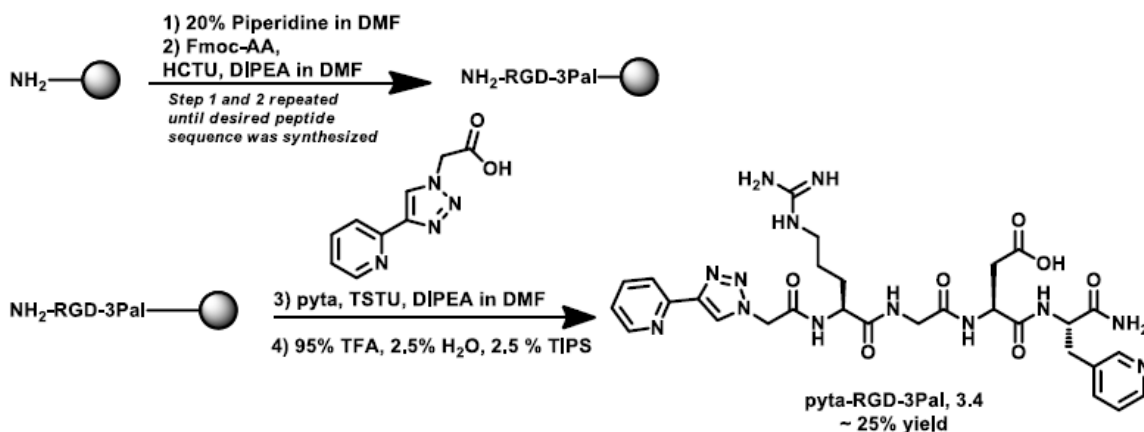
**Figure 3.1** Structures of pyridyl-triazole (pyta) and 3-pyridylalanine (3-Pal)

### 3.2.2 Peptide Synthesis

The peptide, pyta-RGD-3Pal-NH<sub>2</sub>, was synthesized by Fmoc solid-phase peptide chemistry, using rink amide resin as the solid support. Each amino acid couplings was performed for an hour at room temperature, in the presence of a coupling reagent (2-(6-chloro-<sup>1</sup>H-benzotriazole-1-yl)-1,1,3,3-tetramethylaminium hexafluorophosphate, HCTU; 2-(7-aza-<sup>1</sup>H-benzotriazole-1-yl)-1,1,3,3-tetramethyluronium hexafluorophosphate, HATU) and a base (DIPEA) in DMF. Pyridyl-triazole (pyta) was synthesized according to a previously published procedure, scheme 3.1.<sup>14,15</sup> The t-butyl group was thermally cleaved under microwave conditions.<sup>16</sup> Pyridyl-triazole, pyta, was vortexed for an hour at room temperature in the coupling solution, consisting of TSTU (*N,N,N',N'*-tetramethyl-*O*-(*N*-succinimidyl)uronium tetrafluoroborate) and DIPEA in DMF, to prepare the pre-activated ester. Removal of all the protecting groups and cleavage off the resin was achieved by vortexing the resin in a cleavage cocktail (95% (v/v) trifluoroacetic acid (TFA), 2.5% (v/v) triisopropylsilane (TIPS) and 2.5% (v/v) H<sub>2</sub>O). The peptide was precipitated, centrifuged, and lyophilized to remove residual solvents. The linear peptide was then purified by RP-HPLC-MS, with a purity > 95%.



**Scheme 3.1** Synthetic route for pyridyl-triazole (pyta).



**Scheme 3.2** Synthesis of pyta-RGD-3Pal-NH<sub>2</sub>, **3.4**, employing SPPS

### 3.2.3 <sup>1</sup>H-NMR Analysis of pyta-RGD-3-Pal-NH<sub>2</sub>

The linear peptide was characterized by LC-MS, <sup>1</sup>H-NMR and two dimensional gCOSY NMR spectroscopy. The NMR experiments were performed in deuterated dimethyl sulfoxide (DMSO-d<sub>6</sub>) at 25 °C. Bundi et al. reported proton chemical shifts of twenty amino acids in the peptide sequence, TFA-Gly-Gly-X-Ala-OCH<sub>3</sub>; where X is one of the natural twenty amino acids.<sup>17</sup> The linear peptide adopts a random conformation in solution, and proton chemical shifts reported by Bundi et al. were used as a reference for identifying chemical shifts of amino acids in the linear peptide sequence, pyta-RGD-3Pal-NH<sub>2</sub>. Circular Dichroism (CD) spectroscopy confirmed that the linear peptide adopted a random coil conformation. It is important to note that the proton chemical shift of an amino acid is influenced by neighboring amino acids, as demonstrated by Wishart et al.<sup>18</sup> They compared two sets of peptide sequences, Gly-Gly-X-Ala-Gly-Gly and Gly-Gly-X-Pro-Gly-Gly, and found that substituting a proline for an alanine had a significant effect on the chemical shift of H<sub>α</sub>, for the X amino acid. Table 3.1 reports proton chemical shifts of αCH, βCH<sub>2</sub>, NH, and others protons for amino acids present in the backbone of pyta-RGD-3Pal-NH<sub>2</sub>, **3.4**.

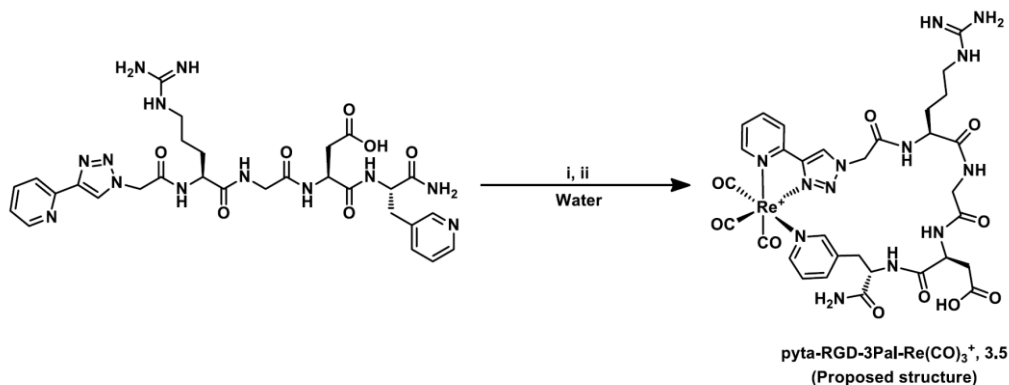
Residue	NH	H $\alpha$	H $\beta$	Others
3-Pyridylalanine	7.55	4.36	3.12, 2.90	
Aspartic acid	8.71	4.25	2.54, 2.23	
Glycine	8.86	3.98, 3.48	-	
Arginine	8.73	4.39	2.02, 1.63	$\gamma$ CH <sub>2</sub> 1.62, 1.54; $\delta$ CH <sub>2</sub> 3.17, 2.99

**Table 3.1** Amino acids' proton shifts (ppm) of the linear peptide, pyta-RGD-3-Pal-NH<sub>2</sub>,

### 3.4

#### 3.2.4 Re(CO)<sub>3</sub><sup>+</sup> Coordination

The synthesis of rhenium tris-carbonyl complexes was demonstrated by reacting the linear peptide, pyta-RGD-3Pal, with two different rhenium (I) centres, Re(CO)<sub>5</sub>Br and [Re(CO)<sub>3</sub>(OH<sub>2</sub>)<sub>3</sub>]OTf. Tris-aqua tris-carbonyl rhenium (I) triflate, [Re(CO)<sub>3</sub>(OH<sub>2</sub>)<sub>3</sub>]OTf,<sup>19</sup> was synthesized according to the previously described procedure by Schmidt et al., from commercially available bromopentacarbonyl rhenium (I), Re(CO)<sub>5</sub>Br. [Re(CO)<sub>3</sub>(OH<sub>2</sub>)<sub>3</sub>]<sup>+</sup> is water soluble and serves as an analogue for [<sup>99m</sup>Tc(CO)<sub>3</sub>(OH<sub>2</sub>)<sub>3</sub>]<sup>+</sup>. Rhenium coordination was established under microwave conditions, in water. Upon coordination, the crude mixture was analyzed by LC-MS, and purified by preparative reverse phase HPLC MS. Both rhenium (I) cores produced similar dominant isomeric traces, according to LC-MS. A single isomer was isolated, with a purity of ~ 90%.



**Scheme 3.3** Re(CO)<sub>3</sub><sup>+</sup> coordination of pyta-RGD-3Pal-NH<sub>2</sub>, **3.4**. *Reactions and conditions* i) 0.95 eq 0.1 M [Re(CO)<sub>3</sub>(OH)<sub>3</sub>]OTf, 105 °C, 1 hour, water; ii) 0.95 eq [Re(CO)<sub>5</sub>]Br 105 °C, 1 hour, water.

### 3.2.5 Characterization of [Re(CO)<sub>3</sub>(pyta-RGD-3-Pal-NH<sub>2</sub>)]OTf

The linear peptide and rhenium coordinated peptide were analyzed by electrospray ionization mass spectrometry, and both the peptides were present with a di-cationic charges. Upon coordination with the metal, an isotopic rhenium signature was observed for <sup>185</sup>Re and <sup>187</sup>Re.

Residue	NH	H $\alpha$	H $\beta$	Others
3-Pyridylalanine	7.37	4.42	3.12, 2.47	
Aspartic acid	7.16	4.30	1.63, 1.62	
Glycine	8.41	3.81, 3.52	-	
Arginine	9.31	4.18	1.78, 1.69	$\gamma$ CH <sub>2</sub> 1.53; $\delta$ CH <sub>2</sub> 3.18

**Table 3.2** Amino acids' proton chemical shifts (ppm) of the coordinated peptide, pyta-RGD-3Pal-NH<sub>2</sub>-Re(CO)<sub>3</sub><sup>+</sup>.

The coordinated peptide was characterized by <sup>1</sup>H-NMR, and two dimensional <sup>1</sup>H-<sup>1</sup>H NMR spectroscopy. The proton chemical shifts of the coordinated peptide are reported in Table 3.2. The NMR experiments were performed in DMSO-d<sub>6</sub> at 25 °C. A number of interesting observations were made when comparing the proton chemical shifts of linear and coordinated peptides. The chemical shifts of the NH for all the amino acids, except arginine, resulted in an up-field shift upon metal coordination. The significant downfield NH shift of arginine could be a result of Re(CO)<sub>3</sub><sup>+</sup> being present in close proximity,

thereby influencing the amide bond. Also, the CH $\alpha$  chemical shifts of 3-pyridylalanine and aspartic acid resulted in a downfield shift; whereas CH arginine had an up-field chemical shift.

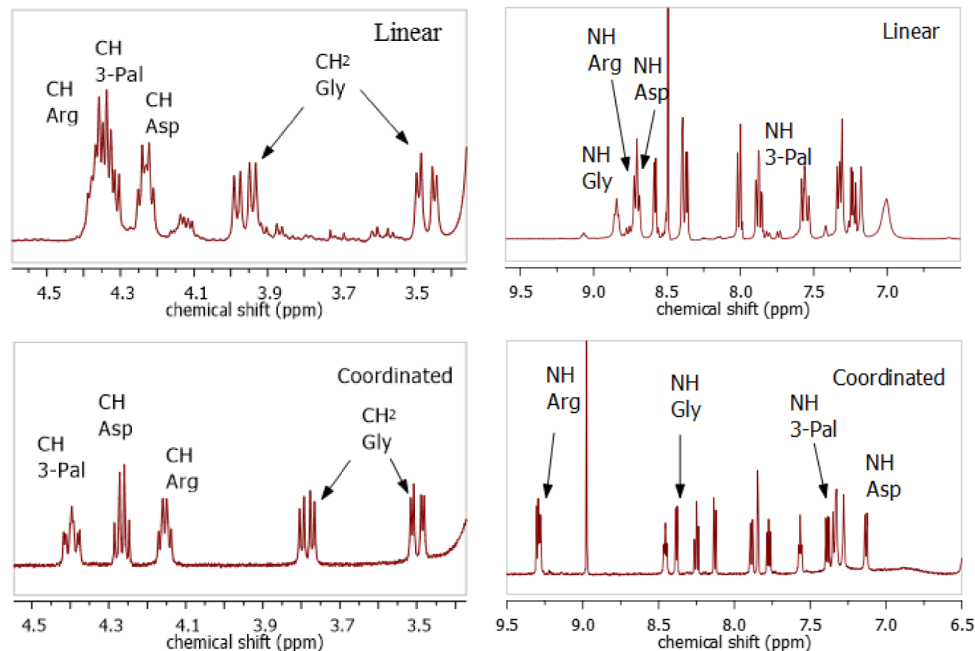


**Figure 3.2** Partial  $^1\text{H}$ -NMR spectra (600 MHz,  $\text{DMSO-d}_6$ , 25  $^\circ\text{C}$ ) of the linear peptide, **3.4** and coordinated peptide, **3.5**

To identify the coordination sphere,  $^1\text{H}$ -NMR spectra of the linear peptide and the rhenium complex were compared.  $^1\text{H}$ - $^1\text{H}$  gCOSY was used to identify proton chemical shifts of linear and coordinated peptides. Upon coordination with  $\text{Re}(\text{CO})_3^+$ , downfield shifts of the aromatic protons for pyridyltriazole and pyridine were observed. This downfield chemical shift was most evident for the triazole proton that shifted from 8.51 ppm in the linear peptide to 9.00 ppm in the  $\text{Re}(\text{CO})_3^+$  coordinated peptide, Figure 3.2. The downfield chemical shifts of these aromatic protons provides evidence that coordination with  $\text{Re}(\text{CO})_3^+$  involves pyridyl-triazole and pyridine, and that the coordination sphere correlates with the proposed structure. Also, the methylene hydrogens (labelled as 10) are significantly separated upon  $\text{Re}(\text{CO})_3^+$  coordination; this further supports the hypothesis that pyridyl-triazole, pyta, is bidentate coordinated to  $\text{Re}(\text{CO})_3^+$ .

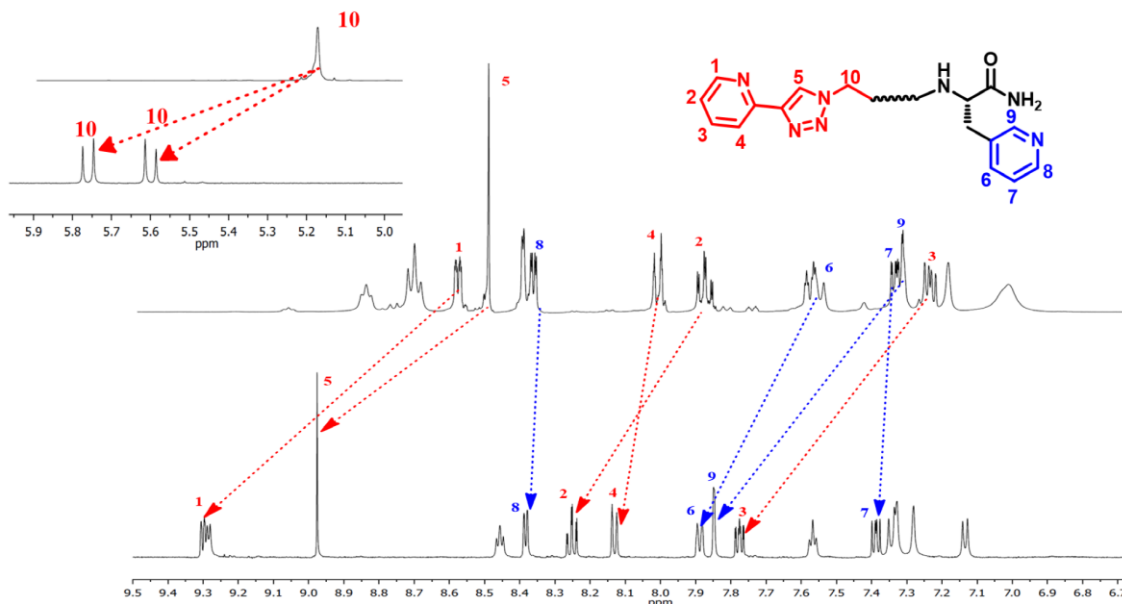


**Figure 3.3** Partial  $^1\text{H}$ -NMR spectra (600 MHz,  $\text{DMSO-d}_6$ ) of the linear peptide (top, **3.4**) and coordinated peptide,  $[\text{Re}(\text{CO})_3(\text{pyta-RGD-3Pal-NH}_2)]\text{OTf}$  (bottom, **3.5**).

### 3.2.6 Circular Dichroism (CD) Spectroscopy

Circular Dichroism (CD) spectroscopy is a widely used technique to determine the secondary structure of proteins and peptides.<sup>20</sup> CD spectroscopy can be used to demonstrate a difference in peptide conformation, for example between a random coil (linear) and an ordered structure (cyclic).<sup>21,22</sup> Analysis of the CD spectrum of the linear peptide, **3.4**, showed one strong minimum at 200 nm. This strong minima is a characteristic of peptides existing in a random coil conformation.<sup>23</sup> The  $\text{Re}(\text{CO})_3^+$  coordinated peptide resulted in two minima at 200 nm and 215 nm, and two maxima at 210 nm and 235 nm. Upon coordinating with a metal, a significant difference in the peptide conformation was observed, suggesting that a turn was created in the peptide backbone. The identification of the secondary structure remains unclear from just CD data. To further explore the secondary structure of the coordinated peptide, variable temperature (VT) NMR and computational studies were performed.

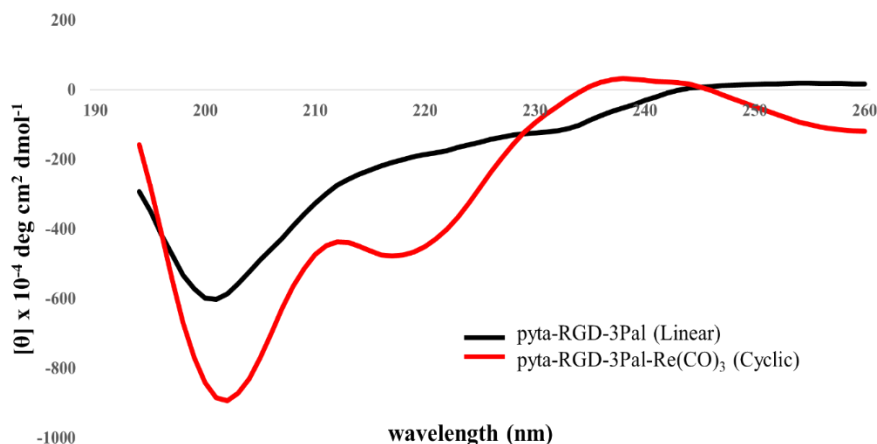


**Figure 3.4** Circular Dichroism (CD) analysis of linear peptide and  $\text{Re}(\text{CO})_3^+$  coordinated peptide in  $\text{H}_2\text{O}$  at 25 °C.

### 3.2.7 Variable Temperature (VT) NMR

$^1\text{H}$ -NMR and CD spectroscopy demonstrated that a turn was established within the peptide backbone. Secondary structure is a result of intra-molecular hydrogen bonding within the peptide backbone that can be evaluated by studying the variable temperature (VT)  $^1\text{H}$ -NMR of the compound.<sup>24,25</sup> The formation of intra-molecular hydrogen bonds results in the chemical shift of the amide proton being less affected by a change in temperature when compared to non-hydrogen bonded or solvent-exposed amide protons.<sup>26</sup> This is due to the amide proton being held in a strong conformational lock by the carbonyl oxygen. A non-hydrogen bonded amide proton shifts significantly up-field as the temperature increases, whereas, a hydrogen bonded amide proton is less strongly affected by temperature change. The hydrogen bonds can be classified as medium and strong interactions. This can be demonstrated by deriving a numerical value ( $\Delta\delta_{\text{NH}}/\Delta T$ ), chemical shift (ppm) divided by change in temperature (K). A temperature gradient of  $\Delta\delta_{\text{NH}}/\Delta T \geq -3 \text{ ppbK}^{-1}$ , corresponds to strong intramolecular hydrogen bonding; and  $\Delta\delta_{\text{NH}}/\Delta T \leq -4.5 \text{ ppbK}^{-1}$  are suggestive of solvent-exposed protons, while intermediate values between the two extremes suggest weak intra-molecular hydrogen bonding.<sup>27,28</sup>

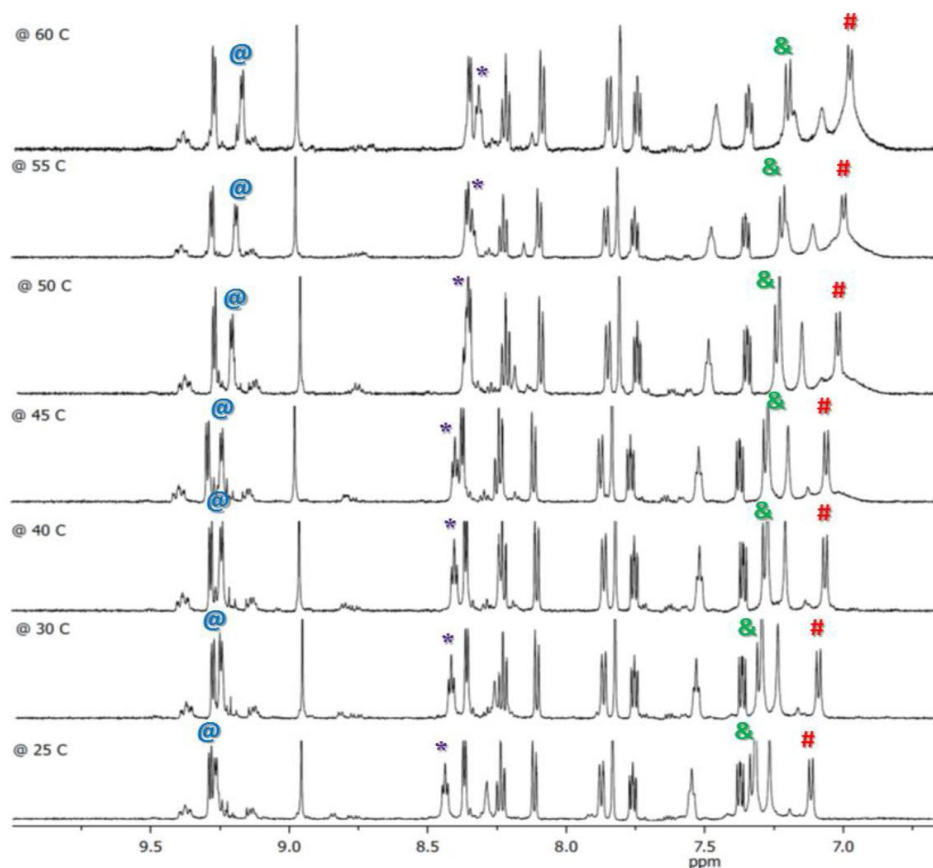


**Figure 3.5** VT NMR analysis of the rhenium coordinated peptide, **3.5**, in DMSO- $d_6$  at 600 MHz.

Amino acid residue ( $N_\alpha H$ )	$\Delta\delta/\Delta T$ (ppb/K)	H Bond
3-Pridylalanine (&)	- 3.1	medium
Aspartic Acid (#)	- 3.4	medium
Glycine (*)	- 3.1	medium
Arginine (@)	- 2.6	strong

**Table 3.3** Chemical shifts of amide protons expressed in numerical values,  $\Delta\delta/\Delta T$  (ppb/K) for each amino acid residues.

VT NMR studies of the rhenium coordinated peptide,  $[\text{Re}(\text{CO})_3(\text{pyta-RGD-3Pal-NH}_2)]^+$ , were carried out in DMSO- $d_6$  from 25-60 °C. The seven  $^1\text{H}$ -NMR spectras for the amide protons were obtained over the range of 35 °C, Figure 3.4. The amide protons are labelled and changes in the chemical shifts of amide protons are observed. Table 3.3 reports numerical values for changes in the chemical shifts of amide protons.

When the chemical shifts were converted to numerical values, all the amide bonds were present in the range of  $0 \geq \Delta\delta/\Delta T \geq -4.5 \text{ ppbK}^{-1}$ , indicating that hydrogen bonding exists within the peptide backbone. This suggested that the amide protons within the peptide backbone are involved in hydrogen bonding, either through backbone carbonyls of the amide bonds or through side chain carbonyls, such as carboxylate functional group on the aspartic acid. The arginine amide proton is considered to be strongly hydrogen bonded, while other amide protons are only moderately hydrogen bonded. The moderate hydrogen bonding could be the result of solvent exposure, as traces of water are present within the sample, or weak intra-molecular hydrogen bonding.

### 3.2.8 Computational Study

To further explore the secondary structure of the peptide backbone, computational studies on the coordinated peptide were performed. Two possible isomers were formed upon metal coordination. All isomers were optimized using density functional theory (DFT), employing B3LYP functional. One of the coordinated isomers, obtained in gas phase, displayed consistent results observed with variable temperature (VT) NMR spectroscopy, Figure 3.5. Multiple intra-molecular hydrogen bonds were observed in the peptide backbone. According to the computational data, all the amide protons, except the aspartic acid amide proton, were hydrogen bonded, which is consistent with the results obtained from variable temperature (VT) NMR studies. The aspartic acid amide proton was hydrogen bonded according to the experimental results but this could be a result of stabilization due to solvent exposure. The optimized structure suggest that the cyclized peptide contains a  $i, i\pm 3$  turn.

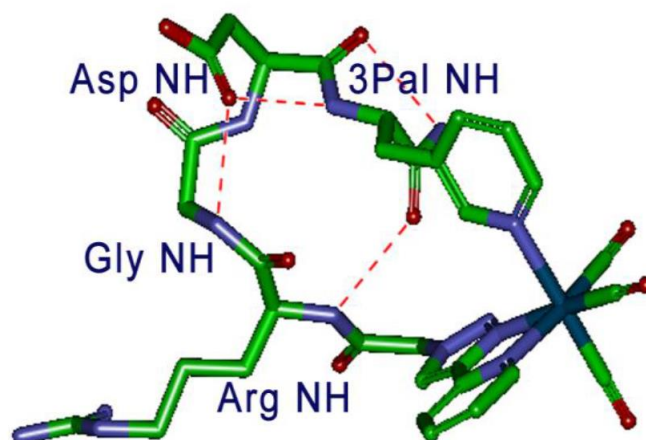
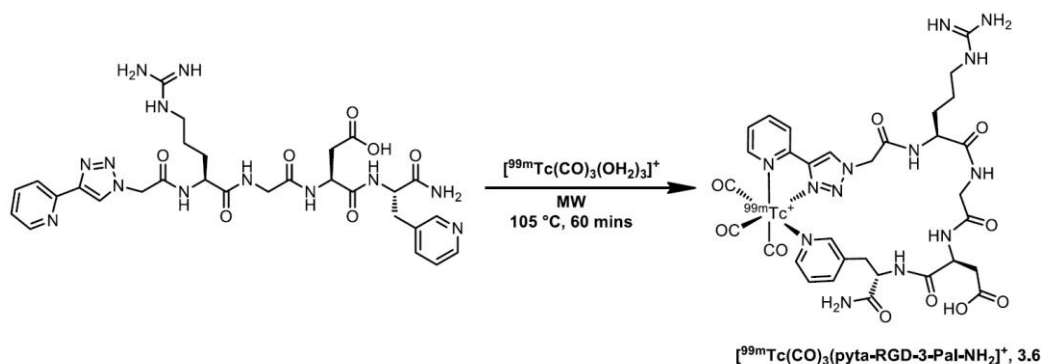


**Figure 3.6** Lowest energy isomer of Re-coordinated peptide, **3.5**, optimized using DFT calculations, displaying intra-molecular hydrogen bonding.

### 3.2.9 $^{99m}\text{Tc}$ Labelling



**Scheme 3.4**  $^{99\text{m}}\text{Tc}(\text{CO})_3^+$  coordination of pyta-RGD-3Pal-NH<sub>2</sub> to give **3.6**.

The linear peptide, pyta-RGD-3Pal-NH<sub>2</sub>, was labelled with technetium-99m to provide  $^{99\text{m}}\text{Tc}$  coordinated peptide,  $[\text{}^{99\text{m}}\text{Tc}(\text{CO})_3(\text{pyta-RGD-3Pal-NH}_2)]$ . The pertechnetate was added to the commercially available isolink kit, and following the microwave reaction conditions reported by Pitchumony et al. resulted in  $[\text{}^{99\text{m}}\text{Tc}(\text{CO})_3(\text{OH}_2)_3]^+$ .<sup>29</sup> The reduced  $^{99\text{m}}\text{Tc}$  was reacted with the linear peptide, producing the radiolabelled peptide. The crude mixture was then purified with Waters Sep-Pak C18 Plus Cartridge. To demonstrate that the linear peptide was coordinated through  $^{99\text{m}}\text{Tc}(\text{CO})_3^+$ , the crude radiolabelled peptide was co-injected with the purified  $\text{Re}(\text{CO})_3^+$  coordinated peptide, and confirmed

by analytical U-HPLC. The retention time of the dominant isomer of the crude radiolabelled peptide in the gamma trace correlated with the purified  $\text{Re}(\text{CO})_3^+$  coordinated peptide in the UV trace, Figure 3.6. From this result, it was concluded that the  $^{99\text{m}}\text{Tc}$  labeling of the linear peptide was successful.

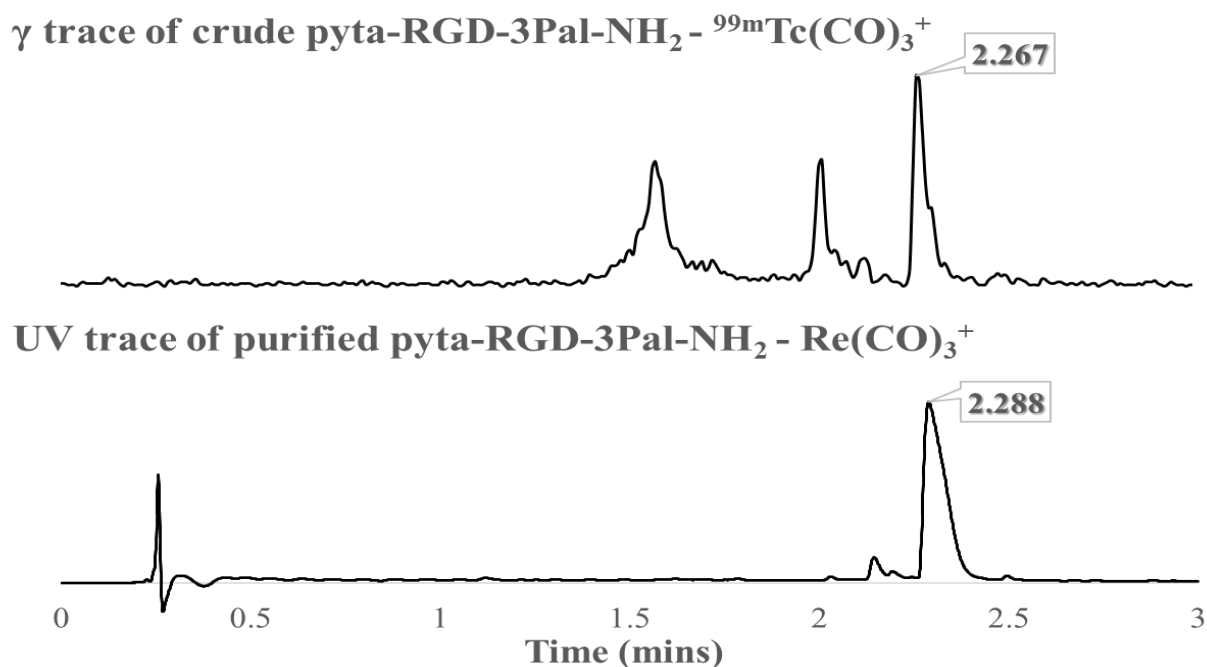


**Figure 3.7** U-HPLC analysis showing correlations between  $\gamma$  trace of crude  $^{99\text{m}}\text{Tc}(\text{CO})_3^+$  labelled peptide and UV trace of purified  $\text{Re}(\text{CO})_3^+$  coordinated peptide.

### 3.2.10 Derivatives of $[\text{Re}(\text{CO})_3(\text{pyta-RGD-3-Pal-NH}_2)]^+$

The protein-peptide interactions highly depend on the structural geometry that the peptide is present in. Changes in the structural geometry can reduce or enhance specific binding affinity of a peptide. To further explore different structural geometry in the RGD backbone, the L-amino acids were replaced with the D-amino acids. This resulted in RGD backbone to adapt different structural geometry upon metal coordination. Figure 3.7 displays derivatives of  $[\text{Re}(\text{CO})_3(\text{pyta-RGD-3-Pal-NH}_2)]\text{OTf}$ . The coordinated peptides were characterized by LC-MS,  $^1\text{H}$ -, and gCOSY NMR spectroscopy.

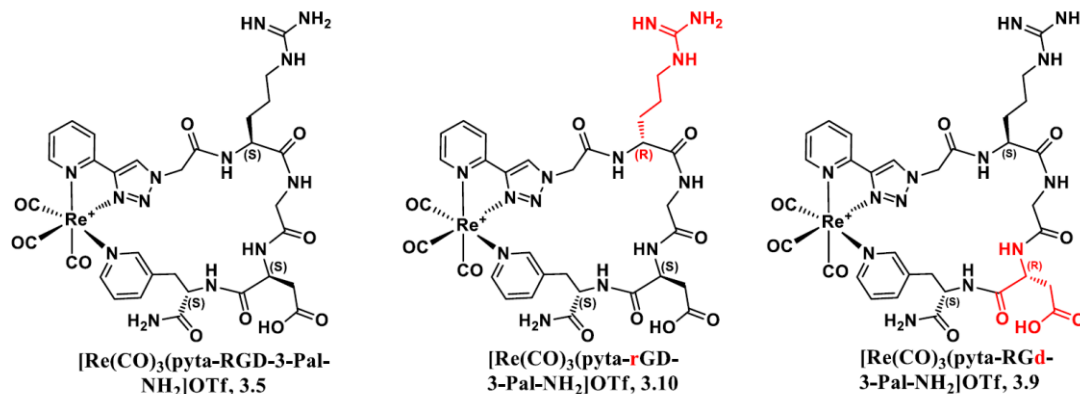


**Figure 3.8** Derivatives of  $[\text{Re}(\text{CO})_3(\text{pyta-RGD-3-Pal-NH}_2)]\text{OTf}$ .

### 3.3 Conclusion

A linear peptide, pyta-RGD-3Pal-NH<sub>2</sub>, was cyclized in a “2+1” fashion through a bi-dentate coordination from two nitrogen atoms on the pyridyl-triazole, and a mono-dentate attack from the nitrogen atom on the pyridine. This was demonstrated by comparing <sup>1</sup>H-NMR spectra of linear and coordinated peptides. Circular Dichroism (CD) data suggested formation of secondary structure upon metal coordination, and hydrogen bonding was observed by variable temperature (VT) NMR spectroscopy studies. Intra-molecular hydrogen bonding displayed by computational data were consistent with VT NMR studies, however, they were not identical. Radiolabelling of the linear peptide with <sup>99m</sup>Tc(CO)<sub>3</sub><sup>+</sup>, resulted in the same structural constraints presented by Re(CO)<sub>3</sub><sup>+</sup> coordination. We successfully demonstrated cyclization of a biological relevant peptide stabilized through <sup>99m</sup>Tc/Re(CO)<sub>3</sub><sup>+</sup> coordination.

### 3.4 Experimental

All the reagents and solvents were purchased from Sigma Aldrich, Chem-Impex, Nova BioChem, and the Fmoc protected amino acids were purchased from Peptide International and Apptec, and were used without further purification. Analytical HPLC-MS was performed using a Waters Atlantis T3 C18 column 4.6 x 150 mm, 5 μm. Preparative RP HPLC-MS was performed using a Waters Atlantis T3 Prep C18 OBD column 19 x 150 mm, 5 μm. A gradient system was used consisting of: CH<sub>3</sub>CN + 0.1%

v/v trifluoroacetic acid, TFA, (solvent A) and H<sub>2</sub>O + 0.1% v/v TFA (solvent B), and the absorbance was detected using a Waters 2998 Photodiode Array Detector. Electrospray Ionization (ESI) mass spectrum was obtained using a Micromass Quatro Micro LCT mass spectrometer. For analytical U-HPLC-MS studies, a Waters, Inc. Acquity UPLC H-Class system was used, combined with a Xevo QToF and a Bioscan Inc. FC-1000 Flow-Count Radio-HPLC Detector System. For analytical UHPLC studies, a Waters Acquity UPLC BEH C18 2.1 x 50 mm, 1.7  $\mu$ m column was used. A gradient solvent system consisting of CH<sub>3</sub>OH + 0.1% formic acid (solvent A) and H<sub>2</sub>O + 0.1% formic acid (solvent B) was used. A Biotage Isolera One flash chromatography system was used for flash column chromatography purification fitted with a Snap 12 g reversed phase C-18 column. Varian INOVA 600 NMR spectrometer was used for <sup>1</sup>H, and gCOSY NMR studies.

### 3.4.1 Small Molecule Synthesis

#### *t*-butyl azido acetate, **3.1**

A modified procedure was used.<sup>14</sup> *tert*-Butyl 2-bromoacetate (19.512g, 100 mmol) and sodium azide (9.751 g, 150 mmol) were dissolved in 3:2 mixture of acetone (60 mL) and water (40 mL). The solution was refluxed (92 °C) for 22 hours. Upon completion of the reaction, the mixture was cooled to room temperature, and concentrated to remove acetone. The organic product was extracted with Et<sub>2</sub>O (3x20 ml). The organic layers were washed with sat. NaCl and dried over sodium sulfate, Na<sub>2</sub>SO<sub>4</sub>. The organic solution was concentrated to give the product, **3.1** (11.5 g, 73 % yield), as a yellow oil. No additional purification was performed prior to further reaction. <sup>1</sup>H NMR (400 MHz, CDCl<sub>3</sub>,  $\delta$ ) 3.72 (s, 2H), 1.48 (s, 9H).

#### *tert*-butyl 2-(4-phenyl-1*H*-1,2,3-triazol-1-yl)acetate, **3.2**

A modified procedure was used.<sup>14</sup> *tert*-Butyl azido acetate (0.489 g, 3.1 mmol) and 2-ethynylpyridine (0.322 g, 3.1 mmol) were dissolved in isopropanol (1 mL) in a 20 mL vial. In another 20 mL vial, copper (II) sulfate pentahydrate (0.041 g, 0.16 mmol) and L-ascorbic acid (0.290 g, 1.6 mmol) were dissolved in H<sub>2</sub>O (2 mL). Solids were completely

dissolved by sonicating for 20 minutes at room temperature. The aqueous solution was added dropwise to the stirring organic solution over 15 minutes. The reaction mixture was stirred at room temperature for 2 hours. The resulting solution was diluted with chloroform (40 mL) and washed thrice with sat. disodium ethylenediaminetetraacetate (3x20 mL). The organic product from the aqueous solution was extracted with chloroform (3x20 mL). The organic layers were combined, dried over Na<sub>2</sub>SO<sub>4</sub>, and concentrated to remove chloroform. The crude product was purified by Biotage Isolera One flash column chromatography fitted with a normal phase cartridge, with methanol (Solvent A) in dichloromethane (Solvent B) using 1–8% gradient to give **3.2** (0.60 g, 75 % yield). <sup>1</sup>H NMR (400 MHz, CDCl<sub>3</sub>, δ) 8.58 (m, 1H), 8.25 (s, 1H), 8.18 (d, J = 7.9 Hz, 1H), 7.78 (td, J = 7.8, 1.8 Hz, 1H), 7.23 (ddd, J = 7.5, 4.9, 1.1 Hz, 1H), 5.12 (s, 2H), 1.49 (s, 9H).

### *2-(4-(pyridin-2-yl)-1H-1,2,3-triazol-1-yl)acetic acid (pyta) 3.3*

In a 20 mL microwave vial, pyridyl-triazole acetate (0.60 g, 0.23 mmol) was dissolved in methanol (18 mL). The solution was heated under microwave conditions for 2.5 hours at 130 °C. The reaction mixture was cooled to room temperature, and precipitates were observed. The reaction mixture was vacuum filtered to give **3.3** (0.12 g, 25 % yield). No further purification was needed. <sup>1</sup>H NMR (400 MHz, D<sub>2</sub>O, δ) 8.84 (s, 1H), 8.72 (d, J = 5.4 Hz, 1H), 8.60 (t, J = 7.9 Hz, 1H), 8.37 (d, J = 8.0 Hz, 1H), 7.97 (t, J = 6.1 Hz, 1H), 5.42 (s, 2H).

## 3.4.2 Peptide Synthesis

### *Pyta-RGD-3-Pal-NH<sub>2</sub>, 3.4*

The Peptide was synthesized from C→N terminus using standard Fmoc Solid Phase Synthesis (Fmoc-SPPS) approach. Synthesis was carried out manually at room temperature. Fmoc protected Rink amide (0.54 mmol/g) resin was used as solid support. The resin was swollen in dichloromethane (DCM) for 15 minutes. The Fmoc group was removed using 20% piperidine in *N,N*-dimethylformamide (DMF) over two cycles (5 and 15 minutes). Coupling reactions were carried out with 3 eq. Fmoc protected amino acid, 3 eq. HCTU (2-(6-chloro-1H-benzotriazole-1-yl)-1,1,3,3-

tetramethylammoniumhexafluorophosphate) and 6 eq. of DIPEA (*N,N*-diisopropylethylamine). Each cycle was vortexed for 60-90 minutes. The resin was washed with excess DMF and DCM after each coupling and de-protection cycles. Pyridyl-triazole, pyta, was vortexed in DMF at room temperature, with 9 eq. of DIPEA and 3 eq. of TSTU (*O*-(*N*-succinimidyl)-1,1,3,3-tetramethyl uranium tetrafluoroborate), for an hour before adding to the resin for coupling reaction. After constructing the desired peptide sequence, the peptide was cleaved off the resin with 95% (v/v) trifluoroacetic acid (TFA), 2.5% (v/v) triisopropylsilane (TIPS) and 2.5% (v/v) H<sub>2</sub>O. The cleavage was performed for 4 hours. The cleaved peptide was precipitated with tert-butyl methyl ether (TBME), and centrifuged at 4000 rpm for 10 minutes. After decanting, the peptide was frozen and lyophilized to remove any remaining solvents. The peptide was purified with reverse phase preparative LC-MS, and the purity was checked by analytical HPLC. The peptide resulted with a purity of > 95%. HRMS: *m/z* calculated for C<sub>32</sub>H<sub>37</sub>N<sub>13</sub>O<sub>10</sub>, 680.2979; observed [M]<sup>+</sup> 680.2443 <sup>1</sup>H-NMR Spectrum (600 MHz, (CD<sub>3</sub>)<sub>2</sub>SO, δ): 10.07 (s, 1H), 8.86 (t, *J* = 5.5 Hz, 1H), 8.72 (t, *J* = 7.3 Hz, 2H), 8.60 (ddd, *J* = 4.8, 1.7, 1.0 Hz, 1H), 8.51 (s, 1H), 8.41 (d, *J* = 2.0 Hz, 1H), 8.38 (dd, *J* = 4.8, 1.6 Hz, 1H), 8.03 (m, 1H), 7.89 (m, 1H), 7.61 – 7.55 (m, 2H), 7.36 – 7.32 (m, 2H), 7.25 (dd, *J* = 7.7, 4.8 Hz, 1H), 7.19 (s, 1H), 7.02 (s, 2H), 5.26 (s, 2H), 4.41 – 4.32 (m, 3H), 4.28 – 4.22 (m, 1H), 3.98 (dd, *J* = 16.9, 6.7 Hz, 1H), 3.49 (dd, *J* = 16.8, 4.8 Hz, 1H), 3.22 – 3.15 (m, 1H), 3.12 (dd, *J* = 14.3, 4.5 Hz, 1H), 2.98 (dd, *J* = 12.8, 8.3 Hz, 1H), 2.90 (dd, *J* = 14.2, 9.1 Hz, 1H), 2.57 – 2.51 (m, 1H), 2.22 (dd, *J* = 15.9, 4.9 Hz, 1H), 2.02 (s, 1H), 1.64 (dd, *J* = 11.9, 7.3 Hz, 1H), 1.50 (dd, *J* = 18.1, 7.9 Hz, 2H).

### *Pyta-RGd-3-Pal-NH<sub>2</sub>*, **3.7**

The peptide was synthesized manually on a Rink Amide resin using general SPPS. ESI-LC-MS: *m/z* calculated for C<sub>33</sub>H<sub>37</sub>N<sub>13</sub>O<sub>10</sub> 680.298 and [M+2H]<sup>2+</sup> 340.653; observed [M+H]<sup>+</sup> 680.338 and [M+2H]<sup>2+</sup> 340.717. <sup>1</sup>H NMR (600 MHz, (CD<sub>3</sub>)<sub>2</sub>SO, δ) 8.78 (d, *J* = 7.4 Hz, 1H), 8.75 – 8.71 (m, 1H), 8.61 (m, 1H), 8.52 (s, 1H), 8.43 (d, *J* = 2.0 Hz, 1H), 8.39 (dd, *J* = 4.8, 1.6 Hz, 1H), 8.18 (d, *J* = 6.9 Hz, 1H), 8.03 (d, *J* = 7.9 Hz, 1H), 7.90 (td, *J* = 7.7, 1.8 Hz, 1H), 7.82 (d, *J* = 8.8 Hz, 1H), 7.63 (dt, *J* = 7.8, 1.8 Hz, 1H), 7.41 (s, 1H), 7.35 (ddd, *J* = 7.5, 4.8, 1.1 Hz, 1H), 7.28 (s, 1H), 7.25 (dd, *J* = 7.7, 4.8 Hz, 1H), 7.00 (s, 2H), 5.31 – 5.22 (m, 2H), 4.32 – 4.27 (m, 2H), 4.10 (d, *J* = 5.3 Hz, 1H), 3.89 (dd, *J* =

17.0, 7.3 Hz, 1H), 3.57 (dd,  $J = 17.0, 4.2$  Hz, 1H), 3.27 (dd,  $J = 13.9, 3.4$  Hz, 1H), 3.18 (dd,  $J = 12.3, 5.7$  Hz, 1H), 3.14 – 3.07 (m, 1H), 2.79 (dd,  $J = 14.0, 11.1$  Hz, 1H), 2.49 – 2.44 (m, 1H), 2.05 – 1.99 (m, 1H), 1.99 – 1.92 (m, 1H), 1.72 (dd,  $J = 16.5, 7.8$  Hz, 1H), 1.66 – 1.51 (m, 2H).

### *Pyta-rGD-3-Pal-NH<sub>2</sub>*, **3.8**

The peptide was synthesized manually on a Rink Amide resin using general SPPS. ESI-LC-MS:  $m/z$  calculated for C<sub>33</sub>H<sub>37</sub>N<sub>13</sub>O<sub>10</sub> 680.298 and [M+2H]<sup>2+</sup> 340.653; observed [M+H]<sup>+</sup> 680.270 and [M+2H]<sup>2+</sup> 340.717. <sup>1</sup>H NMR (599 MHz, dmsO)  $\delta$  8.74 (d,  $J = 7.7$  Hz, 1H), 8.71 (dd,  $J = 11.1, 5.2$  Hz, 1H), 8.63 (d,  $J = 6.6$  Hz, 1H), 8.60 (ddd,  $J = 4.9, 1.6, 0.8$  Hz, 1H), 8.51 (s, 1H), 8.41 (d,  $J = 1.9$  Hz, 1H), 8.38 (dd,  $J = 4.8, 1.6$  Hz, 1H), 8.03 (d,  $J = 7.9$  Hz, 1H), 7.89 (td,  $J = 7.7, 1.8$  Hz, 1H), 7.70 (d,  $J = 8.2$  Hz, 1H), 7.61 (dt,  $J = 7.8, 1.8$  Hz, 1H), 7.38 (s, 1H), 7.34 (ddd,  $J = 7.4, 4.8, 1.1$  Hz, 1H), 7.24 (dd,  $J = 7.7, 4.8$  Hz, 1H), 7.15 (s, 1H), 7.02 (s, 2H), 5.24 (d,  $J = 1.9$  Hz, 2H), 4.35 (ddd,  $J = 15.1, 9.6, 6.4$  Hz, 2H), 4.23 (d,  $J = 6.0$  Hz, 1H), 3.93 (dd,  $J = 16.9, 7.3$  Hz, 1H), 3.52 (dd,  $J = 16.9, 4.3$  Hz, 1H), 3.10 (dd,  $J = 13.7, 4.4$  Hz, 3H), 2.90 (dd,  $J = 10.5, 5.6$  Hz, 1H), 2.46 (dd,  $J = 15.7, 5.3$  Hz, 1H), 2.15 (d,  $J = 16.1$  Hz, 1H), 1.95 (dd,  $J = 14.1, 9.2$  Hz, 1H), 1.65 (ddd,  $J = 18.4, 11.6, 4.8$  Hz, 1H), 1.61 – 1.48 (m, 2H).

## 3.4.3 Metal Coordination

### *[Re(CO)<sub>3</sub>(pyta-RGD-3-Pal-NH<sub>2</sub>)]OTf*, **3.5**

The purified linear peptide, **3.4**, (30.9 mg, 0.046 mmol) was coordinated [Re(CO)<sub>3</sub>(OH<sub>2</sub>)<sub>3</sub>]<sup>+</sup>OTf<sup>-</sup> (451  $\mu$ L of 0.1 M solution, 0.045 mmol) in water (4 mL). The reaction was performed under microwave conditions at 130 °C for an hour. Upon completion of reaction, the crude mixture was lyophilized and purified by preparative HPLC (linear gradient of 22 – 35 % Solvent A in B). The purity of the coordinated peptide was determined by analytical LC-MS with ~ 90 % purity (linear gradient 23 – 75 % Solvent A in B). HRMS:  $m/z$  calculated for C<sub>33</sub>H<sub>37</sub>N<sub>13</sub>O<sub>10</sub><sup>185/187</sup>Re, 948.23/950.23; observed [M]<sup>+</sup>948.2238/950.2157. <sup>1</sup>H NMR (600 MHz, (CD<sub>3</sub>)<sub>2</sub>SO,  $\delta$ ) 12.36 (s, 1H), 9.32 (d,  $J = 5.5$  Hz, 1H), 9.31 (d,  $J = 5.0$  Hz, 1H), 9.00 (s, 1H), 8.48 (t,  $J = 5.8$  Hz, 1H), 8.41 (d,  $J = 5.4$  Hz, 1H), 8.28 (td,  $J = 7.9, 1.4$  Hz, 1H), 8.15 (d,  $J = 7.9$  Hz, 1H), 7.91 (d,  $J =$

8.2 Hz, 1H), 7.87 (s, 1H), 7.80 (m, 1H), 7.59 (t,  $J = 5.9$  Hz, 1H), 7.41 (dd,  $J = 7.9, 5.7$  Hz, 1H), 7.37 (s, 1H), 7.35 (d,  $J = 4.6$  Hz, 1H), 7.30 (s, 1H), 7.16 (d,  $J = 8.1$  Hz, 1H), 5.78 (d,  $J = 16.7$  Hz, 1H), 5.62 (d,  $J = 16.7$  Hz, 1H), 4.42 (ddd,  $J = 12.5, 9.7, 3.2$  Hz, 1H), 4.29 (dd,  $J = 14.9, 8.1$  Hz, 1H), 4.18 (dd,  $J = 12.5, 6.7$  Hz, 1H), 3.81 (dd,  $J = 16.2, 6.7$  Hz, 1H), 3.52 (dd,  $J = 16.1, 4.8$  Hz, 1H), 3.18 (td,  $J = 13.8, 6.9$  Hz, 2H), 3.12 (d,  $J = 11.7$  Hz, 1H), 1.82 – 1.74 (m, 1H), 1.69 (d,  $J = 10.3$  Hz, 1H), 1.66 – 1.59 (m, 2H), 1.58 – 1.50 (m, 1H).

$[^{99m}\text{Tc}(\text{CO})_3(\text{pyta-RGD-3-Pal-NH}_2)]^+$ , **3.6**

$[^{99m}\text{TcO}_4]^-$  (1.0 mL, 337 MBq) was added to a previously prepared isolink kit containing 8.5 mg sodium tartrate, 2.85 mg  $\text{Na}_2\text{B}_4\text{O}_7 \cdot 10\text{H}_2\text{O}$ , 7.15 mg sodium carbonate and 4.5 mg sodium boranocarbonate. To a microwave vessel,  $^{99m}\text{Tc}$  solution (1 mL) was added with 100  $\mu\text{L}$  of 1 M HCl solution, and the reaction was performed for 3.5 minutes at 110  $^\circ\text{C}$  to give  $[^{99m}\text{Tc}(\text{CO})_3(\text{OH}_2)_3]^+$ . 46.7 MBq of  $[^{99m}\text{Tc}(\text{CO})_3(\text{OH}_2)_3]^+$  was added to a separate microwave vessel containing the purified linear peptide (0.5 mg, 0.74  $\mu\text{mol}$ ) in water (1 mL). The labelled peptide was purified with Waters Sep-Pak Plus C18 Cartridge using 25 % acetonitrile in water, to remove unreacted linear peptide. The labelled peptide was mixed with purified  $\text{Re}(\text{CO})_3^+$  coordinated peptide, and the solution was analyzed by analytical Ultra HPLC (UHPLC).

$[\text{Re}(\text{CO})_3(\text{pyta-RGd-3-Pal-NH}_2)]\text{OTf}$ , **3.9**

The reaction was proceeded similar to **3.5**, using the linear peptide **3.7**. ESI-LC-MS:  $m/z$  calculated for  $\text{C}_{33}\text{H}_{37}\text{N}_{13}\text{O}_{10}^{185/187}\text{Re}$ , 948.23/950.23; observed  $[\text{M}]^+$  948.441/950.557.  $^1\text{H}$  NMR (600 MHz,  $(\text{CD}_3)_2\text{SO}$ ,  $\delta$ ) 9.27 (s, 2H), 9.12 (s, 1H), 8.37 (d,  $J = 5.4$  Hz, 1H), 8.25 (t,  $J = 7.7$  Hz, 1H), 8.08 (d,  $J = 7.9$  Hz, 1H), 8.05 (s, 1H), 7.85 (d,  $J = 7.8$  Hz, 1H), 7.79 (s, 1H), 7.76 (t, 1H), 7.74 (s, 1H), 7.63 (t, 1H), 7.33 – 7.27 (m, 3H), 7.24 (s, 1H), 7.09 (s, 1H), 5.75 (d,  $J = 15.8$  Hz, 1H), 5.46 (d,  $J = 15.8$  Hz, 1H), 4.07 (dd,  $J = 13.5, 6.2$  Hz, 1H), 4.00 (dd,  $J = 9.3, 8.3$  Hz, 1H), 3.76 (dd,  $J = 15.8, 6.3$  Hz, 1H), 3.72 – 3.66 (m, 2H), 3.52

(dd,  $J = 15.7, 4.8$  Hz, 3H), 3.15 (d,  $J = 7.1$  Hz, 2H), 2.46 – 2.38 (m, 3H), 2.32 (dd,  $J = 16.8, 8.0$  Hz, 1H), 1.83 – 1.74 (m,  $J = 13.7$  Hz, 1H), 1.71 – 1.51 (m, 4H).

### *[Re(CO)<sub>3</sub>(pyta-rGD-3-Pal-NH<sub>2</sub>)]OTf*, **3.10**

The reaction was proceeded similar to **3.5**, using the linear peptide **3.8**. ESI-LC-MS:  $m/z$  calculated for C<sub>33</sub>H<sub>37</sub>N<sub>13</sub>O<sub>10</sub><sup>185/187</sup>Re, 948.23/950.23; observed [M]<sup>+</sup> 948.2433/950.2352. <sup>1</sup>H NMR (600 MHz, (CD<sub>3</sub>)<sub>2</sub>SO,  $\delta$ ) 12.32 (s, 1H), 9.29 (d,  $J = 5.4$  Hz, 1H), 9.22 (d,  $J = 4.4$  Hz, 1H), 9.16 (s, 1H), 8.64 (m, 1H), 8.28 (t,  $J = 7.8$  Hz, 1H), 8.23 (t,  $J = 7.1$  Hz, 2H), 8.08 (s, 1H), 7.80 (t,  $J = 6.6$  Hz, 1H), 7.57 – 7.53 (m, 2H), 7.46 (d,  $J = 6.6$  Hz, 1H), 7.41 (m, 1H), 7.35 (d,  $J = 9.1$  Hz, 1H), 7.25 (s, 1H), 7.11 (s, 1H), 6.52 (s, 2H), 5.66 (d,  $J = 15.6$  Hz, 1H), 5.39 (d,  $J = 15.7$  Hz, 1H), 4.18 (q,  $J = 7.1$  Hz, 1H), 4.02 – 3.93 (m, 2H), 3.89 (dd,  $J = 16.6, 7.1$  Hz, 1H), 3.55 (dd,  $J = 16.5, 3.9$  Hz, 1H), 3.18 – 3.07 (m, 3H), 2.38 (dd,  $J = 16.8, 7.4$  Hz, 1H), 2.22 (dd,  $J = 16.6, 6.4$  Hz, 1H), 2.08 (d,  $J = 7.4$  Hz, 1H), 1.76 – 1.70 (m, 1H), 1.69 – 1.64 (m,  $J = 5.5$  Hz, 1H), 1.62 – 1.57 (m, 1H), 1.56 – 1.51 (m, 1H).

### 3.4.4 Circular Dichroism (CD) spectroscopy

The samples were dissolved in water, and diluted till absorbance reached a value of 1. The absorbance was measured by UV VIS spectrometer. The spectra were collected at 20 °C with scan rate of 100 nm min<sup>-1</sup>, averaged over ten accumulations. The path length of the cuvette was 0.1 mm. Data were converted to mean residue ellipticity units, and plotted in Graphpad prism.

### 3.4.5 Computational Studies

All the structures were initially constructed by DS viewer 3.5. The optimization of structures was performed using density functional theory (DFT), employing the B3LYP functional. The LANL2DZ pseudopotential and the 6-31G(d) basis set were used to model rhenium and the remaining atoms, respectively. No geometry restraint was applied during all optimizations. The nature of the optimized structures and energy minima were defined by subsequent frequency calculations. All calculated structures were characterized as true minima. All the calculations were performed with Gaussian 09

(RevD.01)<sup>30</sup> on high-performance computing (HPC) facilities within the Compute Canada network.<sup>31</sup>

### 3.5 References

1. Hynes, R. O., Integrins: Bidirectional, allosteric signaling machines. *Cell* **2002**, *110* (6), 673-687.
2. Bednarek, M. A.; Feighner, S. D.; Pong, S. S.; McKee, K. K.; Hreniuk, D. L.; Silva, M. V.; Warren, V. A.; Howard, A. D.; Van der Ploeg, L. H. Y.; Heck, J. V., Structure-function studies on the new growth hormone-releasing peptide, ghrelin: Minimal sequence of ghrelin necessary for activation of growth hormone secretagogue receptor 1a. *J Med Chem* **2000**, *43* (23), 4370-4376.
3. Nakagawa, T.; Hocart, S. J.; Schumann, M.; Tapia, J. A.; Mantey, S. A.; Coy, D. H.; Tokita, K.; Katsuno, T.; Jensen, R. T., Identification of key amino acids in the gastrin-releasing peptide receptor (GRPR) responsible for high affinity binding of gastrin-releasing peptide (GRP). *Biochem Pharmacol* **2005**, *69* (4), 579-593.
4. Chen, K.; Chen, X. Y., Design and Development of Molecular Imaging Probes. *Curr Top Med Chem* **2010**, *10* (12), 1227-1236.
5. Okarvi, S. M., Peptide-based radiopharmaceuticals: Future tools for diagnostic imaging of cancers and other diseases. *Med Res Rev* **2004**, *24* (3), 357-397.
6. Ma, M. T.; Hoang, H. N.; Scully, C. C. G.; Appleton, T. G.; Fairlie, D. P., Metal Clips That Induce Unstructured Pentapeptides To Be alpha-Helical In Water. *J Am Chem Soc* **2009**, *131* (12), 4505-4512.
7. Micklitsch, C. M.; Knerr, P. J.; Branco, M. C.; Nagarkar, R.; Pochan, D. J.; Schneider, J. P., Zinc-Triggered Hydrogelation of a Self-Assembling beta-Hairpin Peptide. *Angew Chem Int Edit* **2011**, *50* (7), 1577-1579.
8. Kelso, M. J.; Beyer, R. L.; Hoangt, H. N.; Lakdawala, A. S.; Snyder, J. P.; Oliver, W. V.; Robertson, T. A.; Appleton, T. G.; Fairlie, D. P., alpha-turn mimetics: short peptide alpha-Helices composed of cyclic metallopentapeptide modules. *J Am Chem Soc* **2004**, *126* (15), 4828-4842.

9. Ma, X. C.; Jia, J. L.; Cao, R.; Wang, X. B.; Fei, H., Histidine-Iridium(III) Coordination-Based Peptide Luminogenic Cyclization and Cyclo-RGD Peptides for Cancer-Cell Targeting. *J Am Chem Soc* **2014**, *136* (51), 17734-17737.
10. Simpson, E. The Development of Metal-Organic Compounds for Use as Molecular Imaging Agents. University of Western Ontario, 2014.
11. Abram, U.; Alberto, R., Technetium and rhenium - Coordination chemistry and nuclear medical applications. *J Brazil Chem Soc* **2006**, *17* (8), 1486-1500.
12. Connell, T. U.; Hayne, D. J.; Ackermann, U.; Tochon-Danguy, H. J.; White, J. M.; Donnelly, P. S., Rhenium and technetium tricarbonyl complexes of 1,4-Substituted pyridyl-1,2, 3-triazole bidentate 'click' ligands conjugated to a targeting RGD peptide. *J Labelled Compd Rad* **2014**, *57* (4), 262-269.
13. Lo, W. K. C.; Huff, G. S.; Cubanski, J. R.; Kennedy, A. D. W.; McAdam, C. J.; McMorran, D. A.; Gordon, K. C.; Crowley, J. D., Comparison of Inverse and Regular 2-Pyridyl-1,2,3-triazole "Click" Complexes: Structures, Stability, Electrochemical, and Photophysical Properties. *Inorganic chemistry* **2015**, *54* (4), 1572-1587.
14. Boulay, A.; Seridi, A.; Zedde, C.; Ladeira, S.; Picard, C.; Maron, L.; Benoist, E., Tricarbonyl Re-I Complexes from Functionalised Pyridine-Triazole Derivatives: From Mononuclear to Unexpected Dimeric Complexes. *Eur J Inorg Chem* **2010**, (32), 5058-5062.
15. Jones, M. R.; Service, E. L.; Thompson, J. R.; Wang, M. C. P.; Kimsey, I. J.; DeToma, A. S.; Ramamoorthy, A.; Lim, M. H.; Storr, T., Dual-function triazole-pyridine derivatives as inhibitors of metal-induced amyloid-beta aggregation. *Metallomics* **2012**, *4* (9), 910-920.
16. Theato, P.; Klok, H.-A., *Functional polymers by post-polymerization modification : concepts, guidelines, and applications*. Wiley-VCH: Weinheim, 2013; p xxii, 414 p.
17. Bundi, A.; Grathwohl, C.; Hochmann, J.; Keller, R. M.; Wagner, G.; Wuthrich, K., Proton Nmr of Protected Tetrapeptides Tfa-Gly-Gly-L-X-L-Ala-Och<sub>3</sub>, Where X Stands for One of 20 Common Amino-Acids. *J Magn Reson* **1975**, *18* (1), 191-198.
18. Wishart, D. S.; Bigam, C. G.; Holm, A.; Hodges, R. S.; Sykes, B. D., H-1, C-13 and N-15 Random Coil Nmr Chemical-Shifts of the Common Amino-Acids .1.

- Investigations of Nearest-Neighbor Effects (Vol 5, Pg 67, 1995). *J Biomol Nmr* **1995**, 5 (3), 332-332.
19. Schmidt, S. P.; Nitschke, J.; Trogler, W. C.; Hockett, S. I.; Angelici, R. J., Manganese(I) and Rhenium(I) Pentacarbonyl(Trifluoromethanesulfonato) Complexes. *Inorg Syn* **1989**, 26, 113-117.
  20. Greenfield, N. J., Methods to estimate the conformation of proteins and polypeptides from circular dichroism data. *Anal Biochem* **1996**, 235 (1), 1-10.
  21. Johnson, W. C., Secondary Structure of Proteins through Circular-Dichroism Spectroscopy. *Annu Rev Biophys Bio* **1988**, 17, 145-166.
  22. Johnson, W. C., Analyzing protein circular dichroism spectra for accurate secondary structures. *Proteins-Structure Function and Genetics* **1999**, 35 (3), 307-312.
  23. Gopal, R.; Park, J. S.; Seo, C. H.; Park, Y., Applications of Circular Dichroism for Structural Analysis of Gelatin and Antimicrobial Peptides. *Int J Mol Sci* **2012**, 13 (3), 3229-3244.
  24. Kessler, H., Peptide Conformations .19. Conformation and Biological-Activity of Cyclic-Peptides. *Angewandte Chemie-International Edition in English* **1982**, 21 (7), 512-523.
  25. Baxter, N. J.; Williamson, M. P., Temperature dependence of H-1 chemical shifts in proteins. *J Biomol Nmr* **1997**, 9 (4), 359-369.
  26. Hickey, J. L.; Simpson, E. J.; Hou, J. Q.; Luyt, L. G., An Integrated Imaging Probe Design: The Synthesis of Tc-99m/Re-Containing Macrocyclic Peptide Scaffolds. *Chem-Eur J* **2015**, 21 (2), 568-578.
  27. Cierpicki, T.; Zhukov, I.; Byrd, R. A.; Otlewski, J., Hydrogen bonds in human ubiquitin reflected in temperature coefficients of amide protons. *J Magn Reson* **2002**, 157 (2), 178-180.
  28. Urry, D. W.; Ohnishi, T.; Long, M. M.; Mitchell, L. W., Studies on Conformation and Interactions of Elastin - Nuclear Magnetic-Resonance of Polyhexapeptide. *Int J Pept Prot Res* **1975**, 7 (5), 367-378.
  29. Pitchumony, T. S.; Banevicius, L.; Janzen, N.; Zubieta, J.; Valliant, J. F., Isostructural Nuclear and Luminescent Probes Derived From Stabilized [2+1]

Rhenium(I)/Technetium(I) Organometallic Complexes. *Inorganic chemistry* **2013**, 52 (23), 13521-13528.

30. Gaussian 09, Revision D.01, M. J. Frisch, G. W. Trucks, H. B. Schlegel, G. E. Scuseria, M. A. Robb, J. R. Cheeseman, G. Scalmani, V. Barone, B. Mennucci, G. A. Petersson, H. Nakatsuji, M. Caricato, X. Li, H. P. Hratchian, A. F. Izmaylov, J. Bloino, G. Zheng, J. L. Sonnenberg, M. Hada, M. Ehara, K. Toyota, R. Fukuda, J. Hasegawa, M. Ishida, T. Nakajima, Y. Honda, O. Kitao, H. Nakai, T. Vreven, J. A. Montgomery, Jr., J. E. Peralta, F. Ogliaro, M. Bearpark, J. J. Heyd, E. Brothers, K. N. Kudin, V. N. Staroverov, T. Keith, R. Kobayashi, J. Normand, K. Raghavachari, A. Rendell, J. C. Burant, S. S. Iyengar, J. Tomasi, M. Cossi, N. Rega, J. M. Millam, M. Klene, J. E. Knox, J. B. Cross, V. Bakken, C. Adamo, J. Jaramillo, R. Gomperts, R. E. Stratmann, O. Yazyev, A. J. Austin, R. Cammi, C. Pomelli, J. W. Ochterski, R. L. Martin, K. Morokuma, V. G. Zakrzewski, G. A. Voth, P. Salvador, J. J. Dannenberg, S. Dapprich, A. D. Daniels, O. Farkas, J. B. Foresman, J. V. Ortiz, J. Cioslowski, and D. J. Fox, Gaussian, Inc., Wallingford CT, 2013.

31. SHARCNET ([www.sharcnet.ca](http://www.sharcnet.ca)) is a consortium of colleges, universities and research institutes operating a network of high-performance computer clusters across south western, central and northern Ontario.

## Chapter 4

### 4 Conclusion

Molecular imaging is a well-established *in-vivo* characterization and visualization technique that provides an insight into the biological events taking place at the molecular and cellular level.<sup>1,2</sup> This technique avoids biopsy, and enables non-invasive identification of disease on-set and progression. Three major components are associated when designing a molecular imaging probe: a) a biological target, b) a targeting entity, and c) a signalling source. Many advances have been made in designing imaging probes for PET and SPECT imaging, for both clinical and research applications. The current generation of radiopharmaceuticals are expensive, lack specificity for targeted receptors, are rapidly excreted from the body, and also lack a repetitive method for synthesizing radiopharmaceuticals. Therefore, the development of new techniques for the design of radiopharmaceuticals that allows for both quick and efficient ways to introduce radio-nuclides, as well as to improve *in-vivo* stability and binding affinity, is an attractive topic of research.

Protein-protein interactions are essential for many biological processes, making them an attractive target for drug discovery and therapeutics.<sup>3,4</sup> Integrins are type I transmembrane proteins that mediate protein-protein interactions, and regulate cell shape, cell cycle, and cell migration.<sup>5,6</sup> Integrins, in particular  $\alpha_v\beta_3$ , are overexpressed at tumor cells, while present at low concentration in normal tissue cells. Preventing protein-protein interactions can serve as a potential therapeutic for tumor suppression. Eight of 24 integrins, including  $\alpha_v\beta_3$ , share an identical recognition site, a tripeptide sequence (RGD), for their protein-protein interactions. Cyclic RGD peptides have been shown to exhibit better binding affinity towards  $\alpha_v\beta_3$ , when compared to their linear counterparts. Introducing structural constraints, through metal-based cyclization, within a peptide backbone, has shown to improve *in-vivo* stability and binding affinity of the original peptide.

In this thesis, the development of cyclic RGD peptides, stabilized through  $^{99\text{m}}\text{Tc}/\text{Re}(\text{CO})_3^+$  coordination, was explored. Mono- and bi-dentate ligands were used at the end terminals of a linear peptide. Cyclization of the linear peptide was demonstrated such that the terminal ligands were able to coordinate with  $^{99\text{m}}\text{Tc}/\text{Re}(\text{CO})_3^+$  in a “2+1” fashion, resulting in a cyclic peptide that represented an integrated design. This is an innovative approach of introducing structural constraints through metal based cyclization, and in doing so triggering biological activity of a peptide.

$^{99\text{m}}\text{Tc}/\text{Re}$  (I) coordination can be achieved by employing natural and un-natural amino acids. Histidine can act as mono-, bi-, and tri-dentate ligand, effectively stabilizing a turn upon metal coordination.<sup>7,8</sup> Simpson demonstrated cyclization of Ac-HAAAH-OH through  $^{99\text{m}}\text{Tc}/\text{Re}(\text{CO})_3^+$  coordination.<sup>8</sup> A “2+1” chelation system was created, with a bi-dentate attack at the C-terminus and mono-dentate coordination at the N-terminus. Coordination of Ac-HRGD-H with  $[\text{Re}(\text{CO})_3(\text{OH}_2)_3]\text{OTf}$  gave numerous isomers that were present in close proximity by chromatography, and isolating a single isomer for further characterization was challenging. To reduce the number of isomers, un-natural amino acids such as 2-pyridylalanine, 3-pyridylalanine, and 4-pyridylalanine were used as a replacement for histidine residues. The coordination of the linear peptide, employing pyridylalanine amino acids, with  $\text{Re}(\text{CO})_3^+$  resulted in fewer number of isomers; and a single isomer for  $[\text{Re}(\text{CO})_3(\text{Ac-3-Pal-RGD-3-Pal-OH})]\text{OTf}$  was isolated. However, the stability of the isolated isomer presented an issue, as it was converted to various isomeric forms.

Employing amino acids as bi-dentate chelators did not provide satisfying results for further characterization. The strong metal chelator, pyridyl-triazole (pyta), was used as a bi-dentate chelator at the N-terminus instead of using an amino acid. A linear peptide, pyta-RGD-3Pal-NH<sub>2</sub>, was synthesized and cyclized in a “2+1” chelation fashion. The linear and coordinated peptides were characterized by <sup>1</sup>H- and 2D-NMR spectroscopy. A turn was created upon metal coordination that was demonstrated by comparing circular dichroism (CD) data of linear and coordinated peptides. Intra-molecular hydrogen bonding was observed by variable temperature (VT) NMR studies. The data obtained from a computational study, where the coordinated peptide was optimized using DFT

calculations, were consistent, but not identical, with VT NMR studies. The linear peptide was radiolabeled with  $^{99m}\text{Tc}(\text{CO})_3^+$ , and resulted in the same dominant isomer presented by  $\text{Re}(\text{CO})_3^+$  coordination.

In conclusion, we successfully demonstrated cyclization of RGD peptides that were stabilized through  $^{99m}\text{Tc}/\text{Re}(\text{CO})_3^+$  coordination and resulted in a “2+1” chelation. To further investigate the cyclic RGD backbone, L-amino acids were replaced with D-amino acids; this resulted in different structural geometry within the peptide backbone. These cyclic rhenium coordinated peptides, will first be tested for their binding affinity towards integrins  $\alpha_v\beta_3$ , by performing competitive *in-vitro* assays, such as enzyme-linked immunosorbent assay (ELISA). The differences in the structural geometry of these cyclized peptides will be compared by computational studies. Finally, *in-vivo* studies on the cyclic peptide with the best *in-vitro* results will be evaluated against human melanoma cell line A375M, which expresses integrin  $\alpha_v\beta_3$ . The  $^{99m}\text{Tc}(\text{CO})_3^+$  labeled peptide has a potential to be used for imaging of angiogenesis associated with cancer.

## 4.1 References

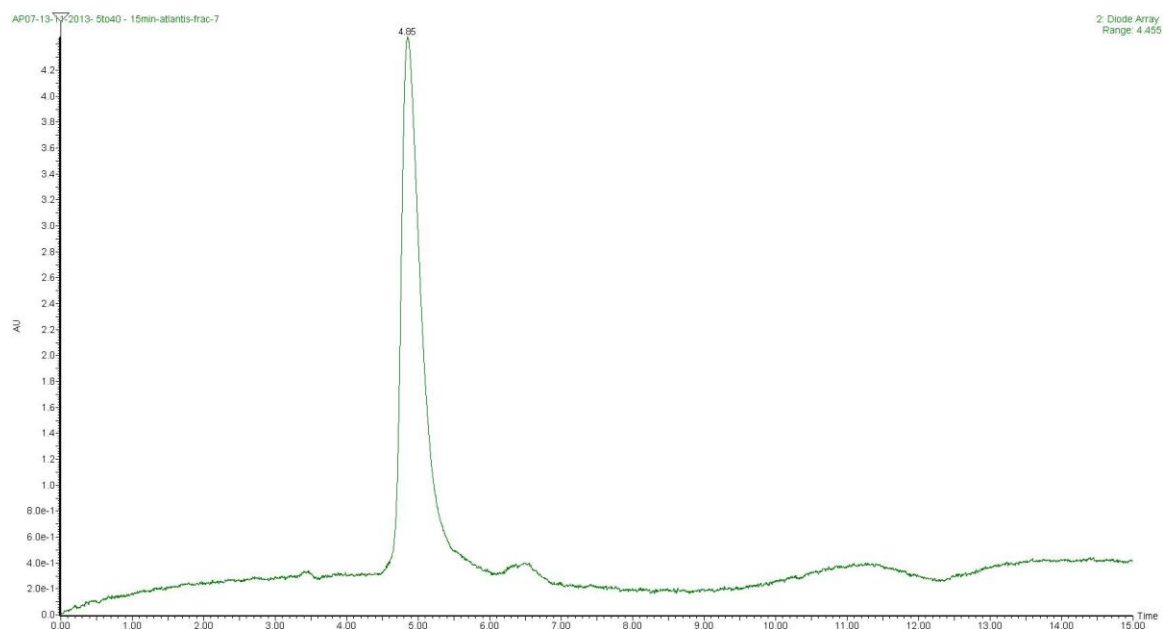
1. James, M. L.; Gambhir, S. S., A Molecular Imaging Primer: Modalities, Imaging Agents, and Applications. *Physiol Rev* **2012**, 92 (2), 897-965.
2. Chen, K.; Chen, X. Y., Design and Development of Molecular Imaging Probes. *Curr Top Med Chem* **2010**, 10 (12), 1227-1236.
3. Arkin, M. R.; Wells, J. A., Small-molecule inhibitors of protein-protein interactions: Progressing towards the dream. *Nat Rev Drug Discov* **2004**, 3 (4), 301-317.
4. Che, Y.; Marshall, G. R., Privileged scaffolds targeting reverse-turn and helix recognition. *Expert Opin Ther Tar* **2008**, 12 (1), 101-114.
5. Desgrosellier, J. S.; Cheresh, D. A., Integrins in cancer: biological implications and therapeutic opportunities. *Nat Rev Cancer* **2010**, 10 (1), 9-22.
6. Brooks, P. C.; Montgomery, A. M. P.; Rosenfeld, M.; Reisfeld, R. A.; Hu, T. H.; Klier, G.; Cheresh, D. A., Integrin Alpha(V)Beta(3) Antagonists Promote Tumor-Regression by Inducing Apoptosis of Angiogenic Blood-Vessels. *Cell* **1994**, 79 (7), 1157-1164.

7. Ma, M. T.; Hoang, H. N.; Scully, C. C. G.; Appleton, T. G.; Fairlie, D. P., Metal Clips That Induce Unstructured Pentapeptides To Be  $\alpha$ -Helical In Water. *J Am Chem Soc* **2009**, *131* (12), 4505-4512.
8. Simpson, E. The Development of Metal-Organic Compounds for Use as Molecular Imaging Agents. University of Western Ontario, 2014.

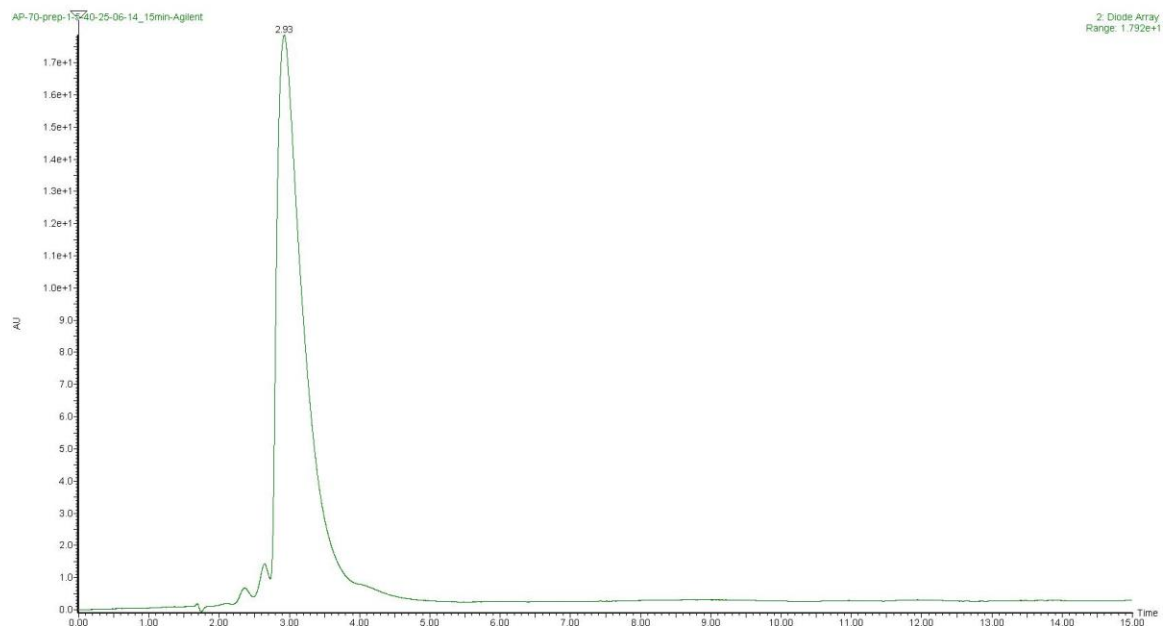
## Appendices

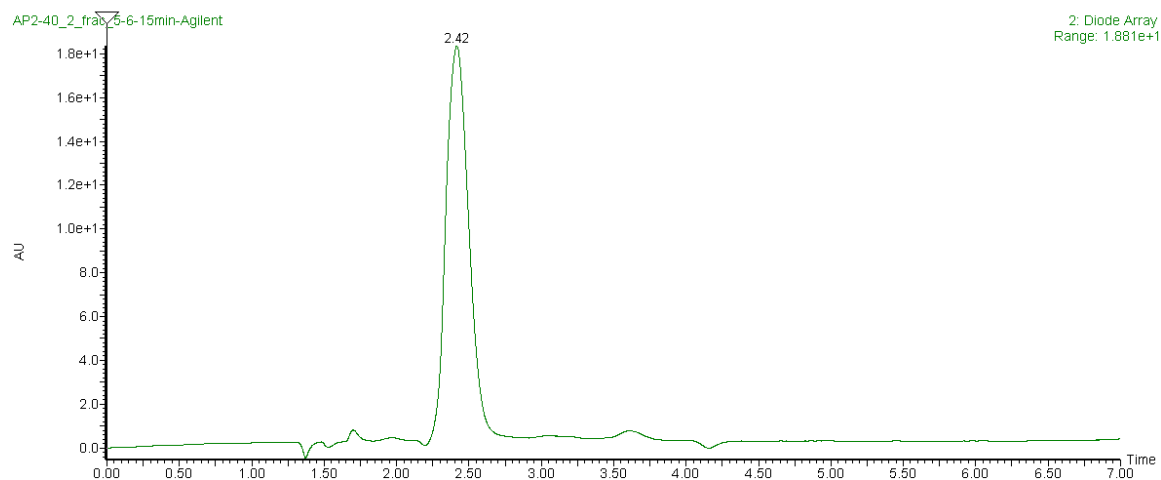
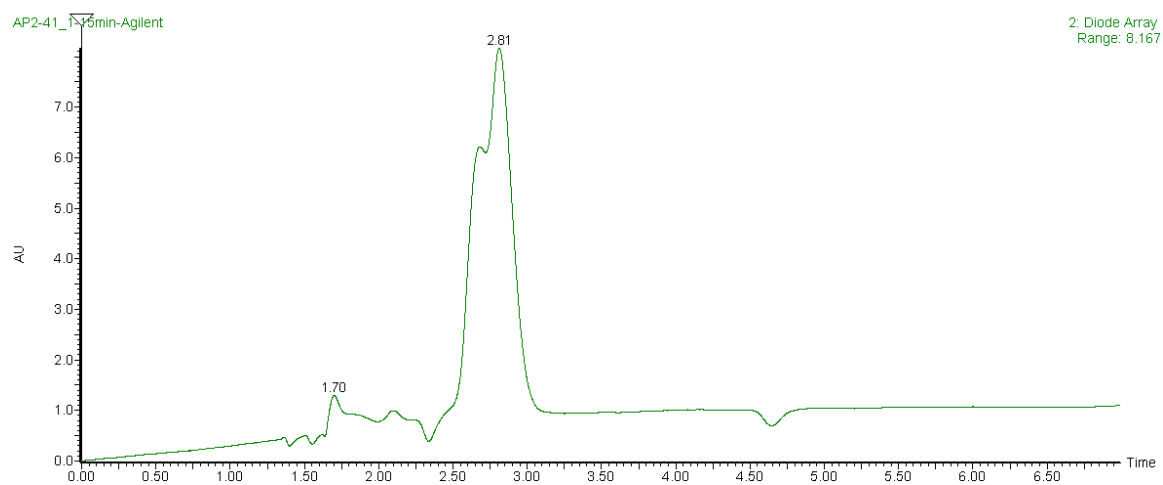
### Appendix A: Chromatograms of selected compounds

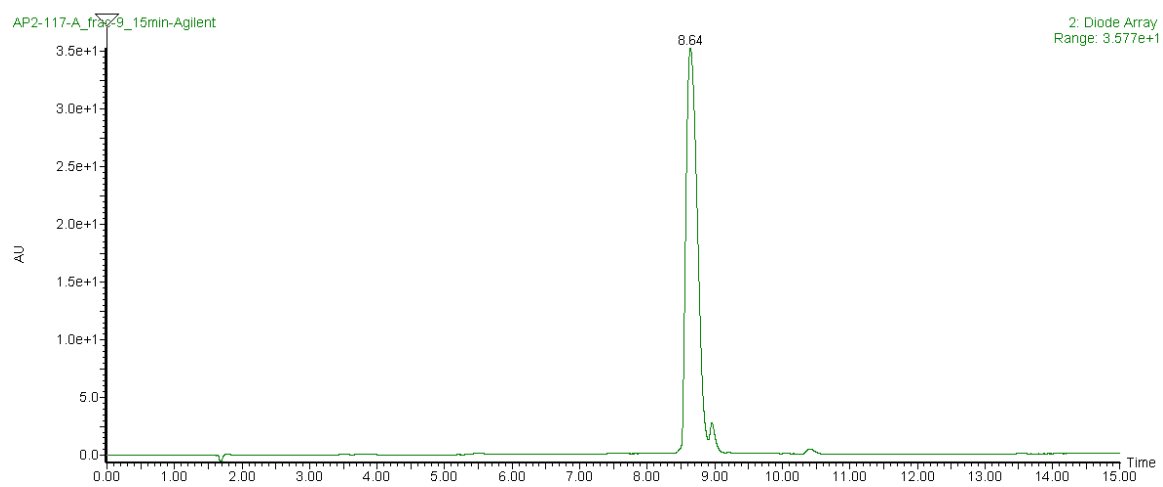
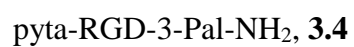
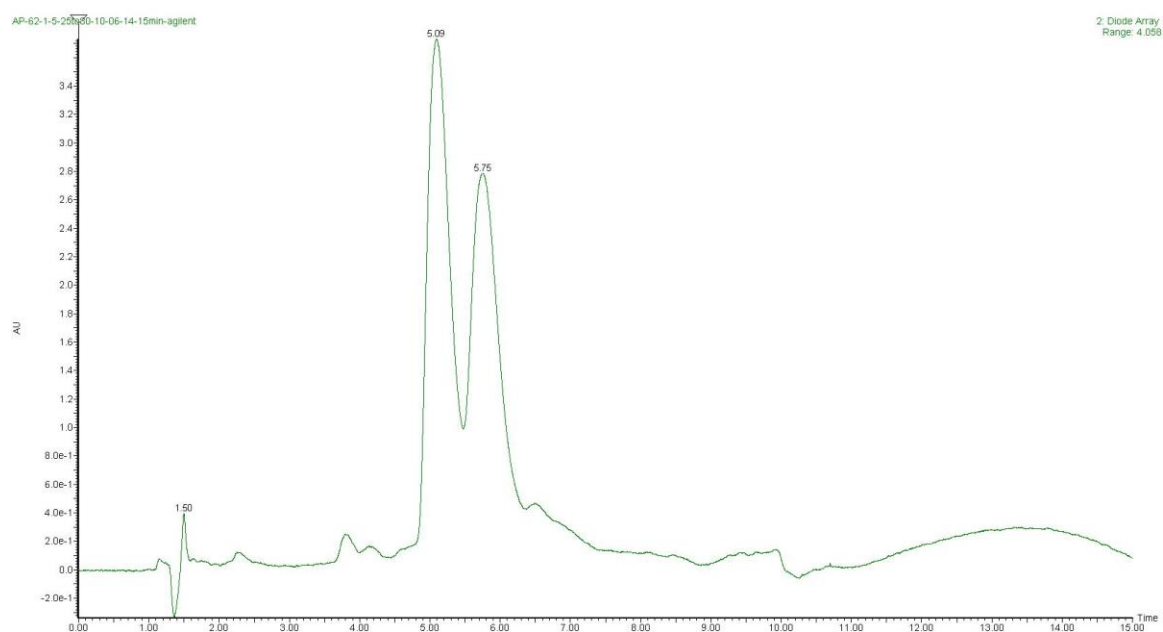
#### Ac-HRGDH-OH, 2.4

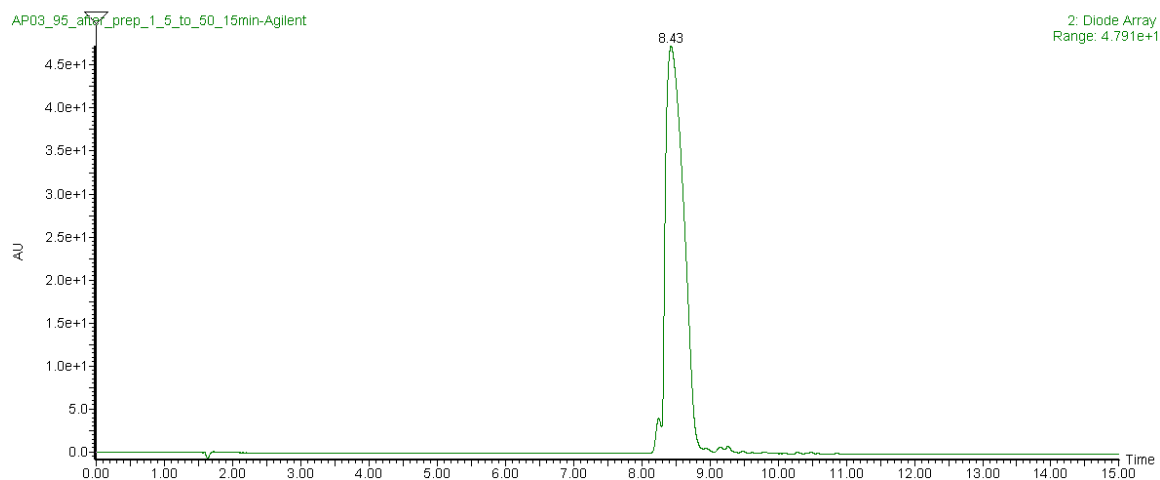
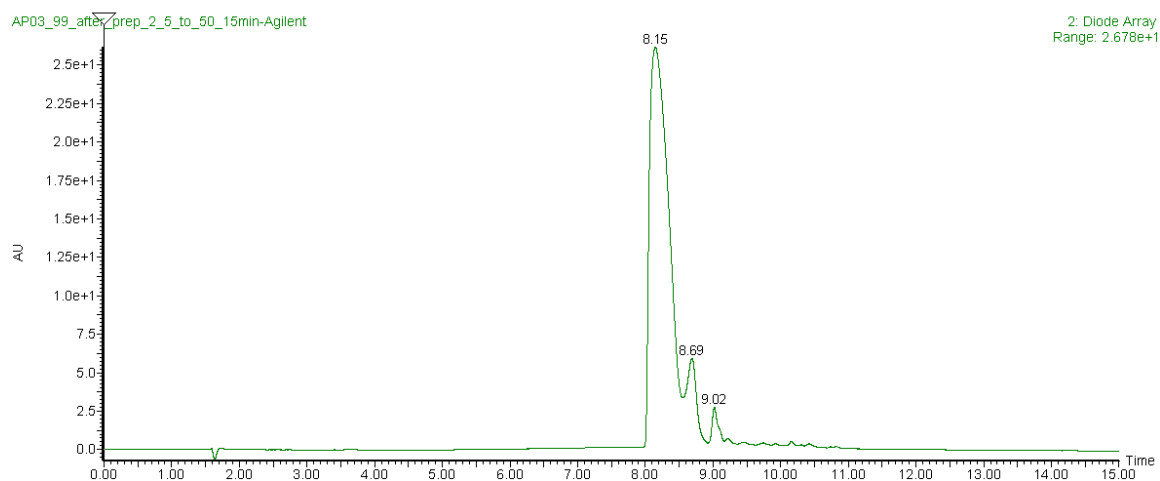


#### Ac-HRGDH-NH<sub>2</sub>

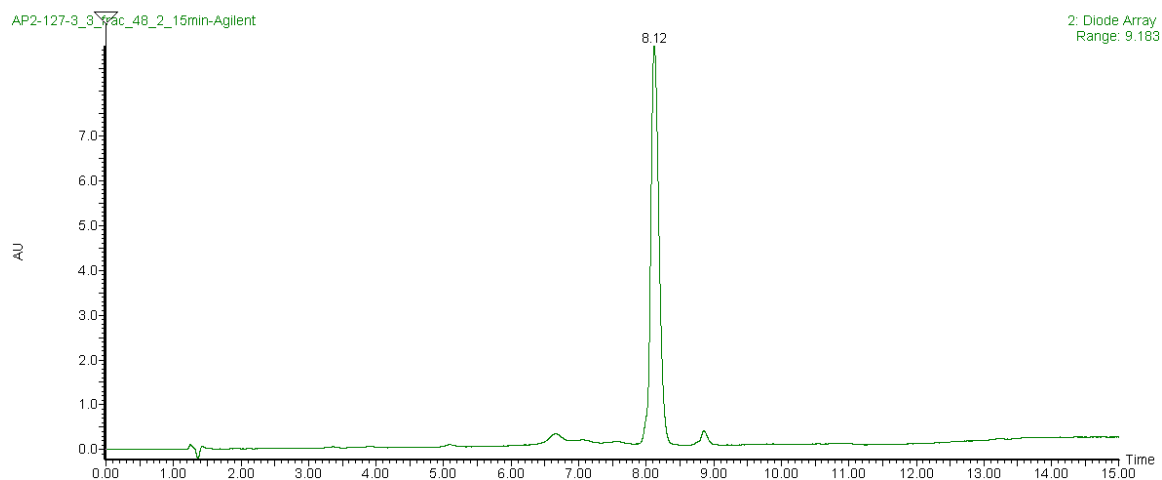


**Ac-3-Pal-RGD-3-Pal-OH, 2.7****Ac-3-Pal-RGD-3-Pal-NH<sub>2</sub>, 2.8**

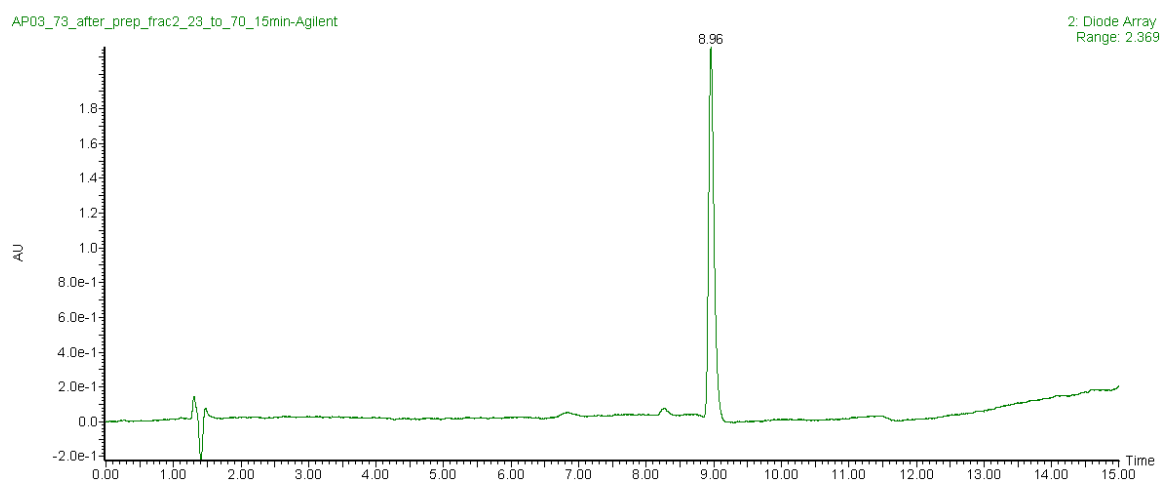


**pyta-RGd-3-Pal-NH<sub>2</sub>, 3.7****pyta-rGD-3-Pal-NH<sub>2</sub>, 3.8**

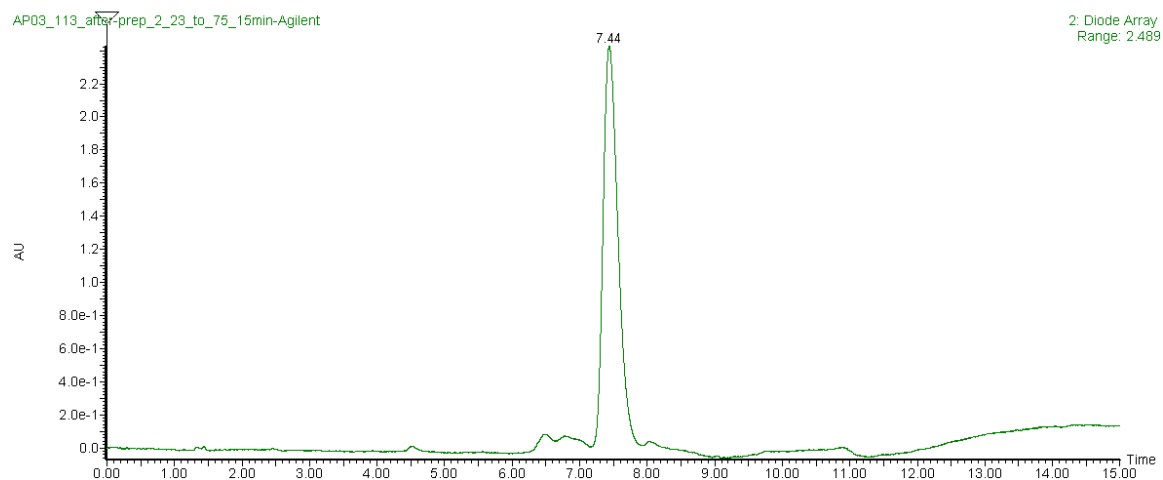
**[Re(CO)<sub>3</sub>(pyta-RGD-3-Pal-NH<sub>2</sub>)]OTf, 3.5**



**[Re(CO)<sub>3</sub>(pyta-RGd-3-Pal-NH<sub>2</sub>)]OTf, 3.9**

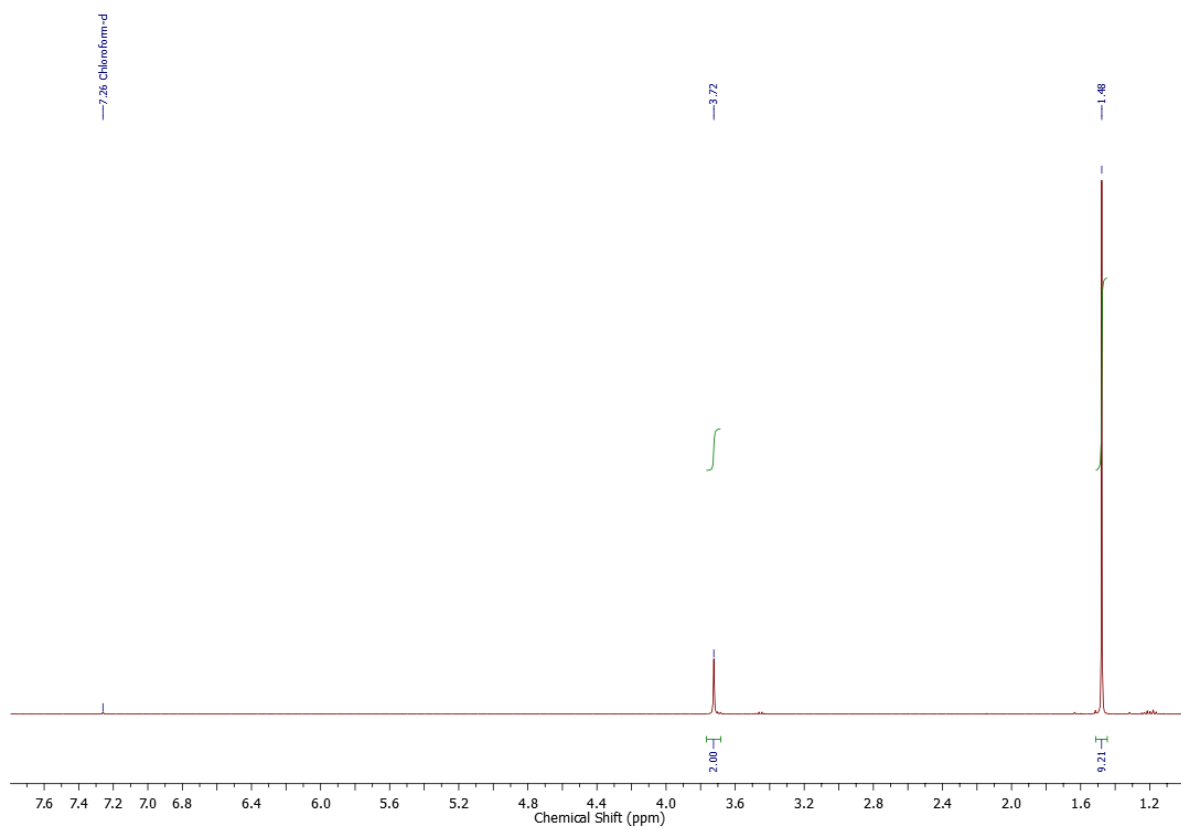


[Re(CO)<sub>3</sub>(pyta-rGD-3-Pal-NH<sub>2</sub>)]OTf, **3.10**

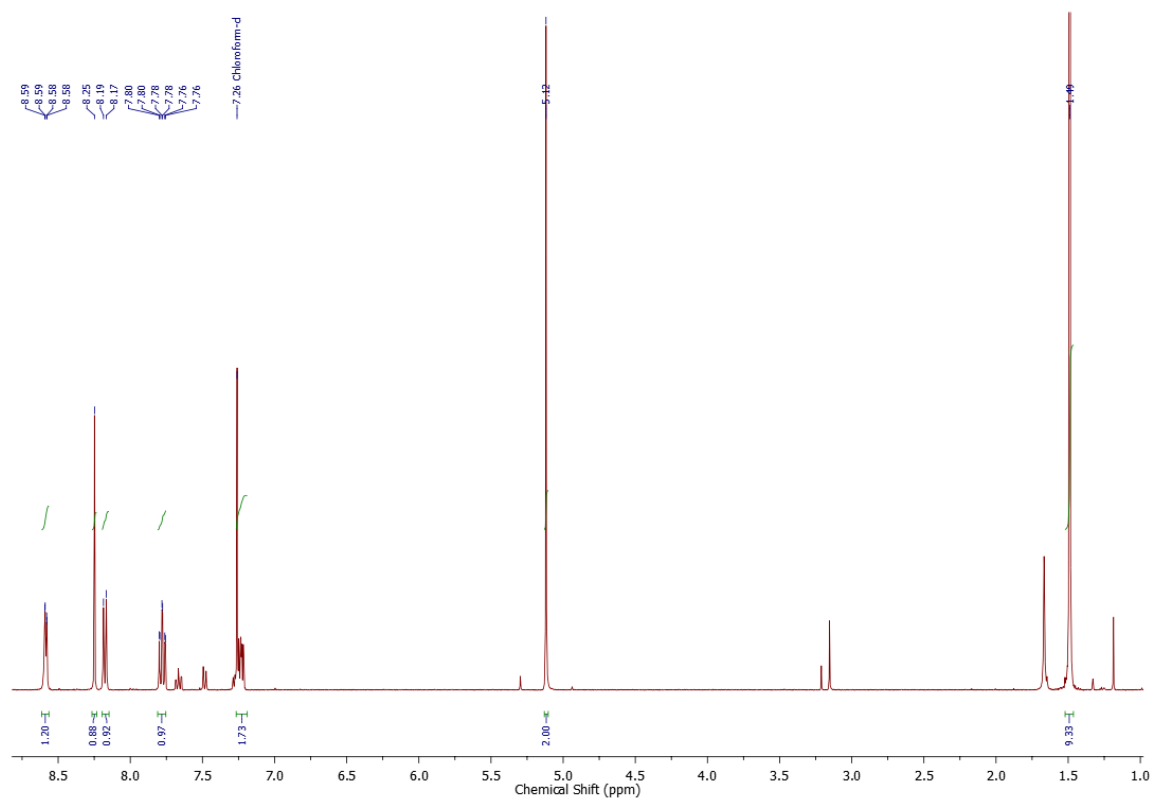


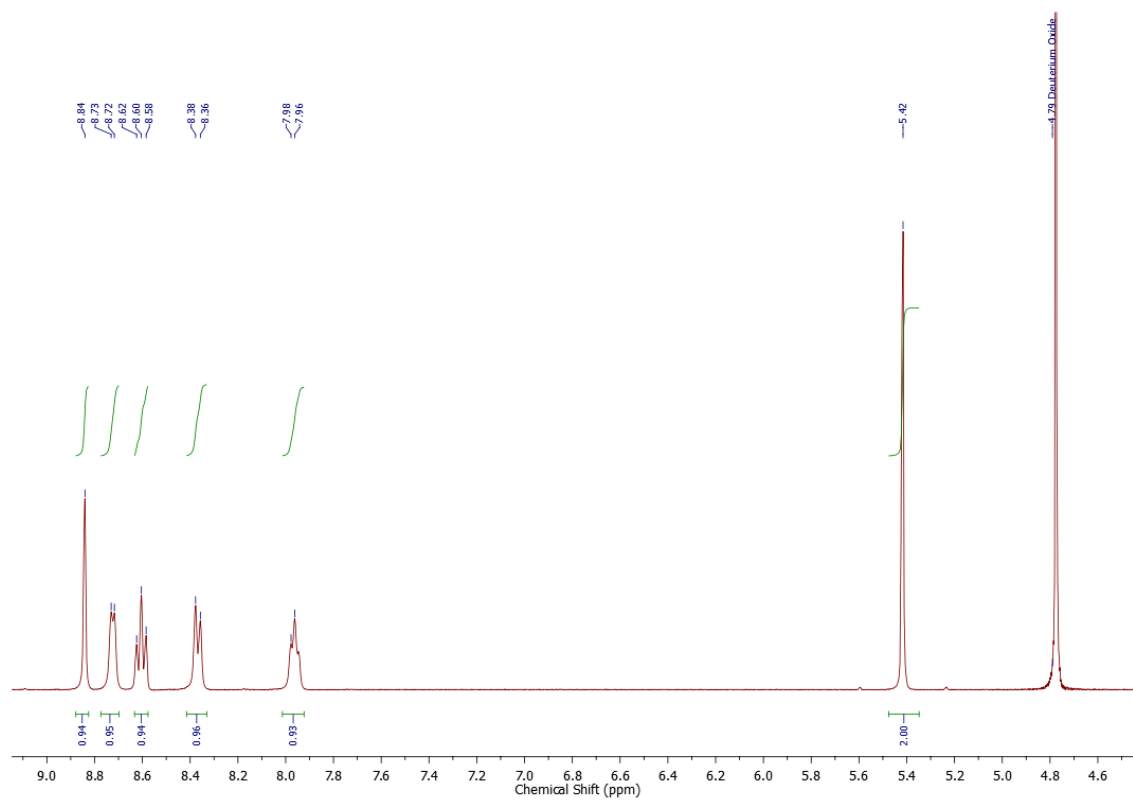
[illegible]

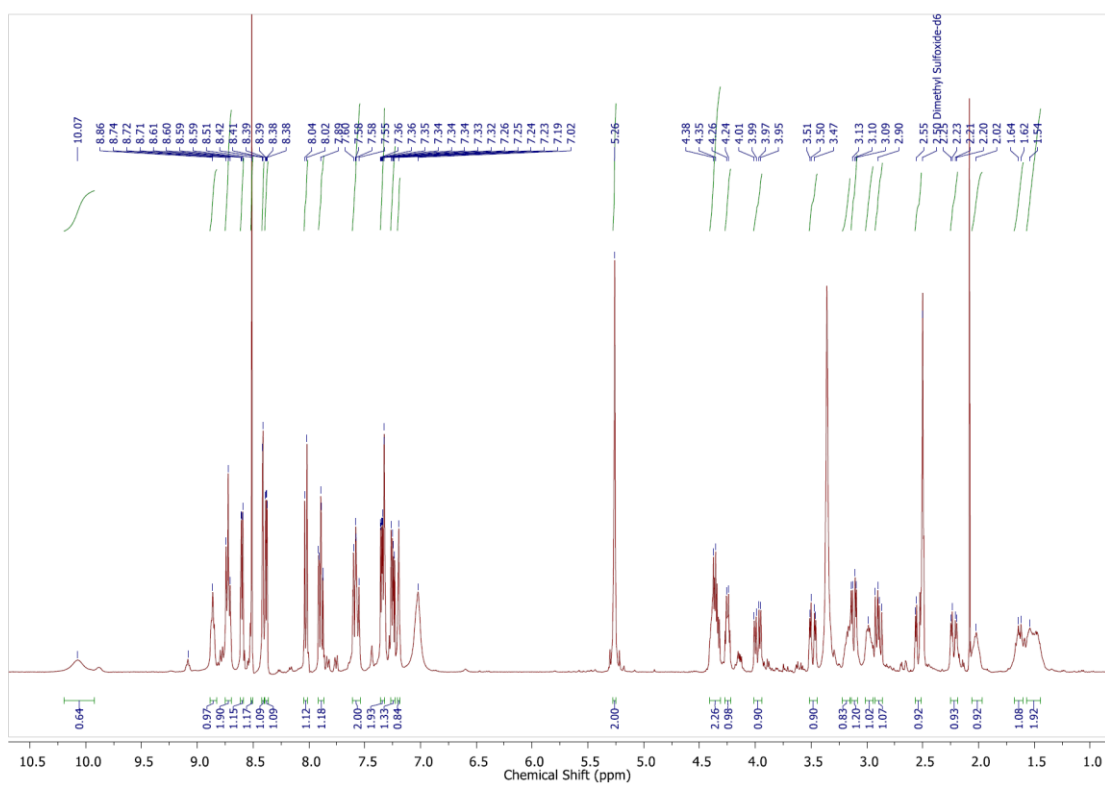
*tert*-butyl azido acetate, **3.1**

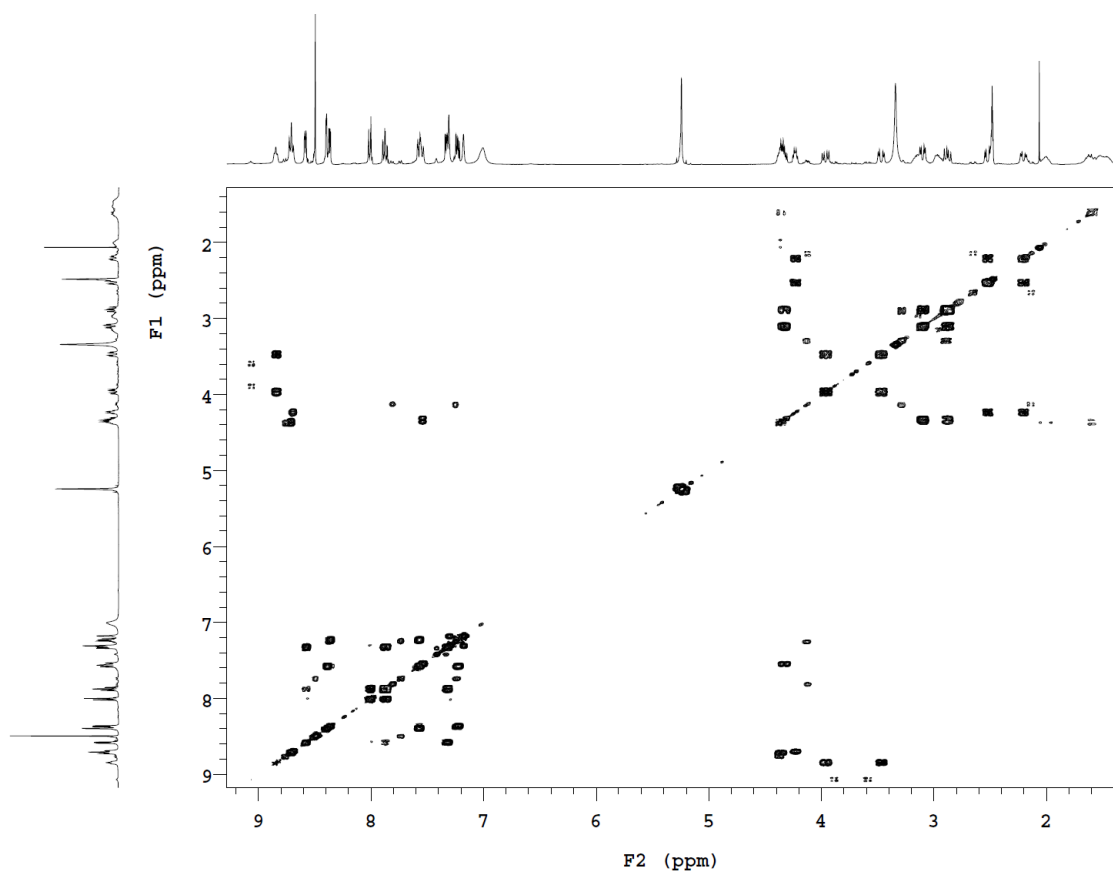


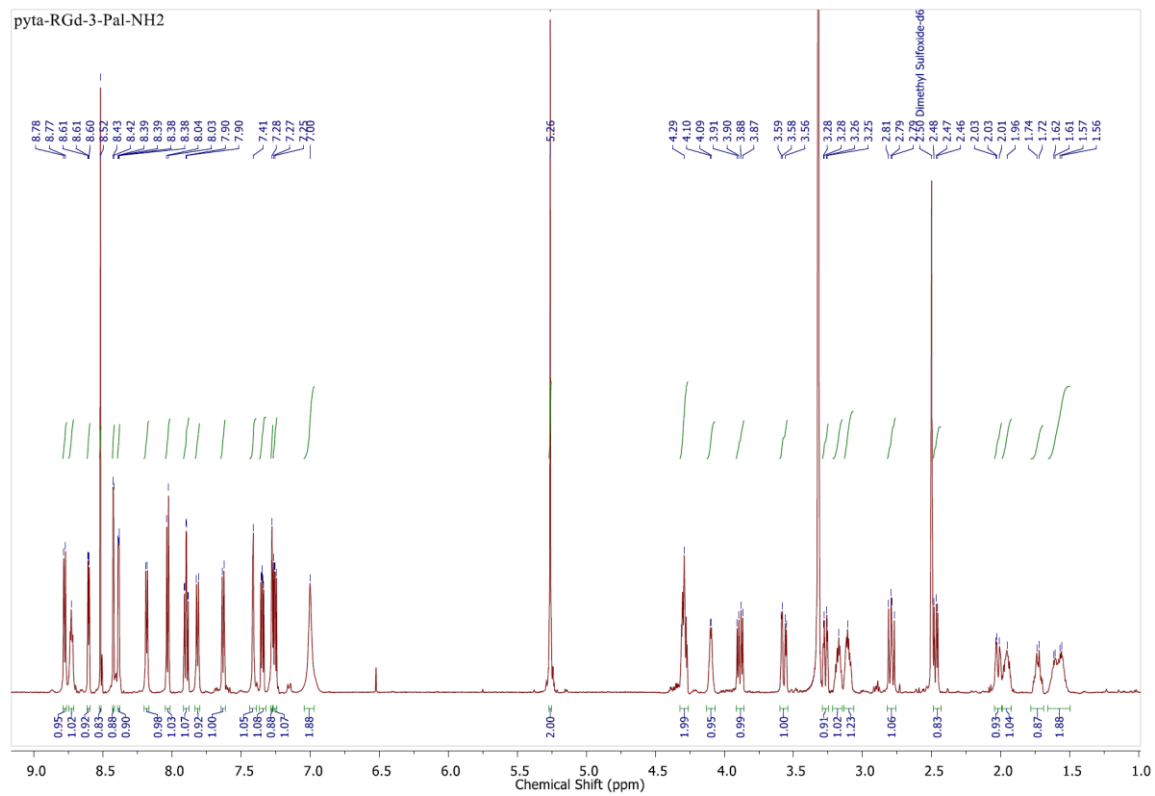
tert-butyl 2-(4-(pyridin-2-yl)-1H-1,2,3-triazol-1-yl)acetate, **3.2**

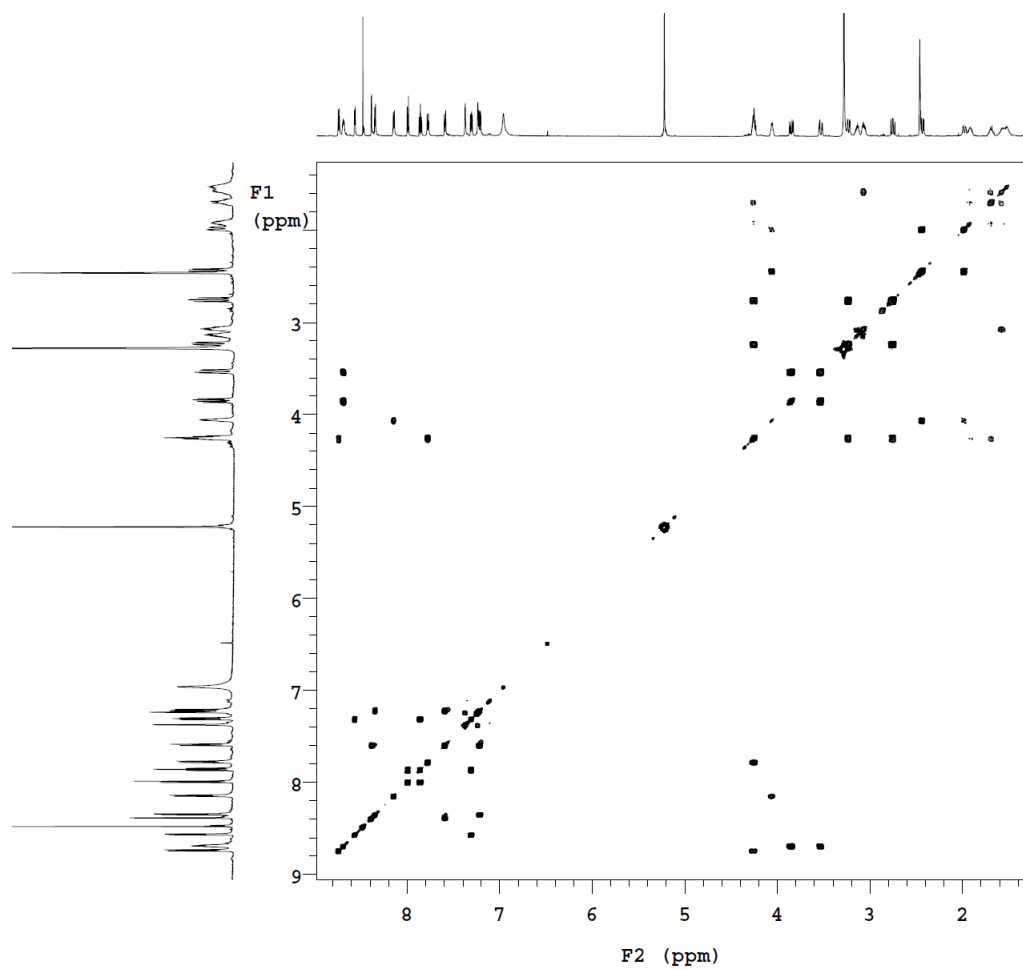


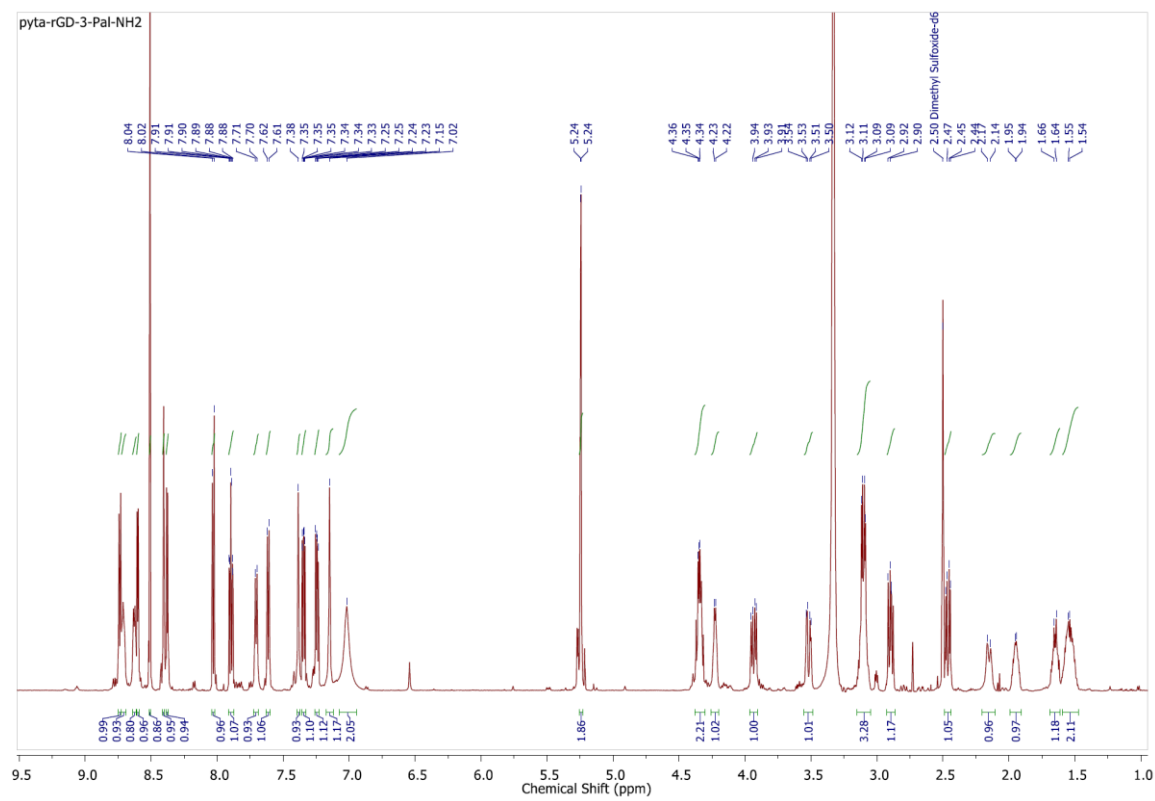
2-(4-(pyridin-2-yl)-1H-1,2,3-triazol-1-yl)acetic acid (pyta), **3.3**

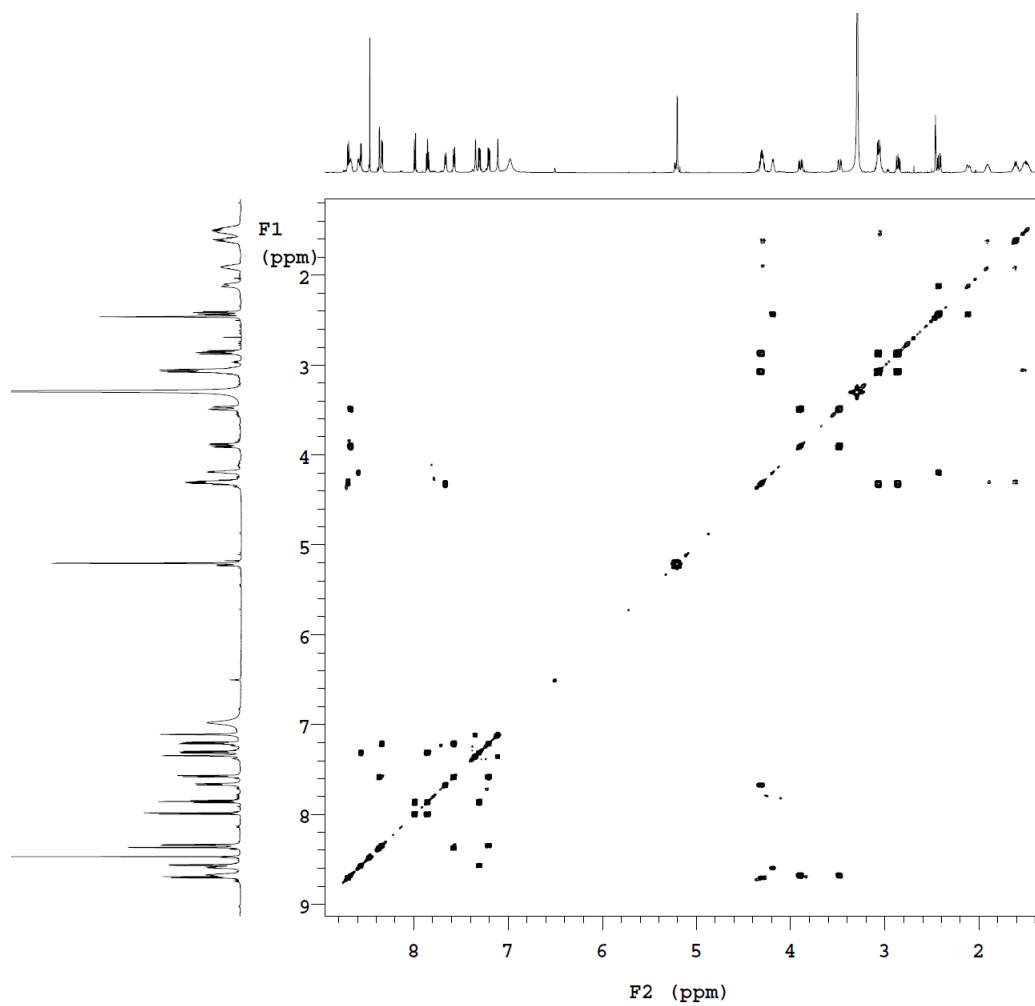
pyta-RGD-3-Pal-NH<sub>2</sub>, 3.4



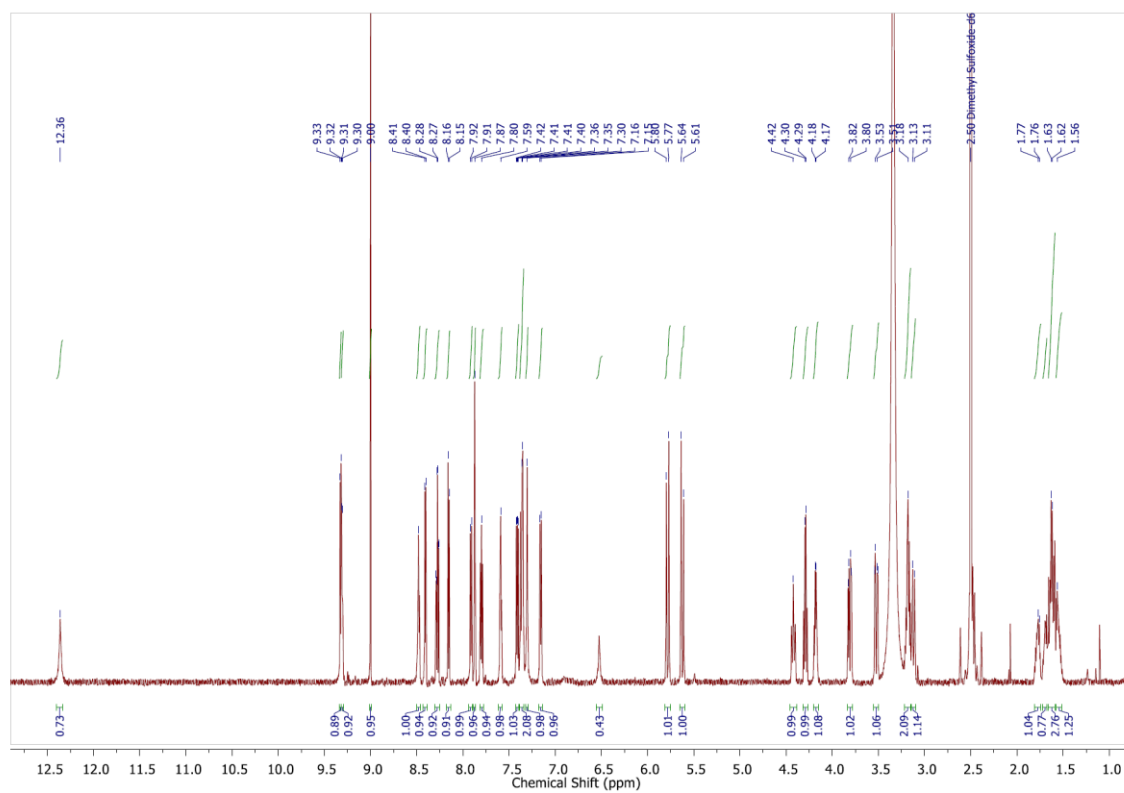
pyta-RGd-3-Pal-NH<sub>2</sub>, **3.7**

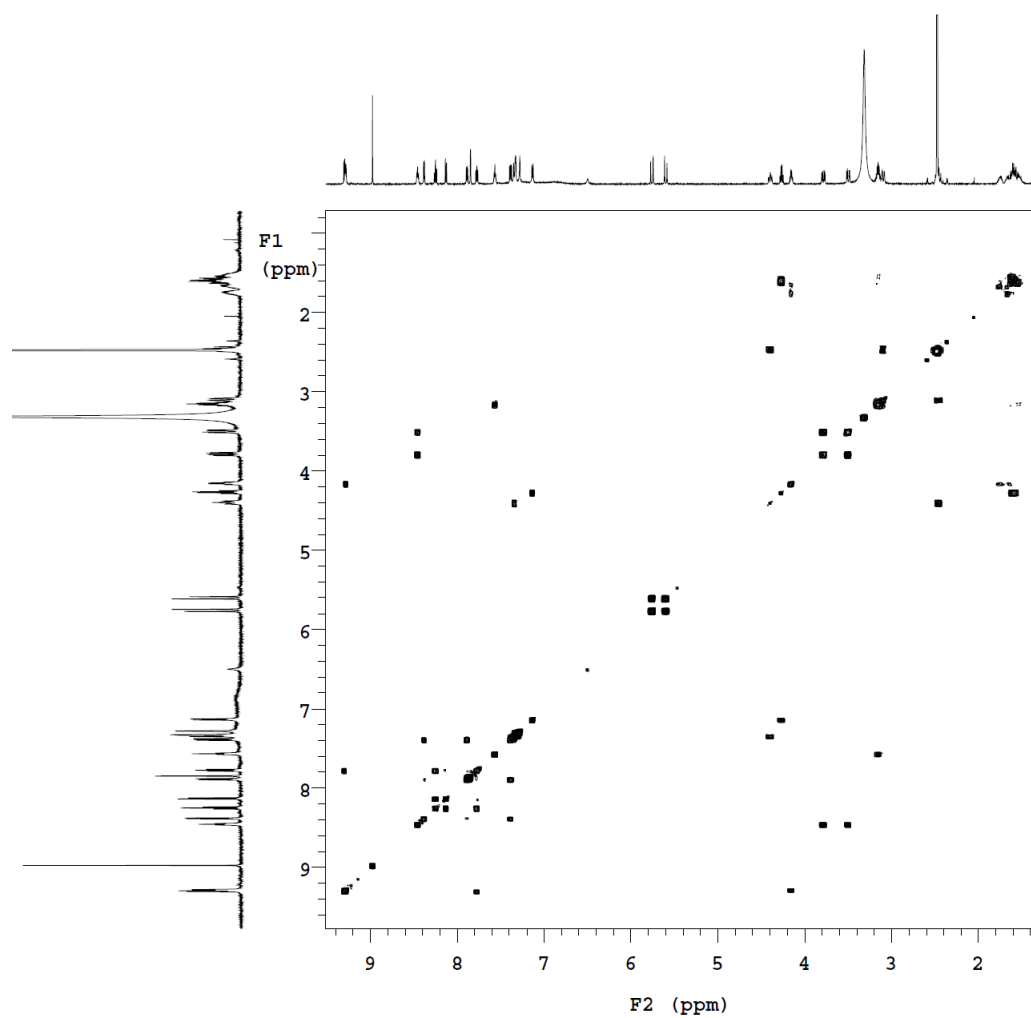


pyta-rGD-3-Pal-NH<sub>2</sub>, **3.8**

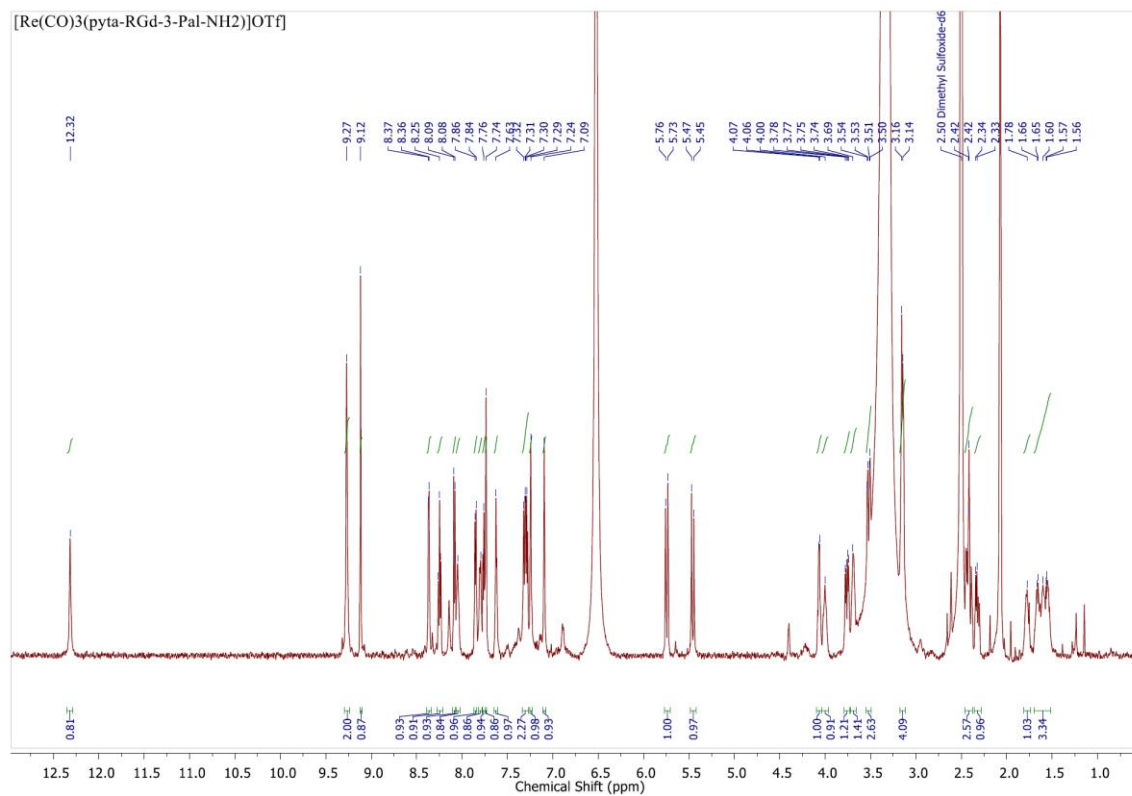


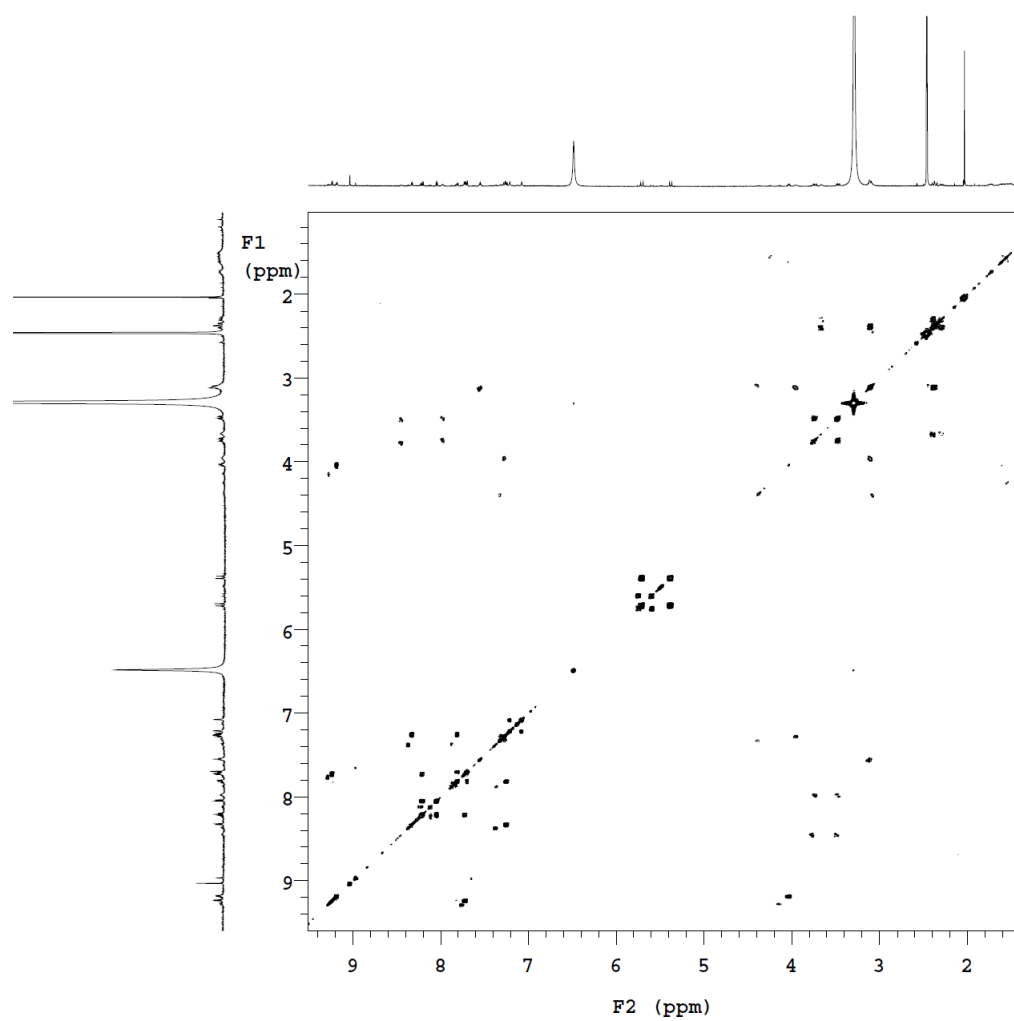
[Re(CO)<sub>3</sub>(pyta-RGD-3-Pal-NH<sub>2</sub>)]OTf, **3.5**



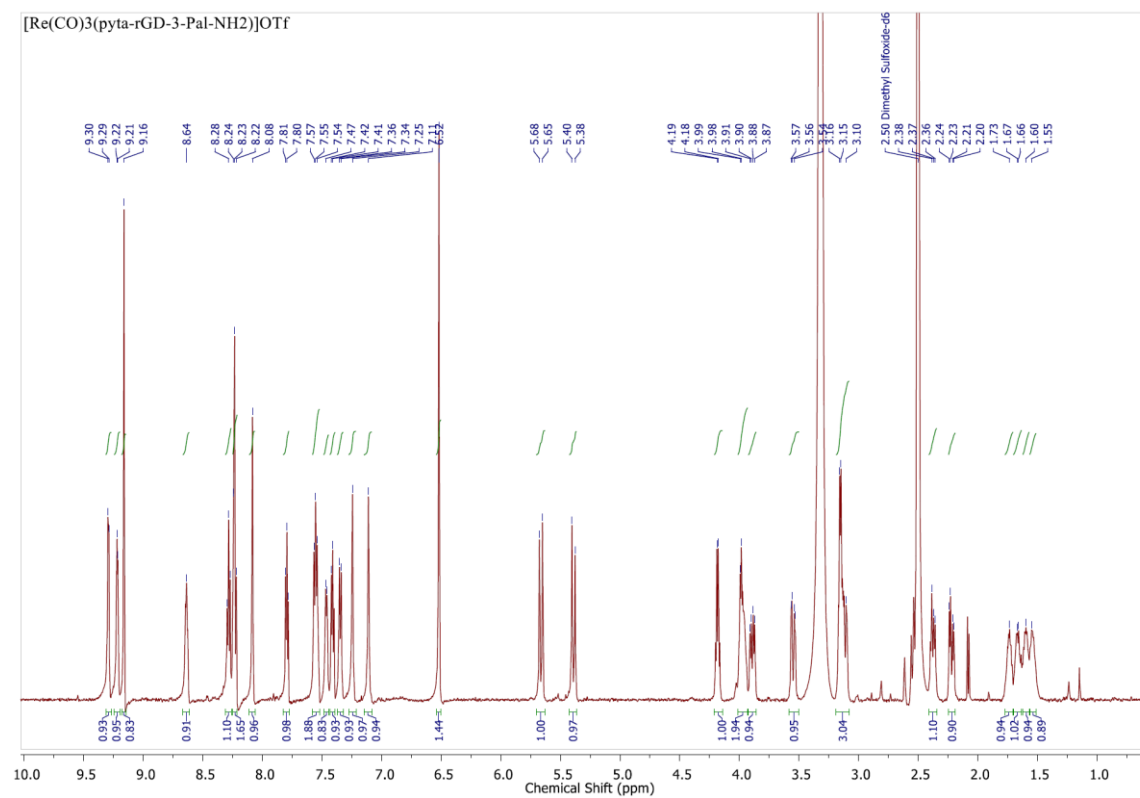


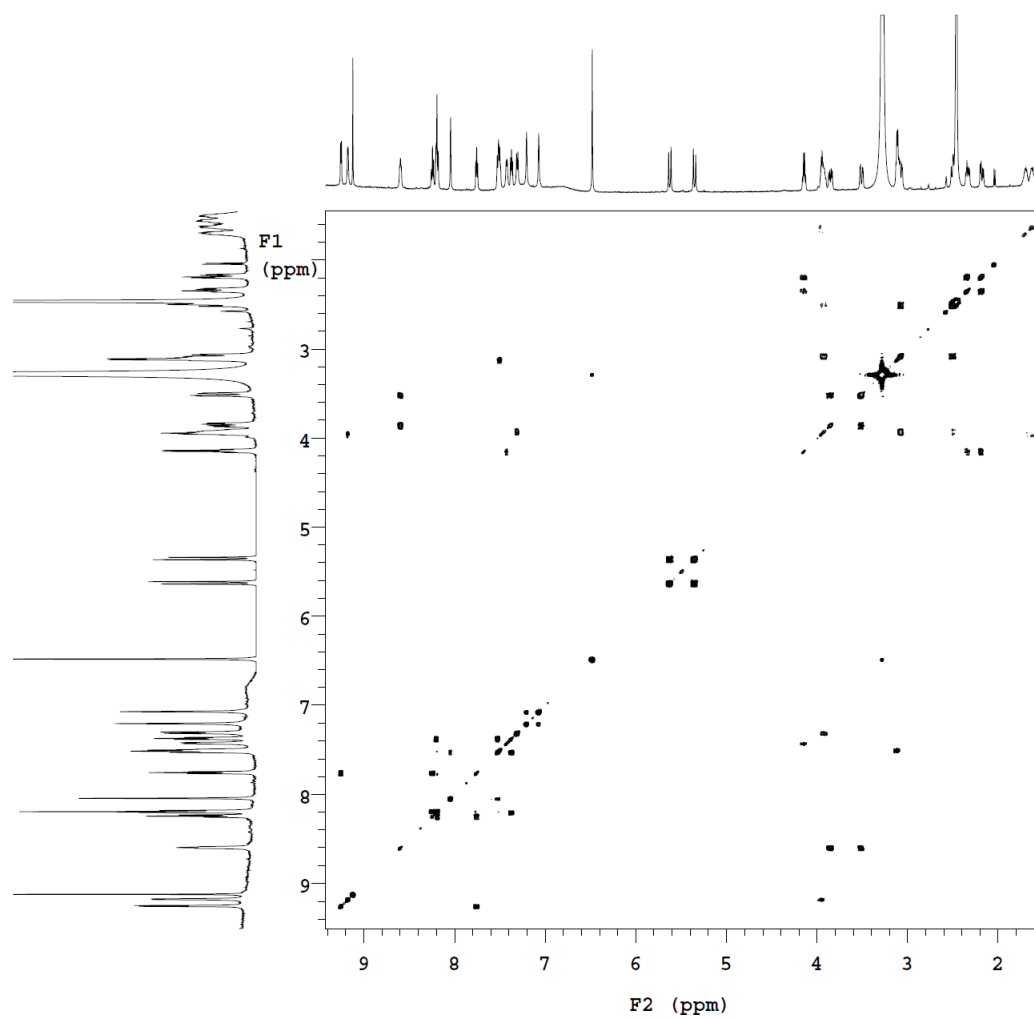
$[\text{Re}(\text{CO})_3(\text{pyta-RGd-3-Pal-NH}_2)]\text{OTf}$ , **3.9**





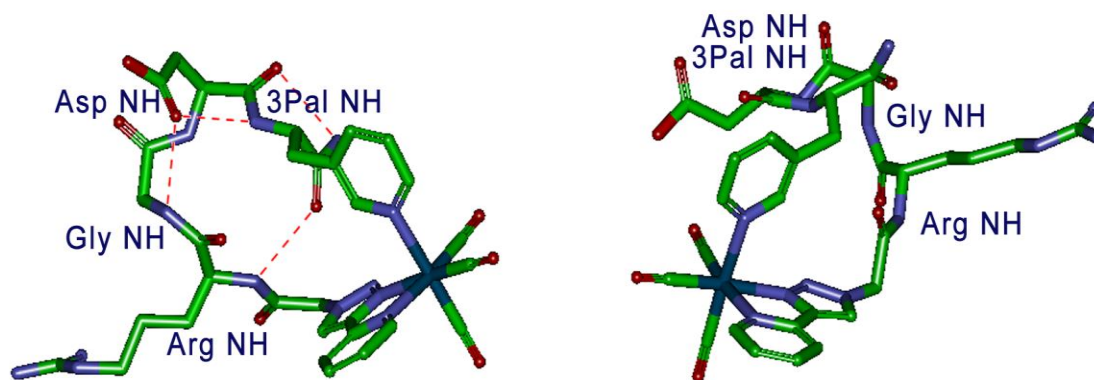
$[\text{Re}(\text{CO})_3(\text{pyta-rGD-3-Pal-NH}_2)]\text{OTf}$ , **3.10**





## Appendix C: Computational study on $\text{Re}(\text{CO})_3^+$ coordinated peptide, **3.5**

3D structures, showing intra-molecular hydrogen bonding (dashed red lines), of two possible isomers for the proposed structure of cyclized peptide, **3.5**



Dear Aagam:

Thank you very much for your request and for your interest in our content.

Please feel free to include the figure in your thesis or dissertation subject to the guidelines listed on our website. I've copied them below:

<http://www.sciencemag.org/site/about/permissions.xhtml#thesis>

#### **Reproducing AAAS Material in your Thesis or Dissertation**

**NOTE:** If you are the Original Author of the AAAS article being reproduced, please refer to your License to Publish for rules on reproducing your paper in a dissertation or thesis. AAAS permits the use of content published in its journals *Science*, *Science Technical Medicine*, and *Science Signaling*, but only provided the following criteria are met.

1. If you are using figure(s)/table(s), permission is granted for use in print and electronic versions of your dissertation or thesis.
2. A full text article may be used only in print versions of a dissertation or thesis. AAAS does not permit the reproduction of full text articles in electronic versions of theses or dissertations.
3. The following credit line must be printed along with the AAAS material: "From [Full Reference Citation]. Reprinted with permission from AAAS."
4. All required credit lines and notices must be visible any time a user accesses any part of the AAAS material and must appear on any printed copies that an authorized user might make.
5. The AAAS material may not be modified or altered except that figures and tables may be modified with permission from the author. Author permission for any such changes must be secured prior to your use.
6. AAAS must publish the full paper prior to your use of any of its text or figures.
7. If the AAAS material covered by this permission was published in *Science* during the years 1974–1994, you must also obtain permission from the author, who may grant or withhold permission, and who may or may not charge a fee if permission is granted. See original article for author's address. This condition does not apply to news articles.
8. If you are an Original Author on the AAAS article being reproduced, please refer to your License to Publish for rules on reproducing your paper in a dissertation or thesis.

Permission covers the distribution of your dissertation or thesis on demand by a third party distributor (e.g. ProQuest / UMI), provided the AAAS material covered by this permission remains in situ and is not distributed by that third party outside of the context of your Thesis/Dissertation.

Permission does not apply to figures/photos/artwork or any other content or materials included in your work that are credited to non-AAAS sources. If the requested material is sourced to or references non-AAAS sources, you must obtain authorization from that source as well before using that material. You agree to hold harmless and indemnify AAAS against any claims arising from your use of any content in your work that is credited to non-AAAS sources.

By using the AAAS Material identified in your request, you agree to abide by all the terms and conditions herein.

AAAS makes no representations or warranties as to the accuracy of any information contained in the AAAS material covered by this permission, including any warranties of merchantability or fitness for a particular purpose.

If how you wish to use our content falls outside of these guidelines or if you have any questions please just let me know.

Best regards,

Lili Catlett

Lili Catlett

Rights, Contracts, and Licensing Associate

The American Association for the Advancement of Science

**From:** Aagam Patel

**Sent:** Thursday, August 20, 2015 1:22 PM

**To:** permissions

**Subject:** Image permission

Date: August 20, 2015

Re: Permission to Use Copyrighted Material in a Master's Thesis

Dear: I am a University of Western Ontario graduate student completing my Master's thesis entitled "The Development of Cyclic RGD Peptides Stabilized Through  $^{99m}\text{Tc}/\text{Re}(\text{CO})_3$ ". My thesis will be available in full-text on the internet for reference, study and / or copy. Except in situations where a thesis is under embargo or restriction, the electronic version will be accessible through the Western Libraries web pages, the Library's web catalogue, and also through web search engines. I will also be granting Library and Archives Canada and ProQuest/UMI a non-exclusive license to reproduce, loan, distribute, or sell single copies of my thesis by any means and in any form or format. These rights will in no way restrict republication of the material in any other form by you or by others authorized by you.

I would like permission to allow inclusion of the following material in my thesis: [Crystal structure of the extracellular segment of integrin alpha V beta 3 in complex with an Arg-Gly-Asp ligand, **Figure 2** on page 154, Science, 2002, volume 296]

The material will be attributed through a citation.

Please confirm in writing or by email that these arrangements meet with your approval.

Sincerely

Aagam Patel

## Curriculum Vitae

**Name:** Aagam Patel

**Post-secondary Education and Degrees:** Ryerson University  
Toronto, Ontario, Canada  
2008-2013 B.Sc. Chemistry

Western University  
London, Ontario, Canada  
2013-2015 M.Sc. Chemistry

**Honours and Awards:** Western Graduate Research Scholarship, Chemistry  
09/13 – 04/14, 09/14 – 04/15

**Related Work Experience** Research Assistant  
Xerox, Canada  
Mississauga, Ontario, Canada  
Sept. 2011 – April 2012

Teaching Assistant  
Western University  
Sept. 2013 – April 2015

### Publications:

Khan, A.; Komejan, S.; Patel, A.; Lombardi, C.; Lough, A.J.; Foucher, D.A.\*; *Reduction of C,O-chelated organotin(IV) dichlorides and dihydrides leading to protected polystannanes*, Journal of Organometallic Chemistry, 776, (2015), 180 – 191

### Conference Abstracts:

Patel, A.; Luyt, L.G.\*; *Turn mimetics induced by Re/Tc (I) tricarbonyl coordination to form cyclic metallopeptides*, June 2015, Canadian Chemistry Conference (Oral Presentation)

Patel, Aagam; Luyt, Leonard G.\*; *Development of cyclic metallopeptides as potential imaging agents for angiogenesis*, June 2015, Oncology Research & Education Day. London, Ontario. (Poster Presentation)